UNIVERSITY OF LISBON

FACULTY OF SCIENCES

PHYSICS DEPARTMENT

NANOTOPOGRAPHIC DEVICE FOR NEURAL SUBTYPES SEGREGATION

ANDREIA ISABEL CÂNDIDO E SILVA

DISSERTAÇÃO

MESTRADO INTEGRADO EM ENGENHARIA BIOMÉDICA E BIOFÍSICA

PERFIL ENGENHARIA CLÍNICA E INSTRUMENTAÇÃO MÉDICA

2014

UNIVERSITY OF LISBON

FACULTY OF SCIENCES

PHYSICS DEPARTMENT

NANOTOPOGRAPHIC DEVICE FOR NEURAL SUBTYPES SEGREGATION

ANDREIA ISABEL CÂNDIDO E SILVA

DISSERTAÇÃO

MESTRADO INTEGRADO EM ENGENHARIA BIOMÉDICA E BIOFÍSICA

PERFIL ENGENHARIA CLÍNICA E INSTRUMENTAÇÃO MÉDICA

ORIENTADOR EXTERNO: Professor Lorenzo Moroni

ORIENTADOR INTERNO: Professor Hugo Ferreira

2014

This thesis is dedicated to my parents, my brother and my sister.

TABLE OF CONTENTS

ACKNOWLEDGEMENTS

This research project would not have been possible without the support of many people. First and foremost, I would like to express my deep gratitude to Dr. Lorenzo Moroni, my external supervisor, for his patient guidance, encouragement, valuable support, and useful critiques of this research work. Special thanks should also be given to Dr. Hugo Ferreira, my internal supervisor, for his useful and constructive recommendations on this project.

I would like to thank Dr. Paul Wieringa for his advice and assistance in keeping my progress on schedule. My grateful thanks are also extended to Prof. Dr. Clemens A. van Blitterswijk for giving me the opportunity to be part of his research group. I also wish to acknowledge the help provided by Dr. Roman Truckenmüller. His willingness to give his time so generously has been very much appreciated.

I would like to express my very great appreciation to Dr. Maqsood Ahmed for his valuable and constructive suggestions during the development of this research. Advice given by David Barata has also been a great help in my research. I am particularly grateful for the assistance given by Bach Le.

I wish to express my deep sense of gratitude to all members of the TR and BST departments who rendered their help to me willingly. I sincerely thank to the MIRA and MESA+ institutes for providing the financial means and laboratory facilities. I would like to thank the Erasmus AN Proalv for their generous financial support.

My thanks and appreciations also go to my Master's colleagues André Girão, Tiago Ramos, Gülistan Kocer, and Quitterie Larrouture who became friends and helped me ever since. I would not have been able to do it without you all. You made my experience so wonderful.

At last but not least, I wish to express my love and gratitude to my beloved family. Mom, dad, brother and sister, you are the only reason I am here. Thank you ever so much.

AGRADECIMENTOS

Este projeto de investigação não teria sido possível sem o apoio de muitas pessoas. Em primeiro lugar, gostaria de expressar a minha profunda gratidão ao Dr. Lorenzo Moroni, o meu orientador externo, pela sua orientação paciente, incentivo, apoio valioso e críticas construtivas para este trabalho de investigação. Agradecimentos especiais devem também ser dados ao Dr. Hugo Ferreira, o meu orientador interno, pelas suas recomendações úteis e construtivas neste projeto.

Também gostaria de agradecer ao Dr. Paul Wieringa pelos seus conselhos e assistência no avanço do meu projeto. Os meus sinceros agradecimentos também se estendem ao Prof. Dr. Clemens A. van Blitterswijk por me ter dado a oportunidade de fazer parte do seu grupo de investigação. Gostaria também de agradecer a ajuda do Dr. Roman Truckenmüller. A sua disponibilidade e generosidade foram muito apreciadas.

Gostaria de expressar o meu grande agradecimento ao Dr. Maqsood Ahmed pelas suas sugestões valiosas e construtivas durante o desenvolvimento desta pesquisa. Os conselhos de David Barata também foram de grande ajuda nesta investigação. Estou particularmente grata pela ajuda prestada por Bach Le. Desejo expressar o meu profundo sentimento de gratidão a todos os membros dos departamentos TR e BST por toda a ajuda que me prestaram. Agradeço sinceramente aos institutos MIRA e MESA+ por terem fornecido meios financeiros e instalações de laboratório. Gostaria de agradecer ao Erasmus NA Proalv pelo seu generoso apoio financeiro.

Os meus agradecimentos e apreciações vão também para os meus colegas de mestrado André Girão, Tiago Ramos, Gülistan Kocer e Quitterie Larrouture que se tornaram meus amigos e me ajudaram desde então. Não teria sido capaz de fazer isto sem todos eles. Tornaram esta experiência maravilhosa. Por último mas não menos importante, gostaria de expressar o meu amor e gratidão à minha amada família. Mãe, pai, mano e mana, vocês são a razão pela qual estou aqui. Serei sempre eternamente grata a vocês.

ABSTRACT

The usability of advanced prostheses can be improved by increasing the degree of motor control over the prosthesis and sensitive feedback to the patient. As nanoscale surface topographies play an important role in axonal outgrowth and guidance, a nanotopographic device was constructed for studying the axonal response of peripheral neurons to different nanograting sizes. This innovative device design incorporates: (1) microfluidic chambers for axonal isolation; (2) physically modified channels with several nanograting ridges; and (3) a bifurcating nanotopography-based approach. The F11 cell line (nociceptive sensory neurons) was chosen as model to analyse cell response in the nanotopographic device. Optimal materials and techniques were used to assure the quality of the device: Channels were molded on PDMS and nanogratings were printed on the COC surface. In parallel, staining and biochemical assays were performed to evaluate the optimal F11 culture conditions, such as DNA, ATP, and LIVE/DEAD assays.

Existing and potential applications of the nanotopographic device were presented. Neurofluidics is an early stage field which develops microfluidic devices for neurobiological research. The nanotopographic device has the potential to be useful in this emerging area by providing insight into topographical preference for each cell type. Based on that, physical segregation of neuron subtypes might be achieved. In response to high and rising amputation rates, these achievements could be useful in the development of highly sophisticated neural-prosthetic interfaces.

Key-words: Neurofluidics, nanotopography, F11 cells, COC, PDMS, bifurcation, axonal isolation and guidance, neuroprostheses.

RESUMO

A usabilidade de próteses avançadas pode ser melhorada através do aumento do controlo motor sobre a prótese e da resposta sensitiva do paciente. Como a topografia da superfície desempenha um papel importante, ao nível da nanoescala, no crescimento e condução dos axónios, o dispositivo nanotopográfico foi construído com o objetivo de estudar a resposta axonal de neurónios periféricos a diferentes tamanhos de nanogradeamentos. O design inovador deste dispositivo incorpora: (1) câmaras microfluídicas para isolamento axonal; (2) canais fisicamente modificados com vários relevos nos nanogradeamentos; e (3) uma abordagem de bifurcação baseada na nanotopografia. A linha celular F11 (neurónios sensitivos nociceptivos) foi escolhida como modelo para analisar a resposta celular no dispositivo nanotopográfico. Materiais e técnicas otimizadas foram usados para assegurar a qualidade do dispositivo: os canais foram moldados em PDMS e os nanogradeamentos impressos na superfície de COC. Em paralelo, colorações e ensaios bioquímicos foram realizados para avaliar as condições ótimas de cultura das F11, nomeadamente os ensaios de ADN, ATP, e LIVE/DEAD.

As potenciais aplicações deste dispositivo nanotopográfico foram apresentadas. A Neurofluídica é um campo em recente desenvolvimento que visa construir dispositivos microfluídicos para a investigação neurobiológica. O dispositivo nanotopográfico tem potencial para ser útil nesta área emergente, fornecendo informação acerca das preferências topográficas de cada tipo de célula. Com base nisto, poderia ser possível obter-se a segregação física de subtipos de neurónios. Em resposta às altas e crescentes taxas de amputações, estes avanços poderiam ser úteis no desenvolvimento de interfaces neuro-protéticas altamente sofisticadas.

Palavras-Chave: Neurofluídica, nanotopografia, células F11, COC, PDMS, bifurcação, isolação e condução axonal, neuroprótese.

LIST OF FIGURES

LIST OF TABLES

ABBREVIATIONS

AAOP - American Academy of Orthotists and Prosthetists

ANOVA - Analysis of Variance

APTES - (3-Aminopropyl)trimethoxysilane

ATP - Adenosine Triphosphate

BDNF - Brain-derived Neurotrophic Factor

COC - Cyclic Oleofin Copolymer

CNS - Central Nervous System

DAPI - 4’,6-Diamidino-2-Phenylindole

DLB - DNA Lysis Buffer

DMEM - Dulbecco’s Modified Eagle Medium

DNA - Deoxyribonucleic Acid

DRG - Dorsal Root Ganglia

EBL - Electron Beam Lithography

ECM - Extracellular Matrix

EDTA - Ethylenediamine Tetraacetic Acid

EthD-1 - Ethdium Homodimer-1

ETOH - Ethanol

FA - Focal Adhesion

FBS - Fetal Bovine Serum

FES - Functional Electrical Stimulation

FGF - Fibroblast Growth Factors

FINE - Flat Interface Nerve Electrode

FSK - Forskolin

GIA - Global Industry Analysts, Inc.

LIFE - Longitudinal Intrafascicular Electrode

MAG - Myelin-associated Glycoprotein

MEA - Multielectrode Array

MT - Microtubule

NG - Nerve Guide

NGC - Nerve Guidance Channel

NGF - Nerve Growth Factor

NIL - Nanoimprint Lithography

NT - Neurotrophin

NTE - Neural Tissue Engineering

PC - Polycarbonate

PBS - Phosphate Buffered Saline

PDMS - Poly(dimethylsiloxane)

PNI - Peripheral Nerve Interface

PNS - Peripheral Nervous System

PS - Polystyrene

RT - Room Temperature

SC - Schwann Cell

SEM - Scanning Emission Microscopy

SPL - Scanning Probe Lithography

TCT - Tissue-culture-treated

TIME - Transverse Intrafascicular Multichannel Electrode

UEA - Utah Electrode Array

USEA - Utah Slanted Electrode Array

UV - Ultraviolet

VEGF - Vascular Endothelial Growth Factor

WD - Working Distance

μCP - Microcontact Printing

CHAPTER 1 - *INTRODUCTION*

1.1. Project Motivation

According to the American Academy of Orthotists and Prosthetists (AAOP), in 2020, 2.4 million people will have an amputation and use prostheses [1]. The most common are the limb amputations, usually caused by vascular complications (Dysvascularity) [2], from issues such as diabetes, a rising incidence disease in developed countries [3].

Prostheses are medical artificial substitutes for replacement of missing or amputee body parts, but its progress has been slow. Recently, developed limb prostheses have been made clinically available for motor rehabilitation of amputees [2]. Advances in components or materials, socket fitting techniques between the residual limb (stump) and the prosthesis, and power sources [3] have contributed to better functionality, efficiency, comfort and lifelike appearance (cosmetically pleasing) [4, 5] of upper and lower limb prostheses.

Although the quality of the interface between the socket and the stump have been greatly improved in the past three decades [4], low dexterity, motility and limited sensory feedback [3] have motivated the substitution of passive and battery powered prostheses. The latest developments are towards body powered prostheses or neuroprostheses, designed to replace lost or impaired motor or sensory functions by communicating directly or indirectly with the nervous system [2].

Compared with human limbs, limb neuroprostheses still have limited performance, mainly due to limitations in the creation of neural interfaces able to provide proper bidirectional connection between the cells of the peripheral nervous system (PNS) of the amputee and the neuroprosthesis. Selectivity is the capacity of a peripheral nerve interface (PNI) to access specific types of neurons, like sensory, motor or autonomic neurons. This constitutes the greatest challenge to develop clinically accepted PNIs suitable for integration with neuroprostheses [2].

A new report by the Global Industry Analysts, Inc. (GIA) reveals that the Global Orthopaedic Prosthetics Market will reach 14.6 billion euros by 2015, especially due to the development of advanced devices [6].

Indeed, innovations in microfluidics, a recent technology using microscale channels to manipulate fluids in a controlled manner at the nanoliter scale has proved to have potential to significantly contribute with three main emerging biomedical areas, namely neuroengineering, nanomedicine and neural tissue engineering (NTE) for the construction of advanced PNIs [7, 8].

Neuroengineering (or neural engineering) has developed a wide range of highly sophisticated stimulating and recording electronic interfaces with different levels of invasiveness and selectivity [2] [9]. At the same time, NTE has created artificial structures and scaffolds that mimic the complexity of nervous tissue [8] [10] and can be incorporated into the PNIs to promote tissue regeneration of injured neurons after amputation [9].

Furthermore, it is known that the macro (>1 mm, overall shape of the scaffold), micro (1 μm-1 mm, cellular level) and nanostructural (<1 μm, subcellular/molecular level) surface properties are important for cell-scaffold interaction [11]. For that reason, the application of nanotechnology to medicine resulted on the “Nanomedicine” or “Nanobiomedicine” field and has been contributing toward the creation of new structures with dimensions on the nanoscale that are useful for tissue engineering purposes [8] [12-14].

Indeed, as different types of neural cells respond positively to different nanotopographical features, which are similar to their natural cellular microenvironment [8], the ability to precisely control the cell response using nanotopography will largely improve the design and development of PNIs.

However, further studies regarding nanoscale features and structures which control neurite growth are still necessary to allow the development of clinically useful platforms for the successful regeneration or replacement of PNS structures [8]. Although the microfluidics field is still at an early stage of development, microfluidic devices are increasingly being used for neuroscience

research and can also be implantable as PNIs, providing a future direction to the new field of neurofluidics [15] (Figure 1).

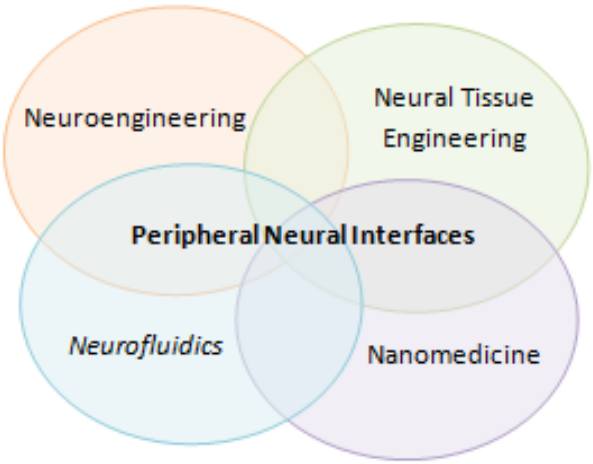

Figure 1 - Recent advances in Neuroengineering, NTE and Nanomedicine fields have been contributing together for the enhancement of PNIs able to be integrated in neuroprostheses. Neurofluidics is a new field that results from the applications of microfluidics to neurobiological research. Future innovations are likely to depend on the strong interaction between all these areas. NTE: Neural Tissue Engineering; PNIs: Peripheral Neural Interfaces.

1.2. Project Aims

The aim of this project is to fabricate and optimize a microfluidic device that can be used as an *in vitro* model to analyze neural cell response to nanotopography. Thus, if cells reveal preferential growth over certain nanotopographical features, scaffolds with optimal surface topography can be fabricated. Moreover, if different neural cell types have specific growth preferences, scaffolds can be designed with the purpose of selective guidance and physical segregation of axons based on their type and function. The *in vivo* integration of these scaffolds with PNIs will then improve selectivity as well as enhance the control over the neuroprosthesis. For instance, motor axons can be nanotopographically guided to electrodes used to electrically stimulate them,

whilst sensory axons are guided to electrodes for signal recording (Figure 2). In this way, the main goals of this project are described below:

1. To fabricate a device suitable for assessing preferential axonal outgrowth of neural cells on certain nanotopographical features;

2. To optimize the design and fabrication techniques of the nanotopographic device, according to cell response.

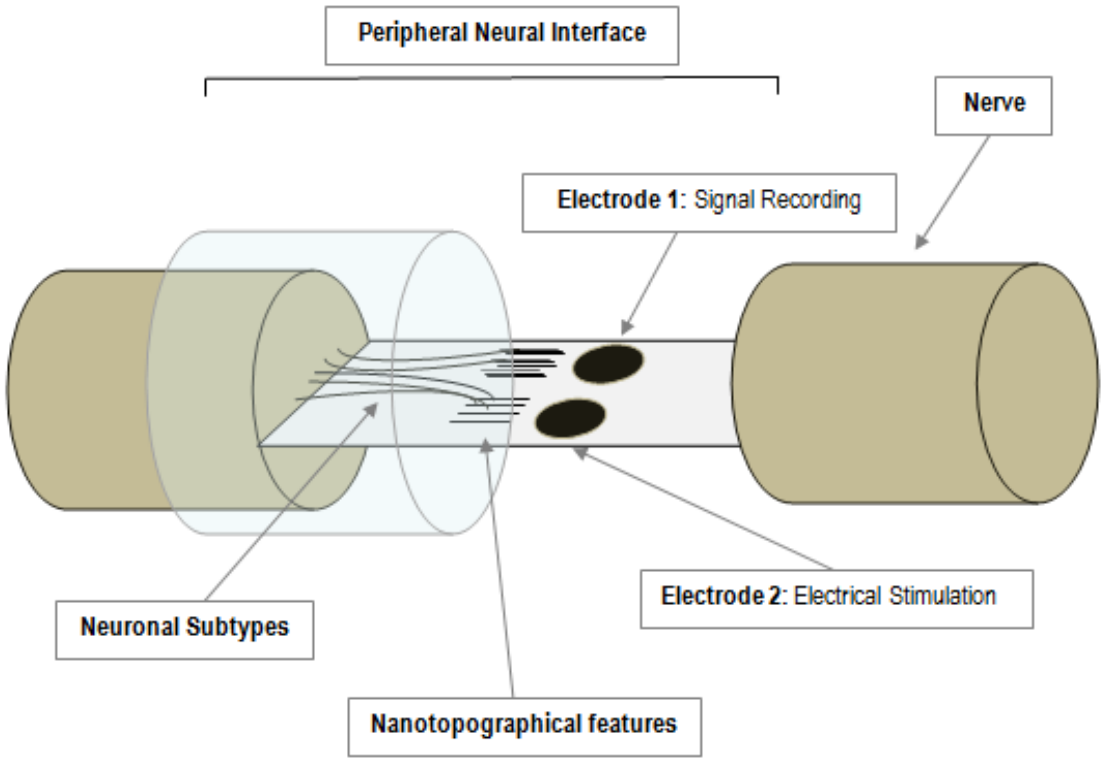

Figure 2 - Specific nanotopographical features on the surface of PNIs will promote guidance, growth and physical segregation of neuronal subtypes allowing a selective control: Electrode 1 promotes signal recording of sensory neurons and electrode 2 induces electrical stimulation of motor neurons. PNIs: Peripheral Neural Interfaces.

To achieve the described objectives, the strategy consisted of fabricating "Y-shaped" nanotopographic patterns on the surface used for neural cells culture and analysing the behaviour of the growing axons. As they encounter the bifurcation, monitoring which pattern they choose (Figure 3B) provides insight into topographical preference. The groove dimensions of the nanograting pattern are constant in all the "Y" structure. However, different ridges widths

were tested (Figure 3A). In addition, a microfluidic platform was used to provide isolation of PNS axons from cell bodies and dendrites in order to facilitate the analysis of the axonal response.

The F11 hybridoma, a dorsal root ganglion-derived cell line, was chosen as model to investigate the response of nociceptive sensory neurons to nanotopographical guidance cues. It was shown previously that F11 axons grow along nanopatterns of 500 nm ridge width [16], so the initial part of the "Y" presents a ridge of 500 nm, while different combinations of ridge widths between 500 nm and 2000 nm were used to test their choices (Figure 3C).

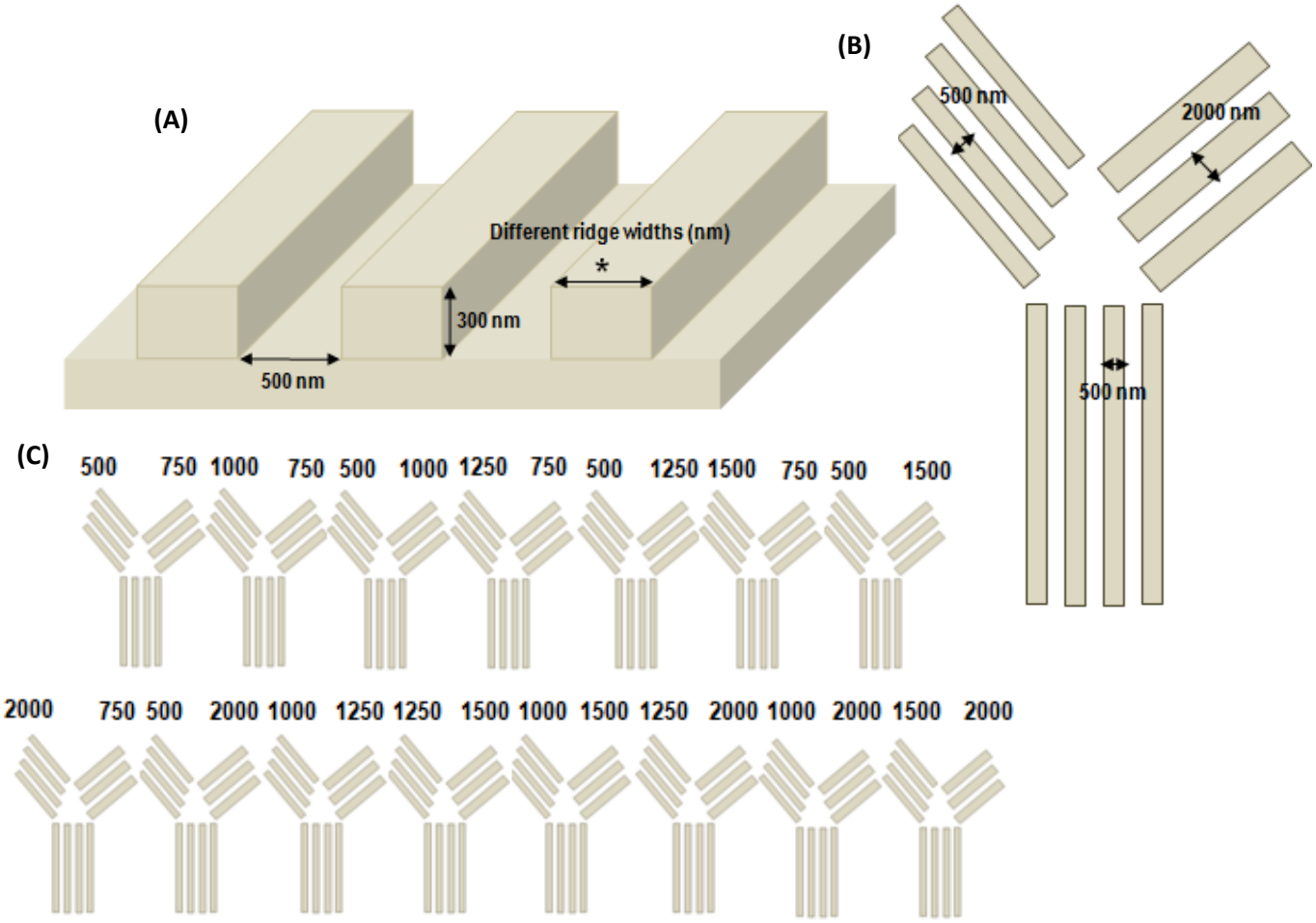

Figure 3 – Nanotopographical patterns were imprinted on the cell culture substrate: (A) Dimensions of the grooves are constant (width of 500 nm and depth of 300 nm) and different ridge widths were studied; (B) The right and left parts of the "Y"-bifurcation had different ridge width constant values between 500 nm and 2000 nm; (C) Different combinations of ridge width values for the bifurcation were used in consecutive imprinted "Ys" on the surface of cell culture.

CHAPTER 2 – *"STATE-OF-ART"*

2.1. Peripheral Nerve Injury and Regeneration

The human nervous system can be anatomically divided into the central nervous system (CNS) and the PNS [17]. The CNS is composed of the brain and the spinal cord, and the PNS contains the peripheral nerves [8]. The neuron is the basic structural and functional unit of the nervous system and each one consists of a cell body (soma) and its extensions (axons and dendrites) [17]. Dendrites transmit electrical signals to the cell body and axons conducts impulses away from the soma [18]. The cell bodies of the sensory neurons are located near the spinal cord in the dorsal root ganglia (DRG) or in cranial ganglia, while the cell bodies of the motor neurons are inside the CNS, spinal cord or brainstem [19]. Axons extend into the body toward their target organs,

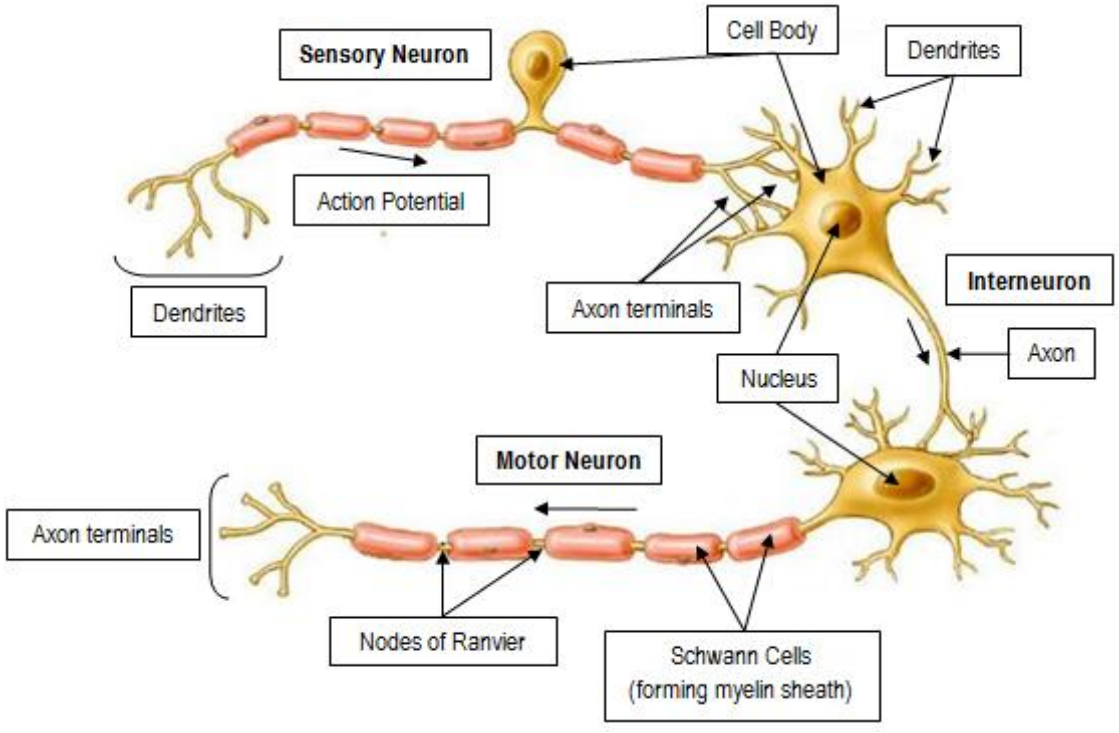

Figure 4 – Basic neuron types: Sensory neurons are unipolar - the axon branches to connect sensory receptors to the spinal cord or brain; motor neurons and interneurons are multipolar, having several dendrites and one axon. The nucleus and the cytoplasm constitute the cell body (soma) of the neuron; dendrites receive and process electrical stimuli from other neurons and axons transmit the action potentials to the axon terminals. SCs form myelin around the axon and line up along it with distinct gaps, called nodes of Ranvier (adapted from [21]). SCs: Schwann Cells.

bundling together en route to form peripheral nerves [20].

Sensory (or afferent) neurons transmit electrical signals from sensory receptors (e.g., in skin, eyes, etc) toward the CNS and motor (or efferent) neurons send electrical signals away from the CNS to muscles or glands (Figure 4) [21]. A single peripheral nerve is filled with several sensory and motor axons, myelinated by Schwann cells (SCs), supported by fibroblasts, and protected by the epineurium (Figure 5) [22].

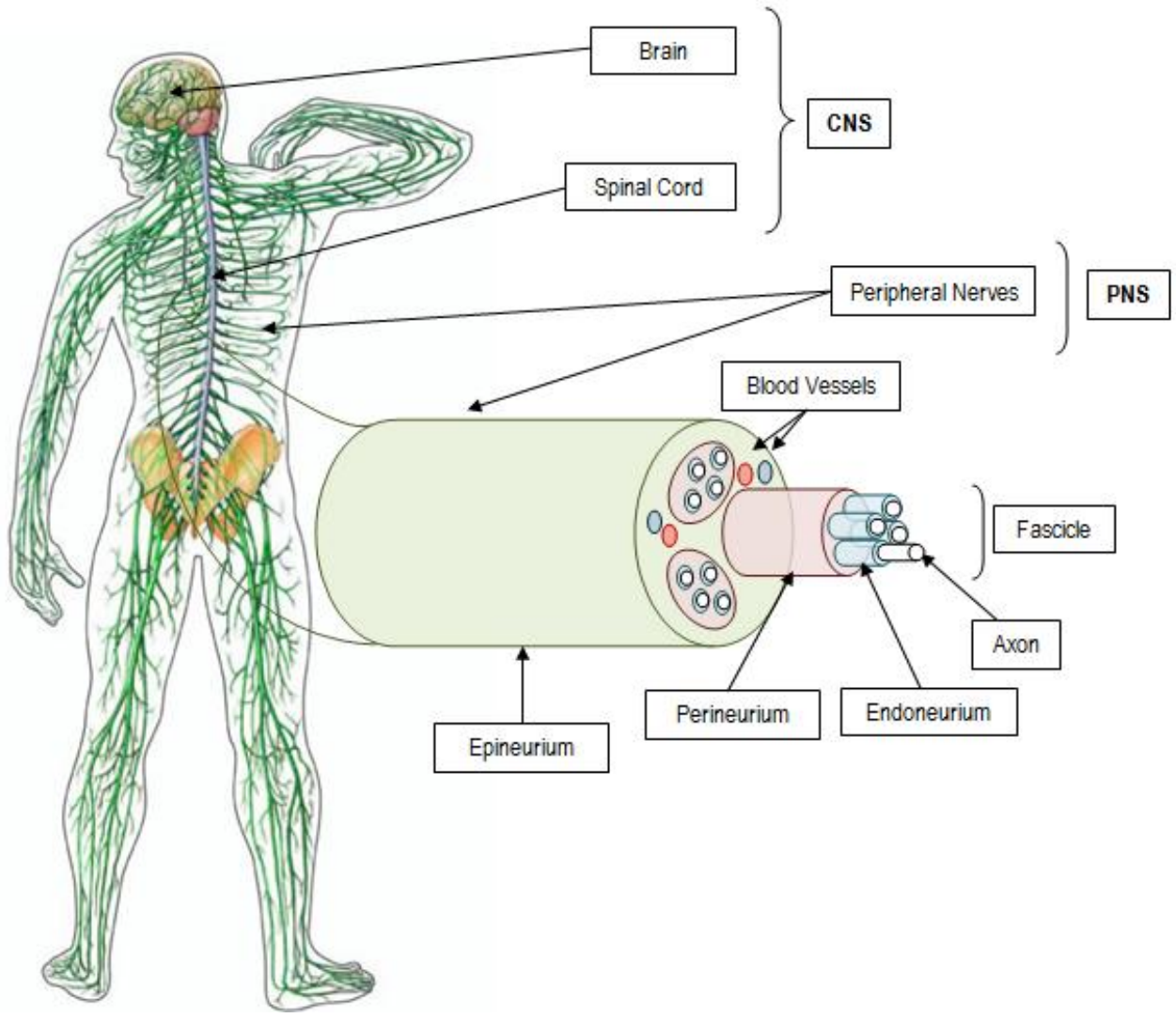

Figure 5 - Anatomy of human nervous system: CNS, composed of the brain and the spinal cord, and PNS constituted by the peripheral nerves. Individual axons and their SCs myelin sheaths are surrounded by connective tissue with collagen fibers, called endoneurium; the perineurium, a connective tissue formed from layers of flat cells and collagen, forms the fascicles. At last, the epineurium is composed of loose fibro-collagenous tissue and binds fascicles into a nerve trunk, vascularised by surrounding blood vessels (adapted from [2] and [22]). CNS: Central Nervous System; PNS: Peripheral Nervous System; SCs: Schwann Cells.

The response to axotomy, or a lesion in the axon, is different in the CNS and PNS [23], namely the nerve degeneration and regeneration mechanisms [8] [24]. The peripheral nerve injuries can result from ischemic (due to the restriction in blood supply), chemical, mechanical, or thermal factors, leading usually to the transection of the axons [23]. However, the capacity of nerve regeneration [8] as well as the intensity and duration of the neural response depends on the severity of the injury, distance between the lesion and the cell body, type of neuron, and age [2]. According to the type and extent of damage to the nerve and surrounding connective tissue, a neuron injury is classified in neuropraxia (nerve remains intact but signalling ability is damaged), axonotmesis (nerve remains intact but with interruptions in impulse conduction) and neurotmesis (injury in axon and surrounding connective tissue) [2].

The molecular mechanisms involved in axonal regeneration are complex and interactions between molecules are still not completely clear [25]. However, after axotomy, the cytoskeleton of the axonal portion that is disconnected from the cell body (distal end) suffers degradation due to calcium-dependent protease activity and separation from the metabolically active cell body, leading to membrane rupture, known as anterograde or Wallerian degeneration. A short distance of the proximal end may also degenerate (retrograde degeneration), but usually survives [8] [25].

Consequently, in the distal end, SCs, previously wrapped around the axon, release myelin lipids (demyelination), and begin to remove myelin and axonal debris (Figure 6A). Simultaneously, genes for myelin-specific proteins are downregulated in SCs. In particular, as myelin-associated glycoprotein (MAG) inhibits peripheral axon regeneration, SCs adopt a non-myelinating phenotype, producing myelin MAG-free to promote axonal growth [2]. Moreover, SCs also secrete cytokines that attract macrophages to complete myelin and axonal clearance [19]. Mast cells around injury site produce histamine and heparin, increasing vascular permeability to attract more macrophages and also contribute to the degradation of myelin debris [8] [18].

After debris clearance, specific growth factors for axon regrowth, or neurotrophic factors, such as neurotrophins (NTs), neuropoetic cytokines and

fibroblast growth factors (FGFs) are released. Nerve growth factor (NGF), neurotrophin-3 (NT-3), and brain-derived neurotrophic factor (BDNF) are NTs produced by SCs to promote axonal regeneration [19]. NGF and vascular endothelial growth factor (VEGF) are also released by mast cells. Tropomyosin-related kinase (Trk) and low affinity receptors (such as p75) in the axonal membrane are activated by NTs, triggering axonal outgrowth. Thus, regeneration begins at the proximal end, where several sprouts (growth cones) are emitted, usually from the nodes of Ranvier, and continues toward the distal end [8] [26].

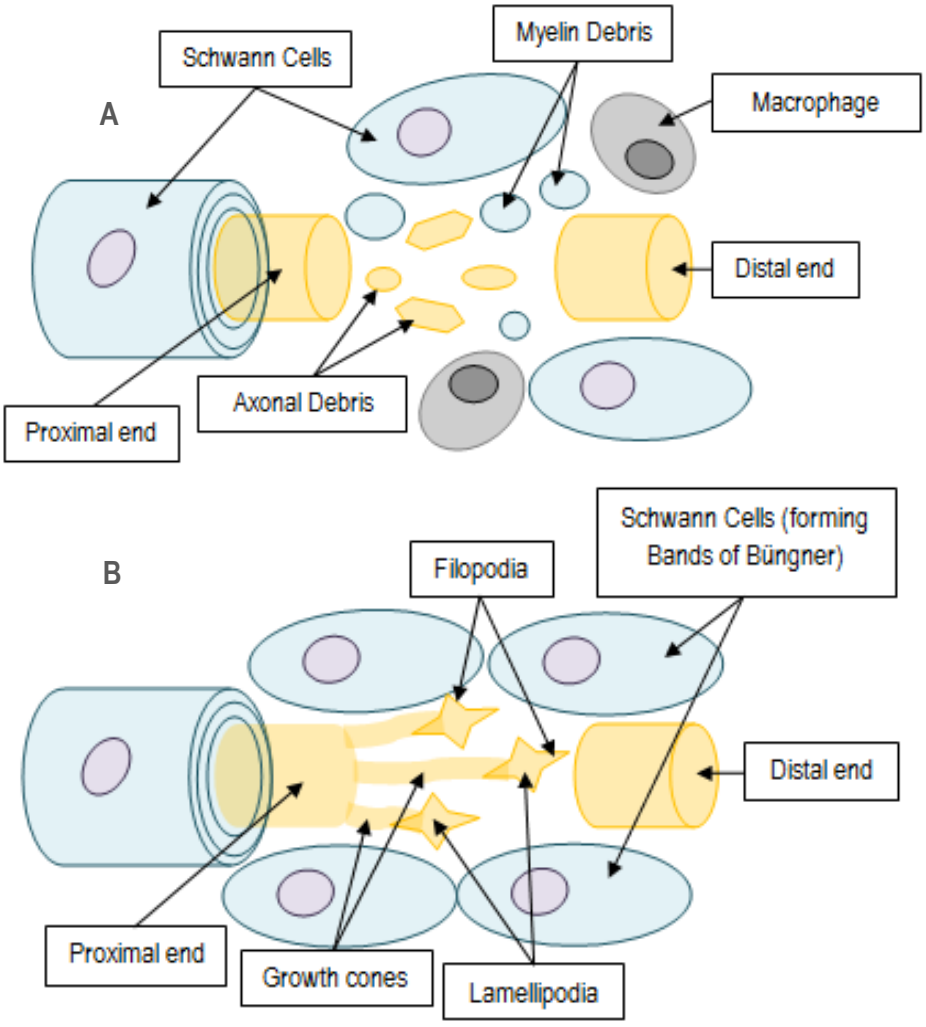

Figure 6 – SCs play an important role in axonal regeneration: (A) 1. Demyelinated damaged axon, 2. Begin clearance of axonal and myelin debris; 3. Produce myelin MAG-free; 4. Release cytokines to attract macrophages; (B) 5. Secrete neurotrophic factors to induce growth cones emergence and development; 6. Form Bands of Büngner with a specialized ECM essential for axon survival and migration (adapted from [25]). SCs: Schwann Cells; MAG: Myelin-associated Glycoprotein; ECM: Extracellular Matrix.

Filopodia and Lamellipodia are the mobile path-finder parts of the growth cone. When filopodia encounter the substrate, membrane receptors bind to extracellular matrix (ECM) molecules, re-organizing cytoskeleton and leading growth cone protrusion [25]. In addition, macrophages produce cytokines that induce SCs to proliferate and form columns of SCs within the remaining tubule of lamina basal. This forms the Bands of Büngner, creating a tubular channels that support [2] and guide regenerating axons to grow to the final targets (Figure 6B) [19] [27]. In the absence of a guide, disperse axonal sprouts and connective tissue form a neuroma (an abnormal growth of nerve tissue) [2].

There are natural mechanisms to compensate for an unsuccessful reinnervation of target organs by regenerating axons, namely the axonal collateral sprouting and the adaptability of the CNS [2].

Collateral sprouting of undamaged axons has different characteristics from regenerative axonal sprouting in response to the absence of other axonal innervations in the same target tissues and results from local secretion of local neurotrophic factors by the denervated cells (Figure 7). Also here, SCs play an important role guiding axonal sprouts to denervated areas. Terminal sprouts emerge from the axon terminals (terminal sprouting) and the nodal sprouts (collateral sprouting) come up from the nodes of Ranvier [2].

However, neither target reinnervation by typical axonal regeneration nor by collateral sprouting promote the full restoration of sensory and motor functions [19]. The diameter, conduction velocity and excitability of regenerated axons remain lower than normal axons for a long time and consequently recovery of reinnervated organs is incomplete [2].

Furthermore, some factors contribute to poor functional recovery after nerve injury: damage of cell body; inability of axonal growth, due to nerve lesion or diseases; and poor specificity of reinnervation by regenerating axons [2].

For that reason, NTE has been developing new strategies for axonal regeneration after injury and several studies *in vivo* show successful recovery of neuronal functions [18].

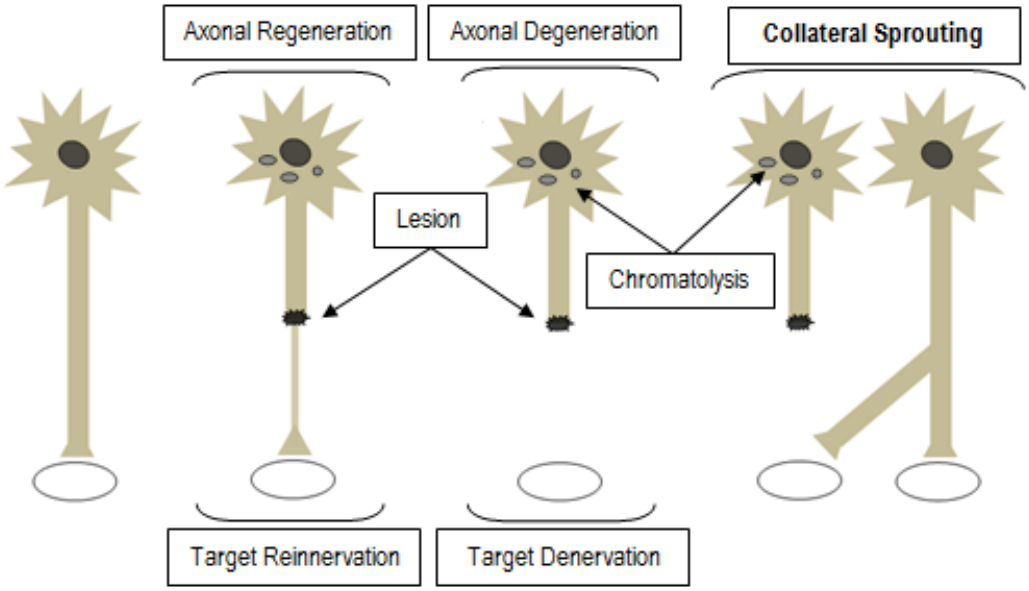

Figure 7 - Axotomized neurons suffer changes in their bodies (chromatolysis), but axonal regeneration usually occurs and target is reinnervated. In case of target denervation, collateral sprouts are induced to grow towards the free target (adapted from [2]).

2.2. Tissue Engineering Strategies for Peripheral Nerve Repair

The complexity of the physiology of the nervous system constitutes a challenge in finding effective treatments for nerve repair. The complete transection of the nerve is the most severe injury [8], but according to the size of the lesion, there are different treatment options for peripheral nerve repair [23] [28].

For small size lesions (few millimetres in length), surgical reconnection of the injured nerve ends (coaptation [8]) is the current clinical treatment [23] [29]. For large size lesions, autologous nerve graft (autograft) from another site in the body or another individual (allograft) is used to fill in the lesion gap and constitutes the gold standard therapy [19].

However, the use of grafts includes risks of morbidity and loss of function at donor site [8], and requires multiple surgeries [23]. Moreover, donor nerves are often few and small [19] and structural and functional restoration of the

injured nerves is incomplete. So, to solve these problems, alternative tissue engineering strategies are being developed for PNS repair [18].

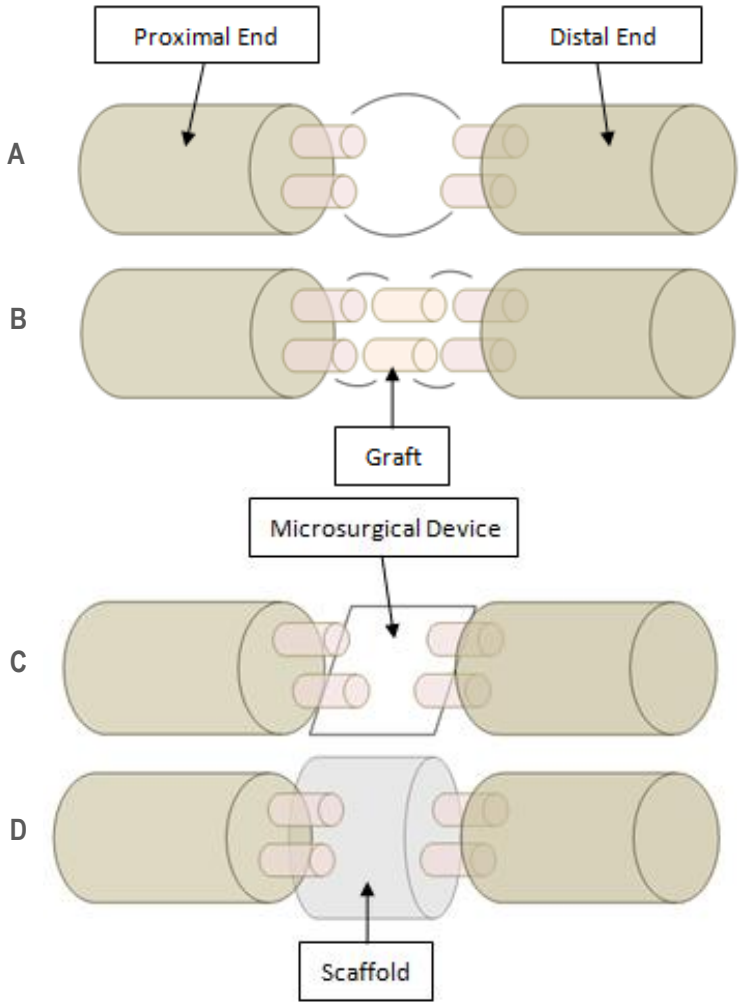

Figure 8 – Nerve repair strategies: (A) Coaptation of proximal and distal ends of damaged axons; (B) Autograft or allograft connects proximal and distal ends; (C) Microsurgical devices promotes axonal cutting (by using a nanoknife or a microbeam laser, and an electrical field for splicing of the ends) and stimulation, by using arrays of electrodes; (D) Scaffolds, fabricated with natural or synthetic polymers, recreate ECM native properties. Besides these strategies, *ex vivo* genetic modification of grafted cells may be a feasible approach for additional axonal growth support (adapted from [29]). ECM: Extracellular Matrix.

NTE is composed of three main parts: the cells (neurons and supporting glial cells - the SCs in PNS), the scaffolds (to support cell growth, differentiation and guidance [19]), and the proteins (such as neurotrophic factors and ECM)

[8]. However, due to electrically excitable nature of neurons, NTE strategies can be separated in four categories: Axonal guidance devices (using tubular scaffolds), cell population recovery (usually by stem cell transplantation or SCs graft [19]), drug delivery (of neurotrophic factors, anti-inflammatory and neuroprotective agents [30]), and electrical stimulation.

Although the combination of these approaches seems to be a feasible solution to nerve repair [23], the typical NTE approach consists in reconnecting damaged axonal ends and consequently achieving target reinnervation. This is done by implanting *in vivo* the artificial scaffolds and substrates that will guide regenerating axons (in a similar way to the Bands of Büngner) (Figure 8) [19].

For small injury gaps, nerve guides (NGs) that are basically tubular artificial scaffolds are placed across the lesion gap in order to guide axonal growth [19], bind the two portions of the damaged axon and create an isolated, well-controlled regeneration environment (Figure 9) [23].

For large gaps, hollow tubes, or nerve guidance channels (NGC), are used [19] because porosity plays an important role in the nerve regeneration process, allowing the migration of cells as well as medium or blood vessel influx into the scaffold [23].

Current strategies for large nerve defects have proved to be alternatives to the autologous nerve grafts, promoting and accelerating functional recovery. However, this recovery is still not complete. For that reason, recent research *in vitro* is focused on developing improved scaffolds that better mimic ECM [8].

Indeed, topographic cues provided by ECM have already proved to influence cell behaviour [8]. In addition, nanotechnology allowed the development of nanotopographic substrates that can be used to induce axonal outgrowth and guidance during neuronal culturing [8] [31]. Thus, the incorporation of nanotopographic surfaces into scaffolds has the potential to physically guide regeneration of nerve across lesions [18].

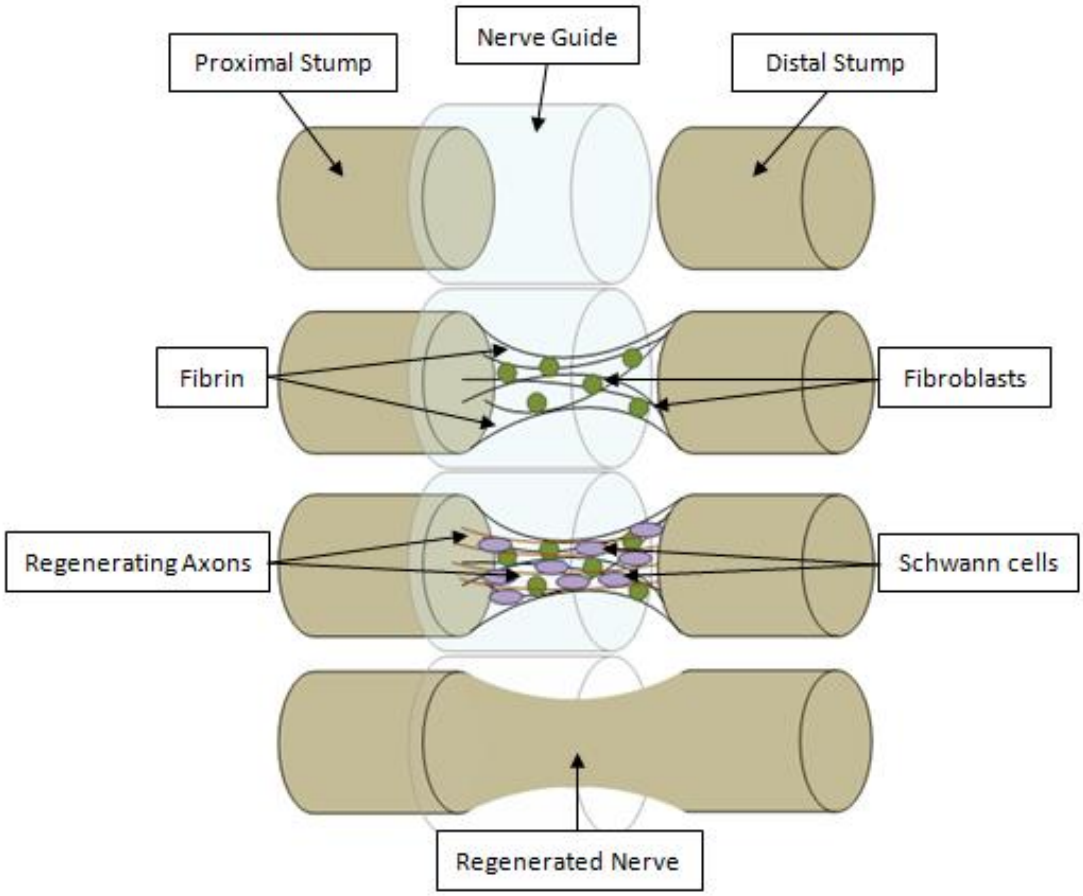

Figure 9 - Axonal regeneration in a NG tube: Fluid phase: fluid and cytokines (including neurotrophic factors) enters into the NG; Matrix Phase: a fibrin matrix is formed and supports the fibroblasts, SCs and axons – Cellular phase; Axonal phase: SCs myelinate axons that are guided by Bands of Bündger towards their targets; the regenerated nerve is usually thinner in the middle of the bridge (adapted from [19]). NG: Nerve Guide; SCs: Schwann Cells.

2.3. Nanotechnologies and Neural Cell Response to Nanotopography

Cells *in vivo* experience a complex environment with nanotopographies provided by the ECM. Thus, a promising route is to recapitulate nanotopographical cues *in vitro* in order to steer and control protein and cellular interactions [8] [32]. With the advancement of micro- and nanofabrication technology, several techniques have been used in fabricating groove-like patterns on a variety of substrates [8] [33].

Although applications of nanotechnology in neuroscience are only in the early stages of development, partially because of the complexities associated with interacting with neural cells, several researchers have shown *in vitro* that surface topography plays an important role in axonal outgrowth guidance as well as SCs activity enhancement. In particular, nanoscale patterned substrates constitute topographical cues and promote better nerve regeneration [34].

2.3.1. Nanofabrication Techniques

As described in a review by Gates et al. [35], new nanofabrication techniques have been developed in the last few decades [35] [36]. Although lithography, namely photolithography (mainly using UV light) and particle beam lithography (usually electron beam lithography, EBL), are the dominant conventional techniques for nanofabrication (Figure 10), several different approaches, such as molding, embossing and printing have been developed for patterning nanoscale structures. Molding and embossing techniques can be divided into two categories depending on the mold type, hard or soft (elastomeric). Molding requires curing a precursor against a topographically patterned substrate, while embossing (or imprinting) transfers a mold with a structured topography into an initially flat polymer film (Figure 11). For example, nanoimprint lithography (NIL) or “hot embossing” results from a pressure-induced transference of a topographic pattern from a rigid mold, usually silicon (Si), into a thermoplastic polymer film heated above its glass-transition temperature (T_g) [35].

Printing techniques (such as microcontact printing, µCP) are also useful in nanofabrication, by transferring a material onto a substrate from a topographically patterned stamp. Moreover, scanning probe lithography (SPL) is a versatile method that allows deposition of clusters of atoms and molecules onto a surface in a well-defined pattern. Edge lithography is another promising approach that uses topographical changes in the edge of patterns, by

selectively removing or depositing material at the edges to create a larger feature in the vertical direction [35].

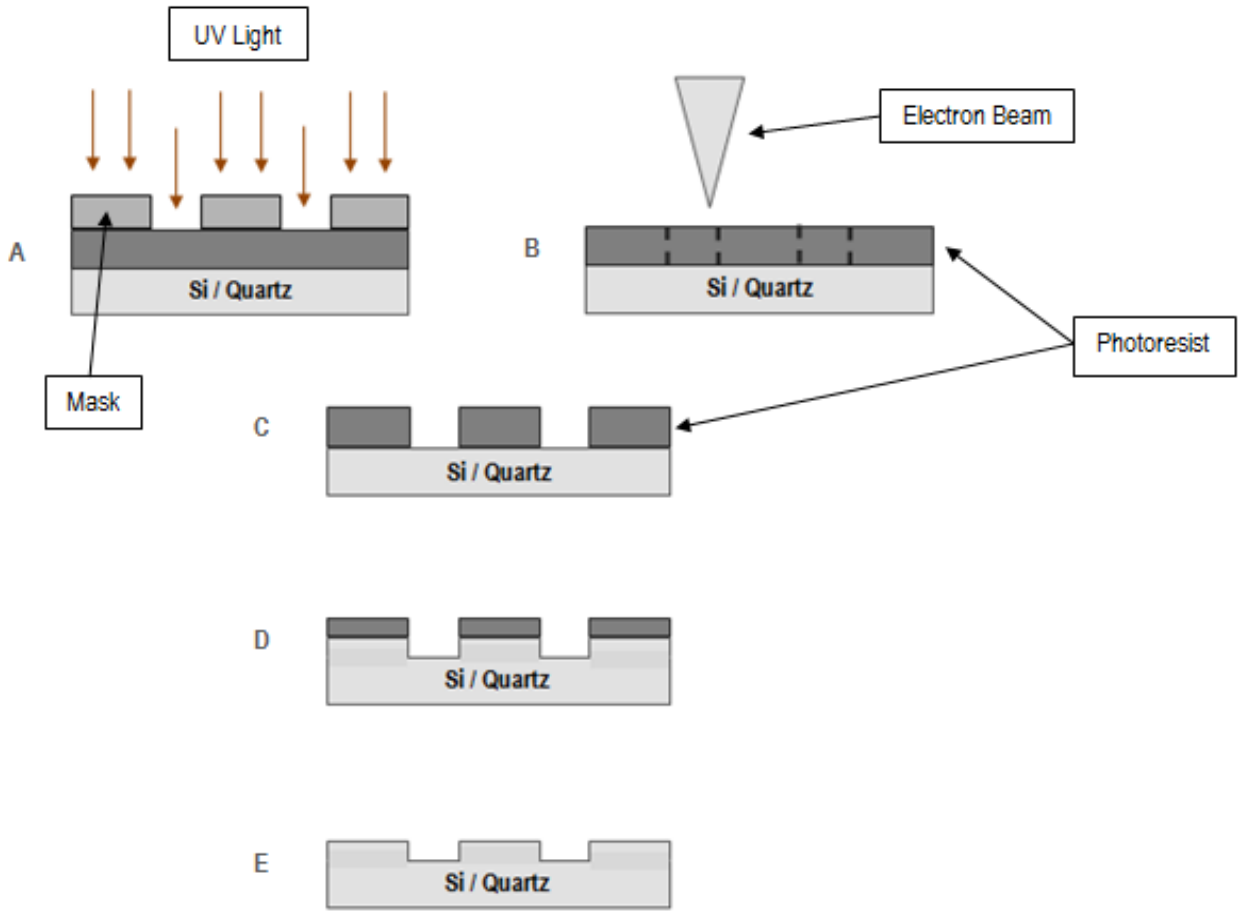

Figure 10 - Conventional lithography (A-E): Photolithography uses UV light and a mask to selectively develop the photoresist (A) while EBL creates nanopatterns directly on the photoresist (B) (adapted from [35]. UV: Ultraviolet; EBL: Electron beam Lithography.

All these techniques use “top-down” approaches to patterning structures (that consist on the incorporation of smaller-scale details into micro/macroscopic materials [37]). Self-assembly is a “bottom-up” nanofabrication strategy and consists on the aggregation of components using covalent and/or non-covalent bonds. These components can aggregate spontaneously (non-templated self-assembly) or interacting with external forces or spatial constraints (template self-assembly) [31] [35]. In addition, different nanoscale topographies can be produced by using chemical techniques, such as chemical etching, polymer demixing, and phase separation as well as electrospinning (application of a high voltage to a flowing viscous polymer

solution) [11] [38]. Several types and combinations of materials have also been tried, such as glass, metal oxides, natural and synthetic polymers [8] [35] [36].

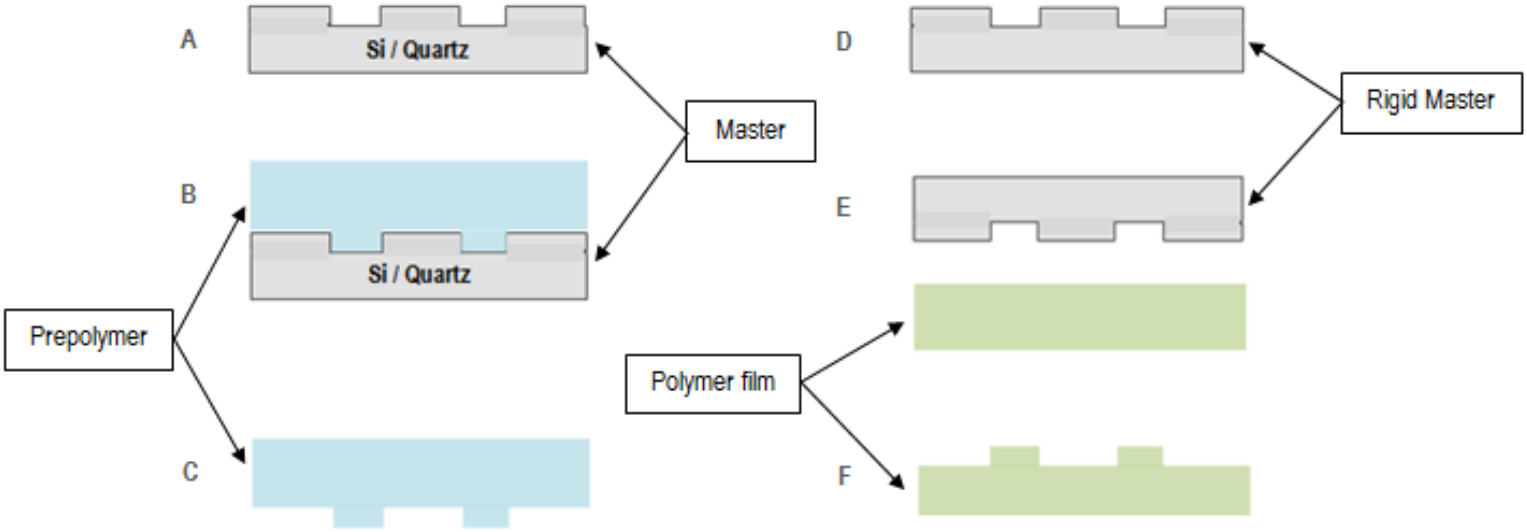

Figure 11 - Molding technique (A-C): Usually a PDMS prepolymer is cured against a patterned master to create nanotopographies on the surface of the PDMS substrate; NIL (D-F): A rigid master transfers topographic nanopatterns on the thermoplastic polymer film by heating the polymer above T_g and applying pressure on the surface (adapted from [35]). PDMS: Polydimethylsiloxane; NIL: Nanoimprint lithography.

2.3.2. Contact Guidance on Nanopatterns

In general, nanotopography can induce two main neural cell responses: cell patterning or contact guidance [39]. Cell patterning consists in the control of the cell position on a surface. For this purpose, there are two main types of approaches: topographical patterning, by using substrates with patterns of shape or texture, and physicochemical patterning, by applying patterns of chemical adhesion or patterns of electrical or physical force on cultured cells [23]; or the combination of both strategies (Figure 12) [40].

Cell patterning has been especially important in neural networks mimicking for CNS repair purposes, by regulating mainly collective cell functions, such as cell adhesion, proliferation and differentiation. Contact guidance, on the other hand, is being crucial in PNS regeneration.

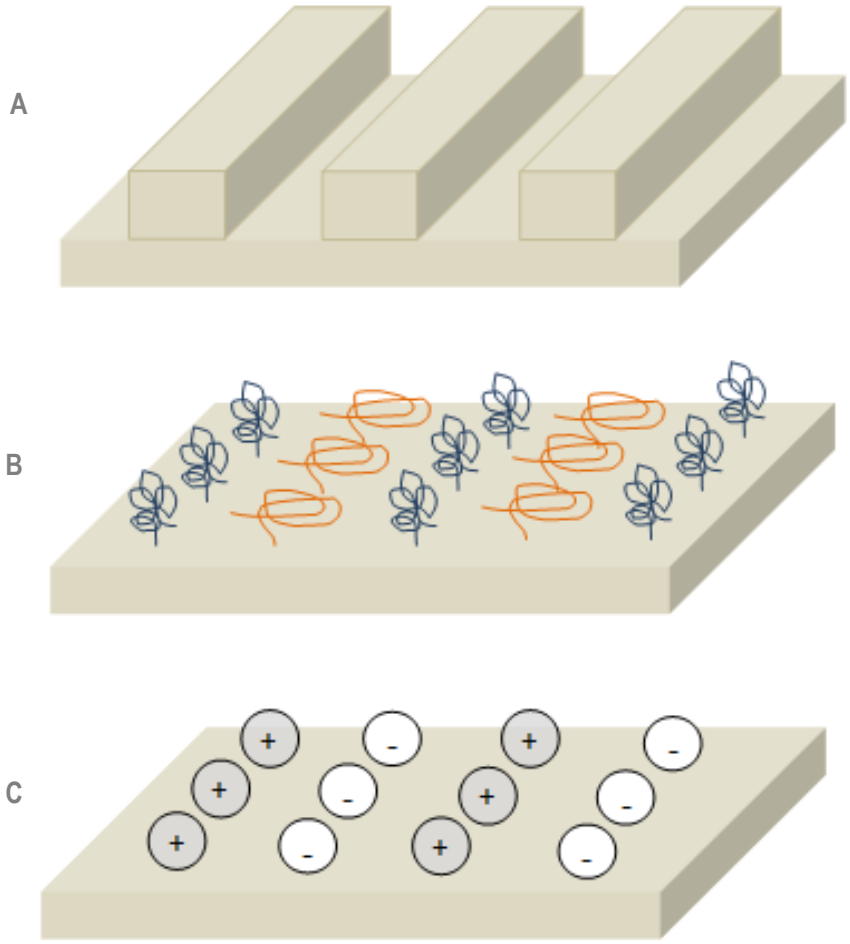

Figure 12 – Cell patterning approaches: (A) Topographical features are grooves with different dimensions, for example; (B) Chemical features results of specific spatial distributions of different biomolecules; and (C) electrical features consists on the application of electrical potential or charge on the surface, for instance (adapted from [40].

The mechanism of contact guidance was described by Weiss in 1934 and refers to the phenomenon that neurites grow on nanopatterns, adjust their orientation and align along those patterns [33]. Axons and dendrites are called *in vitro* collectively neurites and axonal neurite outgrowth can be guided by the geometry and orientation of the surface topographical cues [41] [42].

Indeed, Bettinger et al. [36] showed that contact guidance is an important component in efficient growth cone formation, motility and guidance. However, the molecular mechanisms of cell sensing to nanopatterns, the factors, and the cellular effects are not completely understood [33] [39] [42].

2.3.3. Cell-surface Interactions at the Nanoscale

Cells are sensitive to nanostructures and it is possible to control and manipulate their behaviour *in vitro* and *in vivo* by fabricating surfaces with nanotopographical features [8]. Although it had been proposed that topography may induce changes in protein absorption from the cell culture media, observations proved that cell sensing of topographic is practically independent of the differences in protein adsorption behavior. Cell sensing and response to topography occurs due to a cell-adaptation mechanism, independent of absorbed proteins. Although the molecular mechanisms involved are not completely clear, during adaptation the topographic pattern determines the regulation of specific cell functions [39].

Several studies show that cell adhesion to the surface results from specific binding interactions between transmembrane receptors (integrins) and their ligands absorbed onto the surface. The integrin is a heterodimer of α and β units. Different combinations of these units result in different types of integrins which bind selectively to specific ligands. This binding process induces a change of integrins conformation: cytoplasmatic proteins such as talin bind to the cytoplasmatic tails of integrins inducing other integrins to bind, originating a cluster of integrins; this clustering causes the recruitment of several different types of proteins, such as focal adhesion enzymes (e.g. kinase and Src kinase), adaptor molecules (paxillin, that binds to other proteins), and α-actinin (that binds to the actin cytoskeleton). This assembly of proteins forms the focal adhesion (FA) complex (Figure 13) [43]. This dynamic multimolecular assembly allows mechanical force to transfer between the inside of the cell and the surface of the substrate, where cellular tensile forces are balanced with compressive forces in the substrate [8].

FAs are consequently responsible for cell shape but also are signalling complexes, which initiate cascades of signals that control gene expression. Thus, during cell interaction with the surface, the degree of cell adhesion determines fundamental cell functions, such as survival, proliferation, migration, differentiation and apoptosis [8] [41]. In this way, by using surfaces with

nanofeatures it can be possible to control the FA assembly and consequently cell fate and functions [8].

In particular, *in vivo* and *in vitro* experiments indicate that topographical cues regulate contact guidance. Initially, neurites emerge from the cell body, grow and find their way toward specific targets (neurite path finding). However, both neurite initiation and extension depend on the formation and stabilization of FAs [44]. One primary neurite becomes an axon and begins its fast growth, while the remaining neurites develop into dendrites [45] [46]. Then, neurites probe surrounding environment with membrane projections, the filopodia, allowing a feedback detection mechanism for specific cues [41] [45]. Thus, the filopodia constitutes a mechanosensory system that detects physical or chemical cues on the surface [41]. These cues are converted into biochemical response (mechanotransduction), regulating gene expression [41] [47].

Although the molecular basis of mechanotransduction is complex, it has been reported that cells respond differently to topographic substrates depending on cell type, feature size, distribution and geometry or physical properties of the substrate material [8] [11] [36] [41].

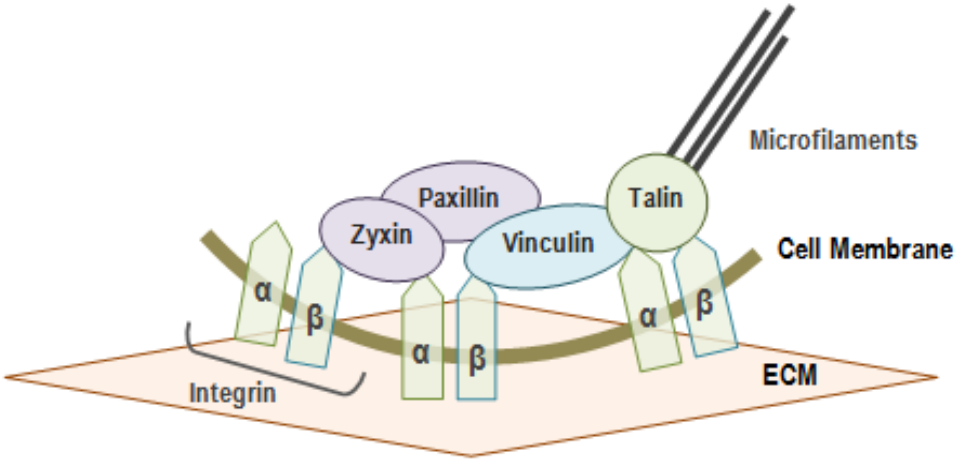

Figure 13 – FA complex: Integrins bind to proteins of the ECM and intracellular proteins link integrins to cell cytoskeleton. This phenomenon also occurs when cells interact with topographical cues (similar to the native ECM) on the surface. F-actin filaments (microfilaments) and microtubules (MTs) are the dynamic cytoskeletal polymers. Together with FAs, they are responsible for promoting shape change and locomotion and consequently axon outgrowth and guidance (adapted from [8]). FA: Focal adhesion; ECM: Extracellular Matrix.

2.3.4. Neural Cell Response to Nanotopographical Features

Based on the pattern, topography can be classified in isotropic or anisotropic [11] [39] [48]. In general, anisotropic topographies, such as grooves and ridges, have been used to study cell alignment (or orientation), while studies with isotropic topographies, such as evenly or randomly distributed pits or protusions, have been focused on collective cell behaviors [39]. Moreover, Bettinger et al. [36] defined three basic nanotopographic geometries used on *in vitro* research, namely nanogratings, nanopost arrays, and nanopit arrays (Figure 14). However, other regular and irregular nanoscale features have been used [39], such as spheres, particles, fibers, and others [41].

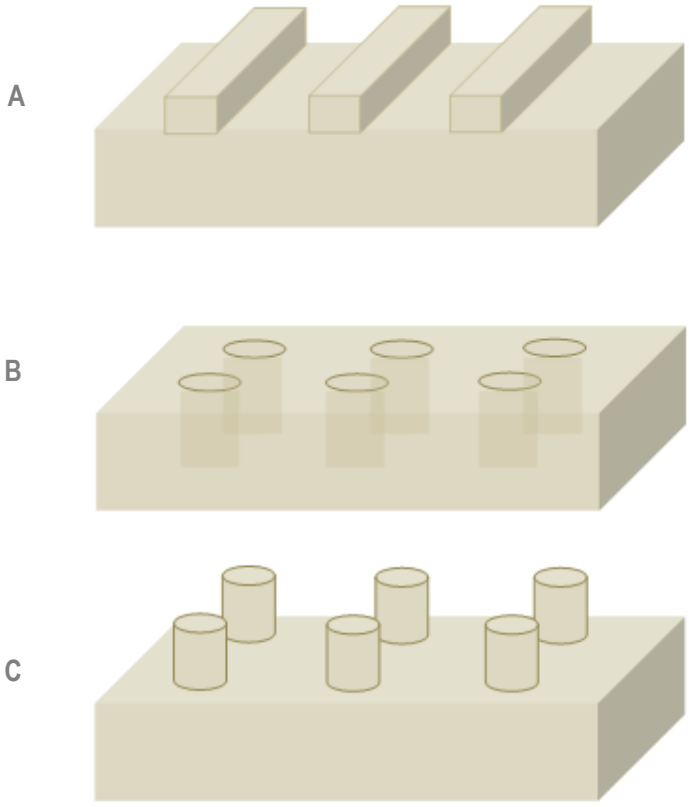

Figure 14 - Basic nanotopographic geometries: (A) Nanogratings, (B) Nanopit arrays; (C) Nanopost arrays (adapted from [36]).

Although the comparison of various isotropic topographies may currently be difficult because of diversities in topographic size, shape, uniformity, or even chemistry [39], many studies have demonstrated neurite outgrowth, alignment or guidance on these surfaces (Table 1) [16] [38] [44] [49-63]. Even though several cell types have been used as models in neural repair approaches, such as neuronal cell lines, primary cells, stem cell or cancer cells (like neuroblastomas) [33], only cell types usually studied for PNS repair purposes were considered in this literature review.

In general, researchers showed that cells cultured on nanogratings presented lower proliferation rates than cells cultured on flat substrates. However, nanogratings have shown to enhance the cell adhesion into several geometrical combinations, while nanoposts and nanopits generally reduce initial cell attachment. For instance, neurites extending from PC 12 cell line cultured on nanogratings have shown enhanced alignment and extension, while reduction of spreading was observed on nanoposts and nanopits [36]..

Moreover, FA formation occurs predominantly on the ridge structures and the width of the FAs is determined by the width of the ridge [64]. Consequently, aligned axonal outgrowth was preferentially observed on ridge edges and elevations rather than in grooves. In these cases, both cell shape and cytoskeleton displayed directional organization [33] [39].

Thus, nanograting substrates can be used to study contact guidance and migration *in vitro*. Nanopost or nanopit substrates can be used to study the filopodia dynamics, FA formation, and other cytoskeleton functions in a controlled manner [36].

Although many of the studies are still qualitative and sometimes produce conflicting results with similar nanotopography [65], results suggest that the topographical structures and chemical properties of the scaffold must be optimized for each cell type [33]. However, more work needs to be done in order to understand if there is a preferential outgrowth of individual neurites over certain nanotopographical features.

Cell Type	Method	Feature type	Cell Response	Reference
PC 12	Chemical Etching	Nanoporous surface	Neurite outgrowth	Moxon et al. [49]
	NIL	Nanograting	Neurite outgrowth and guidance	Ferrari et al. [44], [50]; Cecchini et al. [51]
	Electrospinning	Nanofiber		Koh et al. [52]
	Self-Assembly	Nanopost		Naka et al. [53]
(Rat) DRG	Electrospining	Nanofiber	Neurite outgrowth, alignment or guidance	Xie et al. [38]; Kim et al. [54]; Corey et al. [55]
	Imprinting (μCP)	Nanograting	Neurite outgrowth	Kofron et al. [56]
	Phase inversion		Neurite outgrowth and alignment	Long et al. [57]
	Embossing			Miller et al. [58]
	Molding			Goldner et al. [59]
(Chicken) DRG	Electrospinning	Nanofiber	Neurite outgrowth	Wang et al. [60]
	Self-assembly	Nanopost	Neurite outgrowth and alignment	Dubey et al. [61] Naka et al. [53]
(Mouse) DRG	EBL	Nanopost	Neurite outgrowth and guidance	Krsko et al. [62]
(Rat) Schwann Cell	Electrospinning	Nanofiber	Proliferation and alignment	Gupta et al. [63], Kim et al. [54], Wang et al. [60]
F11	NIL	Nanograting	Neurite outgrowth and alignment	Wieringa et al. [16]

Table 1 – Generalized neural cell response to nanotopographical features. PC12: Pheochromocytoma cell line of the rat adrenal medulla; DRG: Dorsal root ganglion; F11: Hybridoma of mouse neuroblastoma cell line N18TG-2 with embryonic DRG neurons; NIL: Nanoimprint lithography; μCP: Microcontact printing; EBL: Electron beam lithography.

2.3.5. Selective Neurite Outgrowth and Guidance

A review of the literature shows that additional work has to be done on single-cell analysis of neurite outgrowth and guidance over different nanogratings. Table 1 indicates that several researchers have achieved contact guidance of many cell types on different types of nanofeatures. Some of them have even tried to compare cell response to different feature dimensions or types, but none tested the preferential response of individual neurites [66].

Fozdar et al. [67] have already developed competition assays in order to assess the ability of topography to attract axonal formation based on feature size and shape. A grid with arrays of nanopits and nanogratings was constructed and single hippocampal neurons (CNS) were micropositioned in gaps between neighbouring topographies. Results suggest that axons prefer nanoscale (300 nm) over microscale (2000 nm) and holes over lines for a given feature size.

Based on these results, the use of a bifurcating approach in order to create a nanofeature choice system seemed to be an alternative and a feasible approach. Thus, neurons could be placed near to the “Y-shaped” nanogratings and axons would grow over their preferential ridge dimensions.

However, the bifurcation approach was not new. Curley and Moore [68] had already constructed a dual hydrogel “Y” model in order to promote neurite outgrowth in a 3D environment.

In particular, Wieringa et al. [69] in 2010 had shown that the microchannels bifurcating approach was able to promote separation of growing neurites. However, this separation was not based on topography of the surface, but based on physical-space constraints.

Wieringa et al. [16] in 2012 introduced the F11 neural cell line as an *in vitro* model for PNS regeneration purposes and cultured F11 cells on various nanograting substrates. These results indicated that the F11 cells are sensitive to nanotopographical features. Based on that, F11 cell line seemed to be a

feasible *in vitro* peripheral sensory neuron model for nanotopographical guidance.

Ferrari et al. [50] had already tested neurite outgrowth of PC12 cells over six different nanogratings transferred on COC films using NIL (ridge width of 500 nm, depths of 350 nm, and groove widths of 500 nm, 750 nm, 1000 nm, 1250 nm, 1500 nm, and 2000 nm). For that reason, and according to the results showing preferential axonal growth over the ridges, the implementation of ridges with widths of 500 nm, 750 nm, 1000 nm, 1250 nm, 1500 nm, and 2000 nm in the “Y-shape” model seemed to be a feasible approach (Figure 15A).

Thus, several combinations of different ridge width values could be tested by using consecutive “Ys” on the surface of the cell culture substrate. Preferential growth and selection of F11 axons over certain feature sizes could be then evaluated. For instance, axons could choose between 500 nm and 2000 nm of ridge width (Figure 15B).

Furthermore, it was already shown that axons are able to cross ridges or grooves [39]. Goldner et al. [59] showed that DRG neurites can successfully bridge micropatterned grooves (200 µm plateau width). In addition, Fozdar et al. [67] also concluded that neurons positioned in close proximity to topography (<30 µm) recognized and responded to the topography, regardless of feature dimensions. Thus, the maximal gap of 5 µm between the right and left parts of the bifurcation is suitable for axons to choose the right or left patterns without influencing their decisions.

Based on the nanotopographical preferences of each neural cell type, nanofabrication techniques might be applied to provide topographical guiding structures in order to manipulate the axonal outgrowth.

As sufficient electrical recording or stimulation is achieved only when a neuron is located directly on the top of the electrode, these topographical guiding structures might be incorporated into an implantable electrode to improve selectivity and signal transmission across PNIs [40] [70].

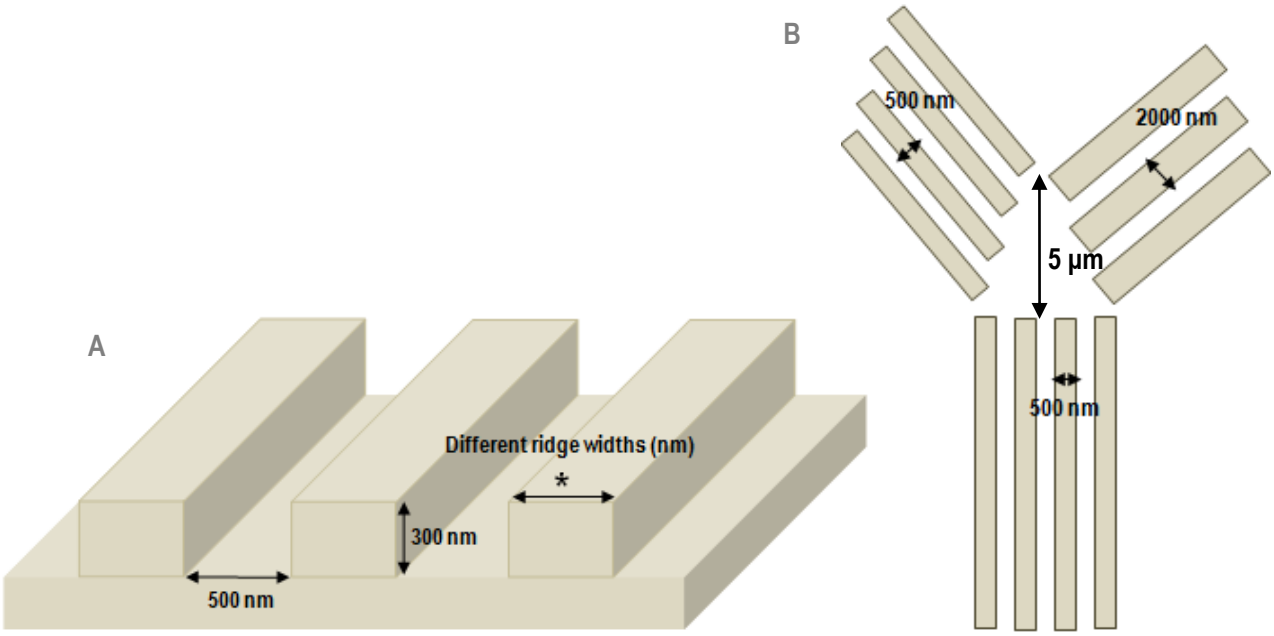

Figure 15 – "Y-shaped" bifurcation approach: (A) Dimensions of the grooves are constant (width of 500 nm and depth of 300 nm), different ridge widths are applied; (B) The right and left parts of the bifurcation of each "Y" have different ridge width constant values between 500 nm and 2000 nm; different combinations of ridge width values are used in consecutive "Ys" on the surface of the cell culture substrate. The maximal gap between the right and left parts of the bifurcation is 5 µm and growing axons need to cross it in order to choose their preferential nanopatterns.

2.4. Neuroengineering Solutions for Selectivity on Peripheral Neural Interfaces

For amputee rehabilitation purposes, the three main approaches of neuroengineering are: restoration (control and repair function of remaining injured structures), replacement (substitute impaired structures with artificial ones, controlled by another natural and functional neural or muscular structures) and neuromodulation (train CNS in order to induce plasticity through artificial substitutes) [71].

Neuroprostheses link the PNS with electronic or robotic devices and have been widely used not only for replacement purposes, but also to restore the sensory and motor functions in disable patients.

According to the Helmholtz's reciprocity theorem, electrodes detect the bioelectrical activity from active neurons (recording) as well as inject electrical current in order to induce activity in neurons (stimulation). Thus, functional electrical stimulation (FES) systems that are basically arrays of electrodes have been implemented on neuroprosthetic devices to interact with neurons and stimulate them to regenerate [20]. FES systems constitute then a bidirectional interface, allowing nerve stimulation and neural signal recording, and also work as feasible PNIs [2], by connecting peripheral nerves to prosthetic devices [72].

PNIs are usually implanted around, between or within a peripheral nerve or spinal root in order to reduce tissue resistance and to increase stimulus intensity or ensure consistent recordings [9] [73]. However, future-generation neuroprostheses are being designed with a greater focus on reducing the tissue encapsulation as well as improve selectivity.

Selectivity is the ability of a PNI to access specific axons with similar properties. Although some nerves contain only one type of axons (sensory, for example), many peripheral nerves are mixed. This mixture complicates the control of the prosthesis because signals originated from motor and sensory axons must be separated. For that reason, the main challenges consist on reducing the size of bioelectrical interfaces to minimize damage to neural tissue (i.e. reduce invasiveness) and maximize selectivity [74] [75].

PNIs can be divided into three categories according to the level of selectivity and invasiveness [2]: the extrafascicular approach, the intrafascicular approach, and the nerve transection approach. In the first two categories, the nerve is not disrupted, while the third category involves nerve transection and transference, and depends on the regenerative capacity of the nerve. Cuff electrodes and flat interface nerve electrode (FINE) are examples of extrafascicular electrodes that do not penetrate but wrap around the nerve bundle. In contrast, the longitudinal intrafascicular electrode (LIFE), the transverse intrafascicular multichannel electrode (TIME), the Utah electrode array (UEA), and the Utah slanted electrode array (USEA) penetrate the nerve fascicle but not the axons. The intraneural multielectrode array (MEA) and regenerative (or sieve) electrodes are inserted on the third category [72]. Farina

et al. [2] reviews advances and progress in PNIs over the past decades, highlighting designs, materials and techniques used.

The closer a stimulation or recording electrode is to an axon, the more selective or specific the signal evoked or recorded [75]. Thus, the invasiveness increases with the selectivity of stimulation (Figure 16). For that reason, interfaces with PNS constitutes a trade-off between functional restoration and reduced invasiveness [73] [20]. Selectivity (influence smaller populations of fibers) and reaching (influence as large a population of fibers as necessary) need to be balanced [2].

Cuff electrodes are less evasive and, consequently, the most highly used PNI in research with animal models or human trials. However, selectivity during recording and stimulation is still limited [2].

Regenerative or sieve electrodes are implanted between the severed stumps of a peripheral nerve, surrounding several axons and forming “holes”, where regenerating axons will eventually grow through. Thus, action potentials recording and individual or small groups of axons stimulation are possible [2].

Navarro et al. [20] shows that the regenerative electrodes are a promising approach, because of improved recording and stimulation selectivity and overall mechanical stability. Although promising results, regenerative electrodes have the disadvantage of the necessity of transacted peripheral nerves, time for regenerating axons growth through the interface [73], and the presence of the distal portion to attract the axon growth and migration [23].

Moreover, electrodes fabricated with conventional techniques physically impede neural regeneration and their performance degrades during chronic implantation, due to the appearance of bundling neurites that further reduce selectivity [2]. Thus, topographical cues could be presented in the vicinity of electrodes in order to guide axons towards implanted regenerative electrodes, facilitating regeneration mechanisms and improving selectivity [75] [69].

Thanks to the micro- and nanofabrication techniques, a lot of work is being done to understand the effect of microscale and nanoscale topology and morphology on cell response to electrode surfaces [2].

However, until now, few studies have successfully incorporated and implemented neuroprosthetic devices *in vivo* that completely overcome the effect of tissue reaction. Also here, nanotopography might be useful to determine and control immune cells response and consequently tissue reaction to PNIs [9], but more research is needed and the new field of microfluidics promises to be helpful [76].

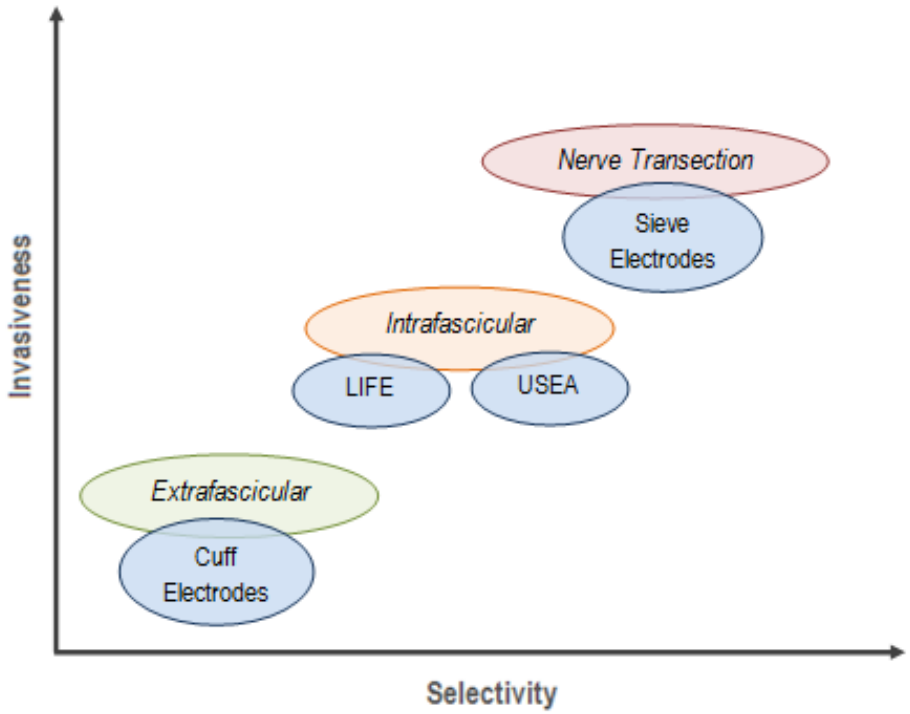

Figure 16 - Three types of peripheral neural electrode-based interfaces: the invasiveness of electrode implantation increases with the selectivity of neural stimulation and recording (adapted from [20]).

2.5. Microfluidics on Neuroscience Research in vitro

Microfluidic systems are designed to control or manipulate small amounts of fluids in channels with dimensions of tens to hundreds of micrometers [70]. Although this field is still at an early stage of development, microfluidics have been contributing to the development of advanced cell culture models for *in vitro* studies [70] [77, 78]. Indeed, several microfluidic cell culture devices are being

used for neuroscience and neurobiological research, because it was shown to provide single-cell and single-molecule analysis [70] [77-79].

2.5.1. Design of microfluidic devices

The main advantages of microfluidic systems for cell study are the ability to recreate cellular microenvironments, precisely control fluid flows, and to reduce time and cost of experiments [80].

However, design considerations must be addressed before planning a microfluidic device for specific cell study applications [70] [78]. For instance, an adequate chamber height must be selected that allows for the optimal flow rate to provide nutrients and remove wastes, without changing cell morphology or even detaching them. Also materials constraints and fabrication methods must be considered and biocompatibility of devices must be tested with the cells of the intended use [78]. Li et al. [81] summarizes the main requirements for materials used in the fabrication of microfluidic devices, according to the applications.

Silicon and glass were used in some of the earliest works in research of microfluidics systems. However, as neither of them had all the properties required for working with living mammalian cells and both are hard to handle, rigid materials have largely been displaced by plastics or elastomers, namely poly(dimethylsiloxane) (PDMS) [70].

PDMS is a silicone rubber material and is the most used polymer for device fabrication due to some physical and mechanical properties, such as biocompatibility, low cost, optical transparency, ease of fabrication and gas permeability. PDMS inhibits cellular adhesion onto its surface, but it can be treated to influence cell attachment and morphology, by changing its hydrophobicity [82]. PDMS can also absorb small hydrophobic molecules or drugs and release oligomers into solution showing disadvantages for some cell studies. Moreover, PDMS is very hydrophobic and even after surface treatment showed hydrophobic recovery [77]. For that reason, thermoplastics such as

cyclic oleofin copolymers (COC), polycarbonate (PC) and polystyrene (PS) are becoming preferable to PDMS for cell culture models in microfluidic systems [77, 78]. For instance, Tsao and DeVoe [83] discussed in their review the advantages of thermoplastics over silicon, glass and elastomeric materials. PC and PS are usually used to produce culture flasks and well plates. Although these polymers are naturally hydrophobic, surface hydrophilicity can be made by oxidizing the surface. In fact, surfaces of these conventional flasks and plates have been oxidized, usually referred as “tissue-culture-treated” (TCT), to make surfaces suitable for adherent cell culture.

However, due to its elasticity and ability to conform to surfaces, PDMS is still useful for compartmentalization in microfluidics. Thus, specific parts of a cell can be biochemically analyzed or manipulated [78].

2.5.2. Compartmentalized microfluidic culture platforms for axonal isolation

Ross Harrison demonstrated in 1910 [45] that neurons can be cultured outside the body. From Harrison’s first culture in the hanging drop (i.e. culture cells in suspended liquid drops) to the present, developments in culture methodologies have emerged and advanced neuroscience research *in vitro*. Culture flasks were firstly developed to culture and analyze neurons, but in the last few decades, patterned substrates and microfluidic devices have been applied on neuronal culturing [45]. As reviewed by Gross et al. [82], many platforms have been designed around the unique anatomy of neural cells. As neural cell bodies and axons have distinct properties and functions, novel designs allowed the isolation and analysis of individual neural cells and single neurites.

Although pipettes remain the standard method for electrical isolation of different compartments (i.e., patch clamping), microfluidic systems have contributed with feasible compartmentalization methods [78]. The Campenot method used a three-compartment Teflon chamber to isolate axons from the

cell bodies of peripheral neurons (Figure 17A). This principle of compartmentalization has been further developed for neuroscience research with many types of neurons [15] [82] [84]. The dual-chamber microfluidic device [76] is the most widely used for neuronal analysis [45] and several modifications have been made on this design over the last years (Figure 17B) [85-88].

Compartmentalized culture systems provide physical separation as well as fluidic isolation for chemical and genetic manipulation of neurons [15]. For instance, axon-specific gene expression and regeneration after physical axotomy were studied [78] [89, 90]. Compartmentalized microfluidic platforms also offer advantages over standard *in vitro* techniques by avoiding problems, such as diffusion constraints and cell population variability. Cost savings are another benefit of microfluidic experiments since the volumes of expensive media and growth factors are less than used in conventional culture flasks [82].

As new microfluidic devices are developed, the control of specific regions of individual dendrites and axons is being possible [45] [88]. Physical modifications of the channels promoted mechanical forces such as gravitational and hydrodynamic forces to act and control transportation, immobilization, isolation, and manipulation of biological molecules and cells [46] [80].

Physically modified microfluidic channels are usually created by bonding two layers with alignment: a micro/nanotopographically patterned substrate and a layer with the impression of microchannels. Several fabrication methods can be used depending on the materials and geometries chose for physical structures and channels [80]. Physically modified microfluidic channels used for cell research were reviewed by Kim et al. [80]. For instance, a microfluidic device having four branch channels with a pattern substrate in the end of each channel used cell adhesion as a physical marker in order to separate different types of cells [80]. Although physically modified microfluidic systems have advantages in cell studies, several problems such as poor selectivity, time consumption for optimizing fluidic control, and fabrication reliability need to be addressed to further advance the microfluidics field [80]. Moreover, the ability to direct the sites of neural attachment and the orientation of axonal outgrowth by using micro- and nanofabrication techniques, combined with isolated

compartments within the culture area, offers significant advantages over standard open culture methods and other conventional manipulation methods [70] [82].

For that reason, the nanotopographic device developed here is the first one combining a nanopatterned substrate for contact guidance with a microfluidic dual-chamber for axonal isolation (Figure 17D).

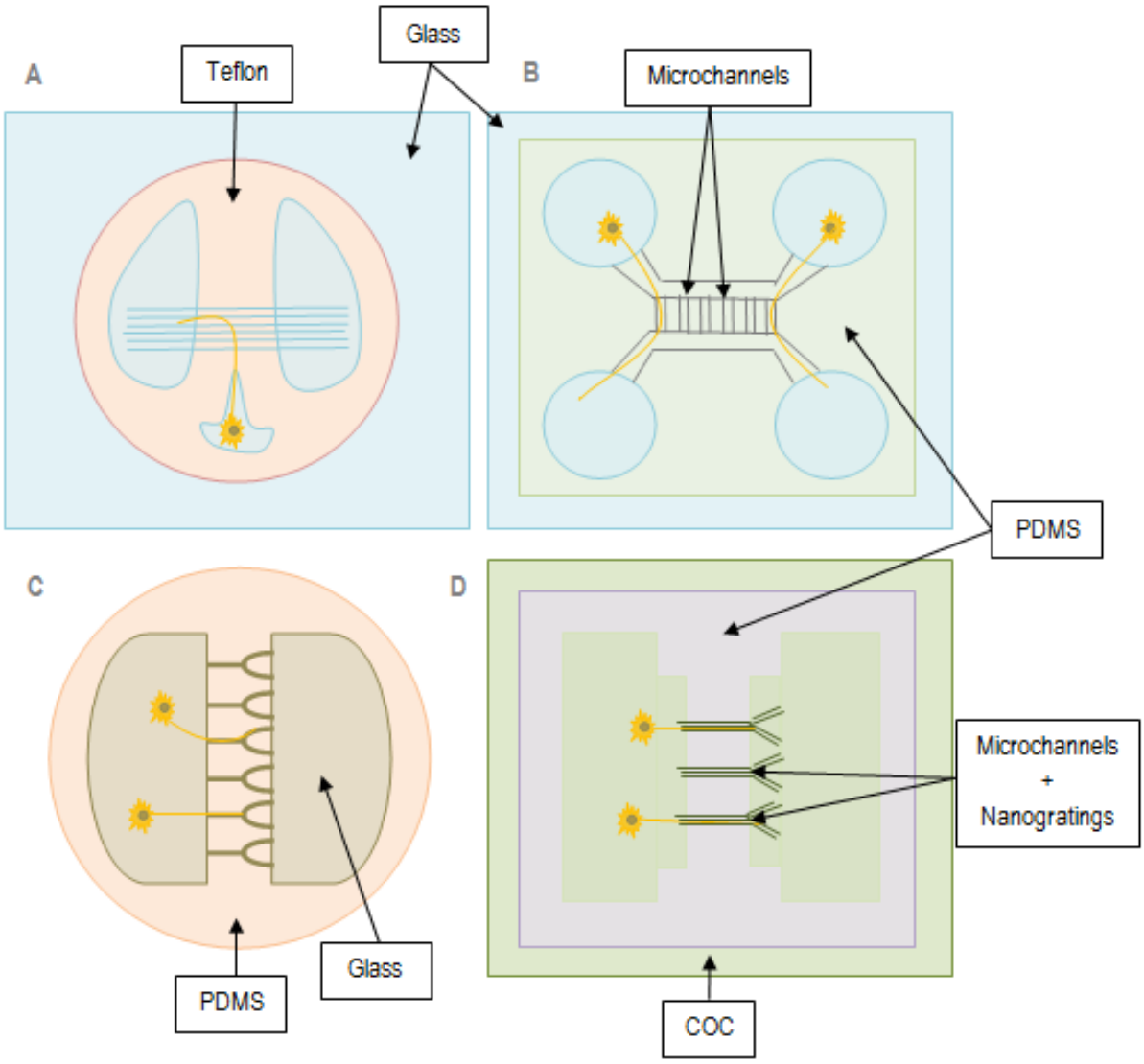

Figure 17 – Main designs used in neuroscience research for axonal isolation purposes: (A) Campenot Chamber, a Teflon platform isolates cell bodies from axons, which grow through scratches in the glass towards other chambers; (B) Dual-chamber microfluidic device, neurons are placed in the soma chambers and axons grow through microchannels towards axonal chambers; (C) Bifurcating microchannels device, neurons are seeded in the origin chamber and axons grow across the bifurcating microchannels in order to achieve the target chamber; (C) Nanotopographic Device, axons are isolated from cell bodies by growing through the physically modified microchannels and chose their preferential nanogratings dimensions. PDMS: Polymethylsiloxane; COC: Cyclic Olefin Copolymer.

CHAPTER 3 – *MATERIALS AND METHODS*

3.1. Device Design

The nanotopographic device was designed to be fabricated by bonding a layer of COC (Zeonor®, T_g=140ºC, 188 µm thickness) containing the Y-shaped nanogratings impressed by NIL with a layer of PDMS (*Dow Corning*® 184 Silicone Elastomer) with microchannels impressed by molding. This device has already been designed by Dr. Paul Wieringa. For that reason, the silica master used on PDMS molding had already been created by him (using the EBL nanofabrication technique, photoresist: SU8). Another silica mold had also been constructed by EBL and it was used as rigid master to transfer nanogratings into COC film.

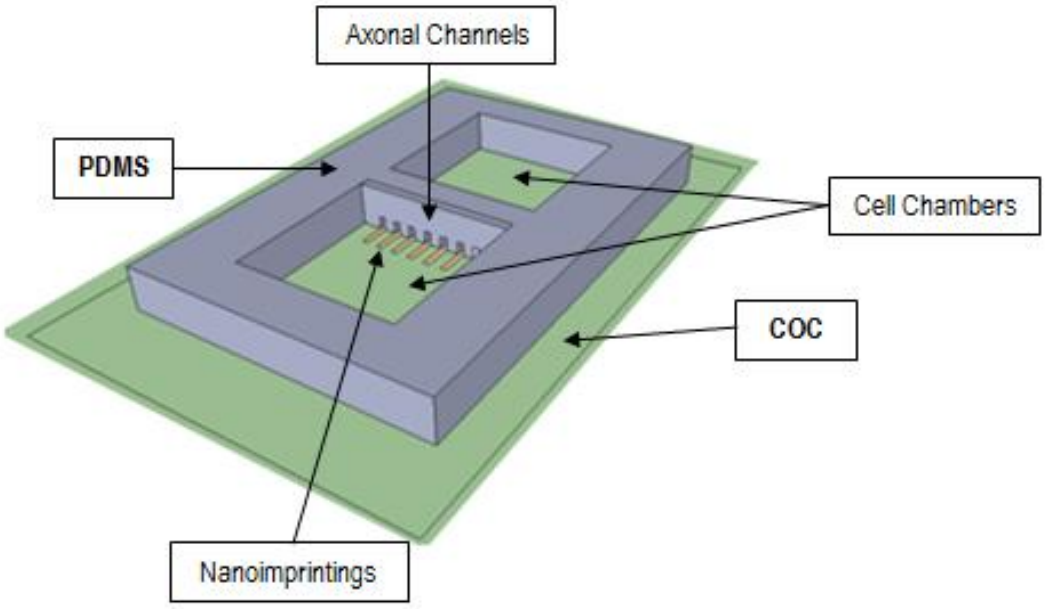

Figure 18 – A SketchUp® model of the nanotopographic device: nanogratings imprinted on COC; PDMS platform separates axons from cell bodies, originates axonal channels aligned with surface nanoimprintings, specifically for axonal growth, and creates cell chambers for cell seeding and culture. COC: Cyclic Olefin Copolymer; PDMS: Polydimethylsiloxane.

The combination of these layers allows creating physically modified channels to promote axonal guidance as well as to isolate axons from cell bodies. Moreover, the PDMS platform was also used to create chambers for cell

seeding (Figure 18). The central “bridge” of the device consists of several consecutive axonal channels. Each one contains a different combination of nanogratings aligned with PDMS platforms (Figure 19A). Combinations were also repeated on the surface several times (Figure 19B).

F11 cells were chosen as model for cell response analysis. Air plasma and (3-Aminopropyl)trimethoxysilane (APTES, Sigma-Aldrich®) treatment were used to bond COC and PDMS, and construct the complete device.

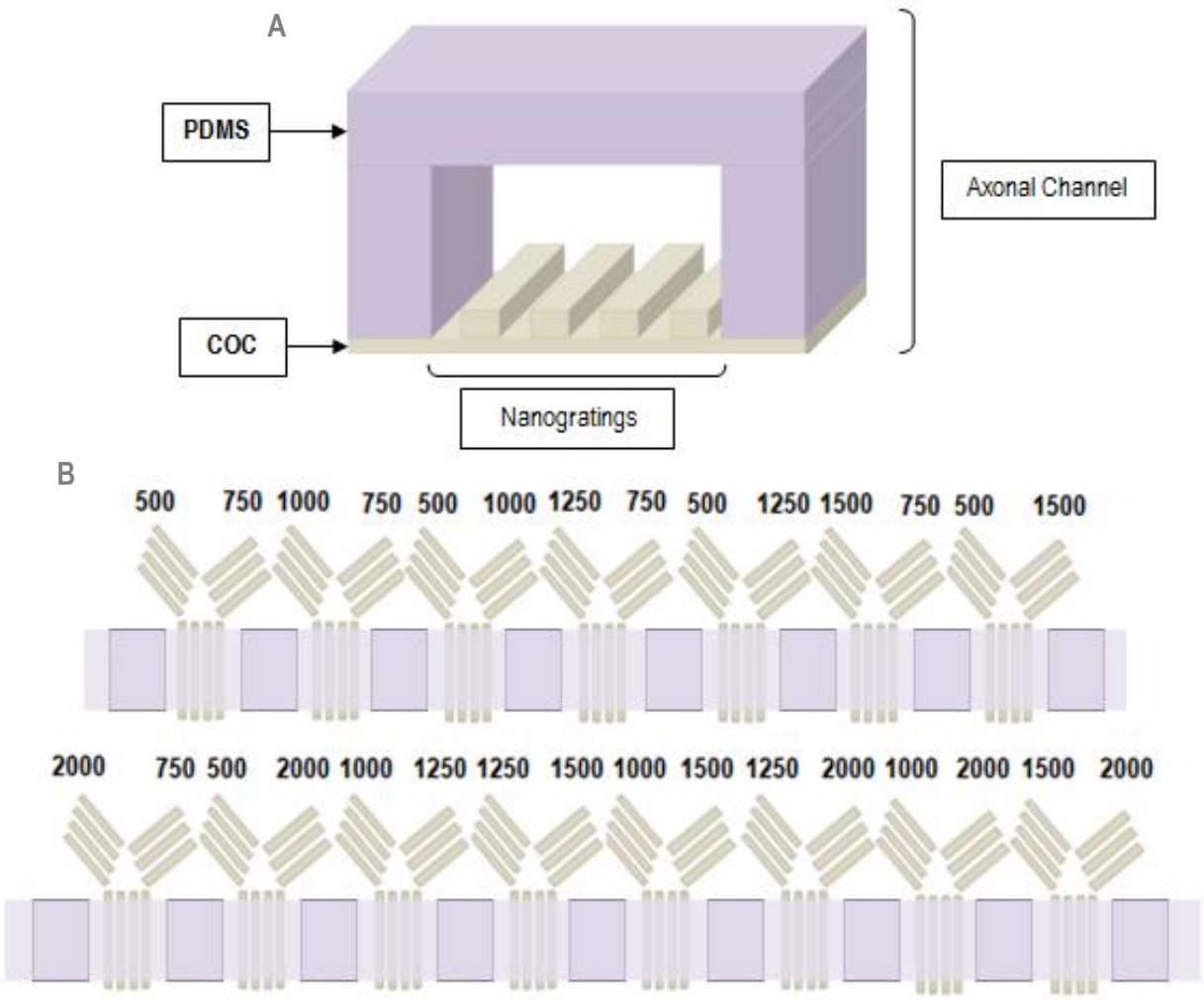

Figure 19 – (A) Each axonal channel consists of “Y-shaped” nanogratings covered by a platform of PDMS; (B) the “bridge” of the device is composed by several consecutive “Ys” with different combinations of ridge width values (500, 750, 1000, 1250, 1500 and 2000 nm). COC: Cyclic Olefin Copolymer; PDMS: Polydimethylsiloxane.

3.2. Device Optimization

During the fabrication process of the nanotopographic device, many parameters were optimized. Ultraviolet (UV) and air plasma treatments were tested for purposes of comparison with bonding efficiencies. Contact angle measurements were performed to quantify hydrophillicity of COC and PDMS after both UV and plasma treatments. Pressure applied during NIL process was also quantified by using a Flexiforce® sensor. Scanning Electron Microscopy (SEM) was used to analyze the optimal conditions for NIL in COC and PDMS molding processes.

3.2.1. UV Surface Treatment

COC and PDMS surfaces were UV-treated by using an Electronic Ultraviolet Crosslinker (Ultra LüM®, wave length 254 nm). Different exposure times (30 and 60 min) were tested for constant values of energy (120 mJ).

3.2.2. Plasma Surface Treatment

A plasma Cleaner/sterilizer (Harrick ® model PDC-002) was used to treat COC and PDMS surfaces. Before treatment, COC sample was cleaned with 70% ETOH and dried with nitrogen (N_2) flow. PDMS sample was cleaned with Scotch® tape. For both surfaces, treatment was performed at a stable pressure value of 0.2 mBar (Pressure display machine, Edwards® AGD Active Gauge Display) and at the highest oxidization intensity (“HI”, power 30 watts). Different exposure times were tested for both COC and PDMS (6 s, 10 s, 15 s, 30 s, 60 s, and 120 s).

3.2.3. Contact Angle Measurements

Contact angles of distilled water on COC and PDMS surfaces were measured for different exposure times of UV and air plasma treatments using an optical goniometer (Contactangle Kruss®) by sessile drop method (Figure 20). The SCA20 OCA Control software® was used to release water droplets of 2 µL (standard parameters) from the syringe onto sample surface, after which images of droplet formation were captured by a high-resolution camera and used to calculate the contact angle. For each sample, 5 locations were tested and contact angles were averaged. Moreover, all measurements were performed 5-10 min after the treatment.

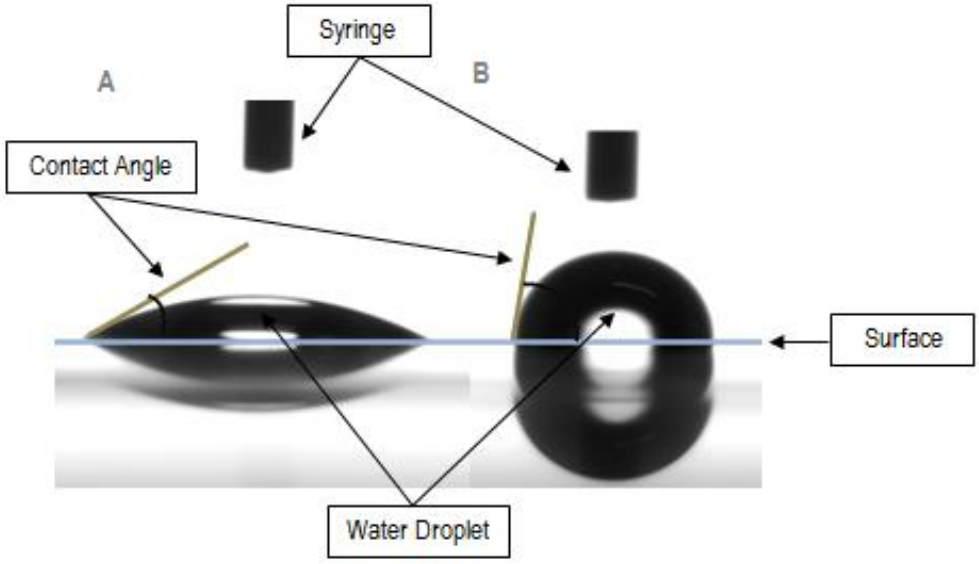

Figure 20 - Contact angle pictures of COC surfaces: (A) Treated-COC shows a hydrophilic surface (low contact angle value); (B) Untreated-COC presents a hydrophobic surface. COC: Cyclic Olefin Copolymer.

3.2.4. Imprinting Pressure Measurements

Paper clips were used to apply pressure and induce the transference of the nanogratings from the silica mold into the COC film. This approach was

based on the work of Goral et al. [91]. Pressure was quantified by using a force sensor (FlexiForce®, model A201 FlexiForce Standard). The *FlexiForce* sensor works as a force sensing resistor in an electrical circuit. Without load, resistance is very high, but as a force is applied to the sensor the resistance decreases [92]. Thus, force was applied to the sensing area of the sensor and resistance was read with a multimeter connected to the two outer pins (Figure 21). The sensor was calibrated by applying objects with different known mass values (0.3-5 kilograms) on the top of the sensing area.

Pressure is defined as the amount of force acting perpendicularly per unit of area:

$$P = \frac{F}{A} \qquad (1)$$

where *P* is the pressure (unit: Pa, Pascal), *F* is the force applied (unit: N, Newton) and *A* is the area (unit: m^2, meter square).

In this case, the force applied perpendicularly to the sensing area is the weight. Thus, pressure was determined by the ratio of the weight of each object and the sensing area (area of the circle, 28 mm^2) of the sensor.

Figure 21 – *FlexiForce* force sensor is composed of small printed electrical circuits, which can be used for force measurements [42].

Resistance (R), measured in function of pressure, presents a logarithmic behavior. Consequently, conductance (C, unit: S, Siemens), the inverse of

resistance (C=1/R) is a linear curve, and therefore useful in calibration. Thus, the obtained calibration curve was used to quantify pressure applied by paper clips on the COC during the imprinting process.

3.2.5. SEM Imaging

First, COC and PDMS samples for SEM imaging were coated with a gold conductive layer, by using a sputter coater (Cressington®) for 40 s at a current of 40 mA. The SEM observations were performed in a Philips® XL 30 ESEM-FEG operated at 10 kV beam accelerating voltage. Working distance (WD) and magnification parameters are shown in each picture. Contrast and brightness were determined automatically.

3.3. Device Fabrication

After optimization procedures, nanotopographic devices were fabricated using the same optimal conditions and techniques.

3.3.1. PDMS Molding

Firstly, the silica mold was carefully cleaned with N_2 flow. The PDMS cast was prepared by pouring PDMS prepolymer onto the silica mold template, followed by curing and PDMS removal. For preparation of the PDMS prepolymer mixture (*Dow Corning* ® 184 Silicone Elastomer), 2 g of curing agent was added to 20 g of elastomer (ratio 1:10) in a centrifuge tube (Polypropylene, 50 mL, Sterile, Nunc ™, Thermoscientific ®) and mixed for 3 min with a metal spatula. In order to remove air bubbles, the tube was centrifuged at 3000 rpm for 1 min (Eppendorf ® Centrifuge 5810 R). A vacuum chamber was also used to remove air bubbles from the PDMS mixture. PDMS

baking was performed in a Binder® oven for 1h at 80ºC. At last, PDMS cast was removed and borders and chambers were cut. On the opposite sides of the "bridge", 2 holes were punched by using a blunt needle (BD ™ Blunt Filter Needle, 18 G 1 ½").

3.3.2. NIL in COC

First, the protective layer was removed; the COC film was cleaned with 70% ETOH, and dried with N_2 flow. COC film, silica mold, rubber, and glass coverslip (22x22 mm) and slides were clumped with 2 paper clips which were used to generate pressure. Glass was used to increase pressure and rubber was added to avoid mold breaking (Figure 22). The assembled components were then put in the oven at 190ºC for 1h (Binder ®). After cooling, components were disassembled.

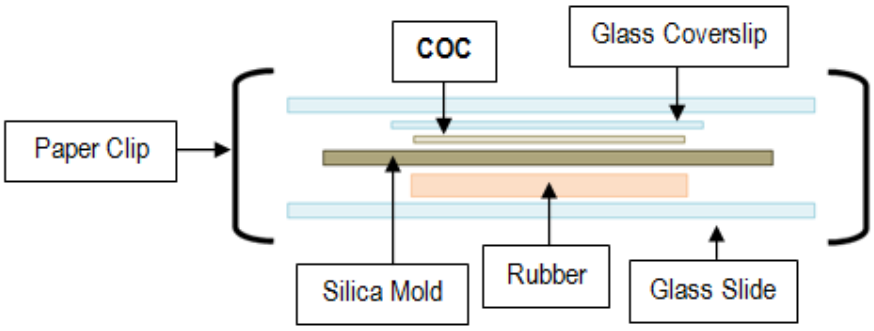

Figure 22 – Paper clips-based hot embossing setup: the assembled components (COC film, silica mold, rubber, and glass coverslip and slides) were clamped together by two paper clips (which were used to generate pressure) and then heated to 190ºC for 1h. COC: Cyclic Olefin Copolymer.

3.3.3. Plasma Bonding and Alignment

Similarly to what was described previously, the COC and PDMS samples were treated with air plasma for 6 s and 60 s of exposure time, respectively.

The treated-COC sample was then put floating in demi-water and the PDMS in APTES solution diluted in demi-water (1% aq) for 20 min. In order to align the COC and PDMS surfaces, the COC sample was dried with N_2 flow and a 20 µL drop of (filtered) ethanol (ETOH) or isopropanol was then put on the top of the COC (to avoid friction between surfaces). The channels/walls of PDMS were aligned with the imprinted-"Ys" on COC under the microscope. COC-PDMS bonding was complete after 1-2 hours (Figure 23). This approach was based on the work of Sunkara et al. [93].

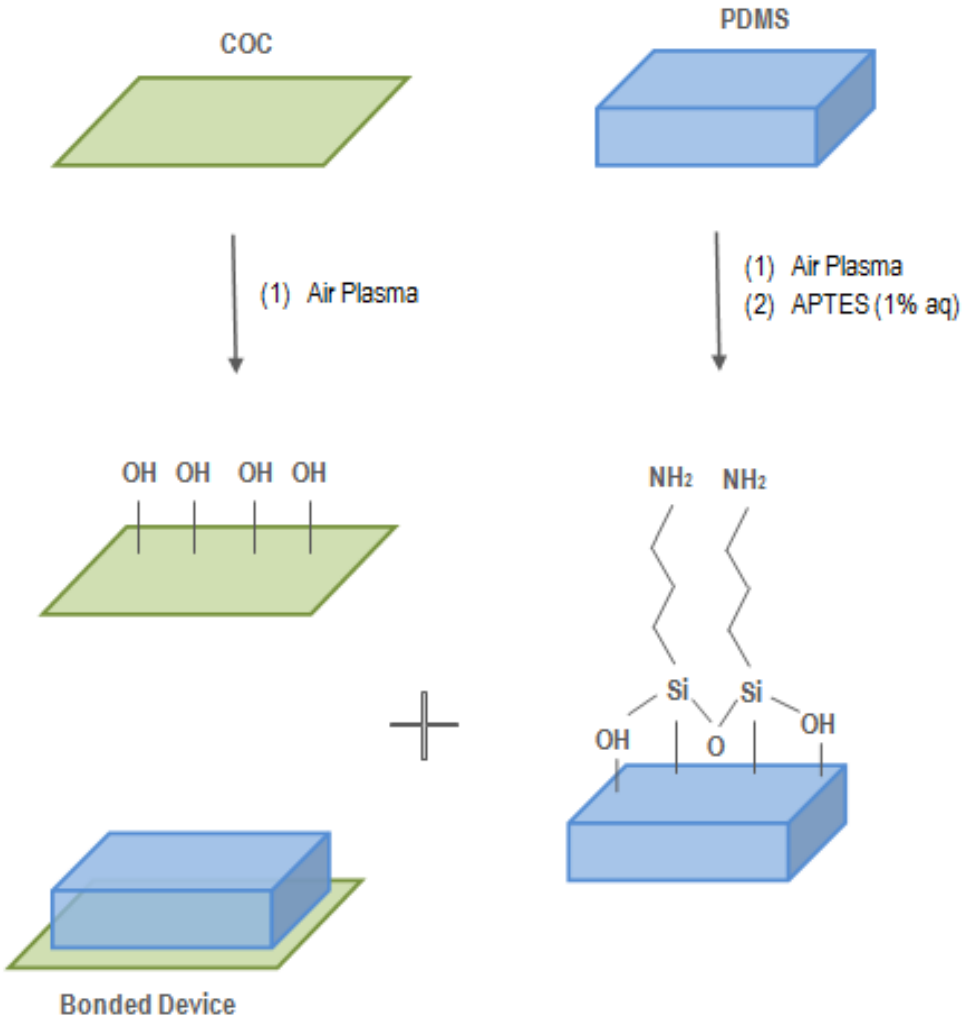

Figure 23 - Bonding process: COC and PDMS surfaces are both treated with (1) air plasma treatment (6 and 60 seconds of exposure time, respectively) and PDMS is also treated with (2) APTES diluted in distilled water (1% aq). Surfaces bond after 2 hours of contact (adapted from [93]).

3.4. Cell Response Analysis

Biochemical tests were performed in order to determine the optimal conditions for F11 cell growth inside the nanotopographic device. Biocompatibility of different substrates and different media conditions were tested for F11 response analysis. Phalloidin and 4',6-diamidino-2-phenylindole (DAPI) staining was used to evaluate cell morphological changes over different culture conditions. Adenosine triphosphate (ATP) assay was also performed to measure cellular metabolic activity. DNA and LIVE/DEAD assays were used to analyze cell culture viability. Cell tracking was also useful to determine the proper cell culturing time in the nanotopographic device.

3.4.1. Cell Culture

F11 hybridoma cells are a fusion of a mouse DRG and a rat neuroblastoma. In contrast to a typical heterogeneous DRG population, this F11 cell line showed to be homogeneous, exhibiting markers and receptors of nociceptive sensory neurons (i.e., related to the perception of pain) and responding electrically to nociceptive stimuli [16].

They were grown in Dulbecco's Modified Eagle Medium (DMEM) (Gibco® DMEM with High Glucose, L-glutamine, Phenol Red) with the addition of 10% fetal bovine serum (FBS heat inactivated, Gibco®), penicillin (10 units/mL), and streptomycin (10 mg/mL) (i.e., Pen-Strep) in an incubator at 37ºC and 5% CO_2. The cells were grown in T75 flasks (Nunc, Thermo-Scientific®) and the media was refreshed every 2 days until the cell growth was confluent (approximately every 4 days), at which point the cells were dissociated using 0.05% Trypsin-EDTA (Ethylenedinitrilotetraacetic acid) with Phenol Red (Gibco®) and splitted 1:15. The experiments used cells from passages 2-10.

3.4.2. Cell Seeding

Standard TCT 24 well-plates (Nunc, Thermo-Scientific®) were used to perform both biocompatibility and media conditions experiments. Technical and biological triplicates were also performed for each experiment. Circles of treated- and untreated-COC, and coverslips (Menzel-Gläser®, Thermo-Scientific®) were placed inside the wells and fixed with rubber rings. Wells were sterilized with 70% ETOH for 30 minutes. The plate was then left for 1 hour to allow for ETOH evaporation. Wells were washed 2x with distilled water and Phosphate buffered saline (PBS, Gibco®) in order to remove residual ethanol. PBS was then removed, the culture media was added, and the plate was warmed inside an incubator (Sanyo®) to promote proteins attachment to the surface. The cells were trypsinized, resuspended in culture media and seeded on the wells with a density of approximately 10000 cells/cm^2. The plate was left inside the incubator to allow the cells to attach. After 4h, the media was replaced. In the case of the media conditions experiment, three different media conditions were investigated. For that, different amounts of FBS and Forskolin (FSK, 24 mM) were added to the DMEM media containing Pen-Strep: 10% FBS, 1% FBS, and 1% FBS + FSK; comparing cell culture substrates of treated-COC and control TCT. For simplification purposes, the three different media conditions were further described as 10% FBS, 1% FBS and 1% FBS + FSK.

Before cell seeding in the nanotopographic device, the chambers were filled with 70% ETOH as well as punched holes were used to aspirate or add ETOH and eliminate eventual air bubbles. Both chambers were then sterilized with 70% ETOH for 1h. ETOH was removed and cleaned by dilution with cell culture water (PAA®, The Cell Culture Company) (x5). Water was also removed and PBS (Gibco®) was added (x3). After 10 min, PBS was removed and culture media was added, and the device was warmed inside the incubator at 37ºC to promote protein attachment to the surface. Media was then removed and 20 µL F11 cell suspension (1 000-2 000 cells inside) was added to the “Ys” chamber (1st chamber) as well as 20 µL media to the other chamber (in order to stop flow between chambers). The device was slightly tilted to induce cell proximity to the

bridge of channels (but not crossing it). Media was then replaced with 1% FBS + FSK. Different seeding densities were tested, such as 500-1000 cells/device, 5000 cells/device, and 10000 cells/device. Also different seeding approaches were tried (like tilting time and position) in order to determine the optimal cell seeding density and method. Bright field pictures were taken with the NIKON® Eclipse TS100.

3.4.3. Phalloidin-DAPI Staining

Phalloidin 488 is a high-specificity filamentous actin (F-actin) probe conjugated to a green-fluorescent dye with excitation ideally suited to the 488 nm laser line. Alexa Fluor® 488 Phalloidin (maximal excitation/emission: 490/525 nm, Molecular Probes®, Life Technologies®) was used to visualize cell cytoskeleton. A FITC filter was used to detect Alexa Fluor® 488-stained cells. DAPI (maximal excitation/emission: 350/470 nm, Sigma-Aldrich®) is a blue-fluorescent dye that binds to DNA. It is excited by the violet (405 nm) laser line. DAPI's spectral properties make it ideal for use with green and red fluorophores in multicolor experiments and it was also used to stain the nuclei of the F11 cells (a DAPI filter was used to detect DAPI-stained nuclei).

After 2 days of culture, the media was removed and the plate was washed 2x with PBS; 10% formalin was dispensed for 20 min at room temperature (RT) and then washed 2x with PBS; 0.5% Triton-X was added for 10 min and removed by washing wells 3x with PBS. After 5 min, PBS + 1% BSA (bovine serum albumin, Sigma®) was added for 30 min. Phalloidin 488 and DAPI were diluted in PBS + 1% BSA (200 µL PBS + 1% BSA + 5 µL Phalloidin; 200 µL PBS + 1% BSA / 14 = 14.3 µL DAPI). Diluted Phalloidin 488 was added in each well and incubated for 20 min at RT. After 2x PBS washing, diluted DAPI was added and incubated for 10 min at RT, and washed 2x PBS.

Phalloidin 568 (red-orange fluorescent dye, Alexa Fluor® 568 Phalloidin, maximal excitation/emission: 578/603 nm, Molecular Probes®, Life Technologies) and DAPI staining was performed in the nanotopographic

devices after 4 days of culture. A different phalloidin probe was used in the devices in order to determine which one enabled more sensitive detection. A Texas Red® filter was used to detect Alexa Fluor® 568-stained cells. The media was removed and the chambers of the device were washed 3x PBS. Cells were left in 10% formalin for 30 min at RT and then washed 2x PBS. 0.5% Triton-X was added for 15 min and removed by washing chambers 3x PBS. After 5 min, PBS + 1% BSA was added for 45 min. Diluted Phalloidin 568 was added and incubated for 30 min. After 2x PBS washing, diluted DAPI was added and incubated for 15 min. After 2x PBS washing, pictures were taken with the NIKON® Eclipse E600 microscope.

3.4.4. DNA and ATP Assays

After 2 days of culture, media was removed and the plate was washed 2x PBS. Glo lysis buffer (Promega®) was dispensed for 5 minutes and cell lysate was then transferred to Eppendorf® microcentrifuge tubes. Tubes were centrifuged (after vortex for 10 seconds) at 12 000 g for 15 seconds (at RT). Supernatants were transferred to new tubes and frozen at -20ºC. After 1 day, black and white 96 well-plates (Nunc®) were used to perform DNA and ATP assays, respectively. Triplicates of cell lysate were assessed for both assays. In the case of the DNA assay, 45 µL of cell lysate and 45 µL of DNA lysis buffer (DLB) were added per well and incubated for 1 hour (at RT in darkness). DLB was prepared by adding component B of the DNA assay kit (Cyquant® DNA Proliferation Assay kit) to a solution already prepared (distilled water; 1.05 g NaCl and EDTA 37.22 mg per 100 mL of distilled water) as well as 1 µL RNase per mL of solution. Component C (DNA standard, λ) was diluted (1 µL of λ in 99 µL DLB) in order to prepare DNA standard series in tubes. Different concentrations of diluted λ in DLB were prepared (1 µg/mL, 500 ng/mL, 200 ng/mL and 20 ng/mL) and added in triplicated wells. Component A (or CyQuant® GR dye) was diluted 100 times in DLB and 90 µL of diluted dye were added to each well. The plate was then incubated for 20 minutes to promote

color development, because the dye exhibits fluorescence enhancement when bound to cellular nucleic acids.

To perform the ATP assay, 45 µL of cell lysate and 45 µL of the CellTiter-Glo® compound (CellTiter-Glo® Luminescent Cell Viability Assay, Promega®) were added per well and incubated for 10 minutes. The luminescence of the luciferase in this compound is proportional to the ATP present in each sample. The ATP standard was prepared by diluting ATP (Adenosine 5'-triphosphate disodium salt, A 2383, Sigma®) with distilled water (Gibco®): 10^{-7}, 10^{-8}, 10^{-9}, and 10^{-10} g/mL.

The amounts of DNA and ATP in each lysate sample were measured by using the Victor® Multilabel Reader (Perkin Elmer®) for both biocompatibility and media conditions experiments.

3.4.5. LIVE/DEAD Assay

The LIVE/DEAD® Viability/Cytotoxicity Assay Kit (Molecular Probes®, Life Technologies®) was used to analyze the viability of cells cultured in different substrates: COC samples treated air plasma and UV. The Calcein AM (Component A) becomes green fluorescent inside live cells (enzymatic conversion) while the Ethidium homodimer-1 (EthD-1, Component B) only enters inside death cells and becomes red fluorescent by binding to DNA. This two-color fluorescence cell viability assay allowed the simultaneous determination of live and dead cells.

After 2 days of culture, media was removed and wells washed with PBS (x2). LIVE/DEAD solution were prepared and added in each well: 3 µL of EthD-1 per 1 mL of PBS and 0.5 µL of Calcein per 2 mL of PBS. The plate was then placed in the incubator for 30 min. The solution was removed and the wells washed with PBS. Imaging was immediately performed with the NIKON® Eclipse E600 microscope.

3.4.6. Cell Tracker

One day after cell seeding, media was refreshed with media and cell tracker (Invitrogen®, Celltracker^{TM} Green CMFDA probes for long-term tracing of living cells): 1 mL media + 1 µL cell tracker (1:1000) and incubated at 37ºC for 1h. Cells were then washed 2x with PBS and media refreshed.

3.4.7. Statistical Analysis

The statistical significance of the DNA assay results obtained from the biological triplicates was evaluated. Comparison of means was performed by One-way Analysis of Variance (ANOVA) with Tukey's posttest. ANOVA provides a statistical test of whether or not the means of the experimental groups (in this case, cell culture substrates or media conditions) are different. When there were differences, Tukey's test was used to find which groups were significantly different from each other by comparing all possible pairs of means. Differences were considered significant if $\rho<0.05$.

3.4.8. Image Processing

Image processing and analysis tools in ImageJ® software were used to adjust brightness and contrast, and to create a combined image from the different channels of the fluorescent microscopic images.

CHAPTER 4 – *RESULTS*

4.1. Preliminary Results

Preliminary experiments were performed in order to test the efficiency of the COC treated with both UV and air plasma techniques in terms of biocompatibility for F11 cells as well as in terms of bonding with PDMS.

The COC samples were exposed to 30 min of UV or 60 s of air plasma. After 2 days of culture, LIVE/DEAD assay was performed in order to analyze F11 cell response to different surface treatments. Many F11 cells were attached to the COC surface treated with UV, with only a few dead cells observed (Figure 24A). Very similar results were also obtained for cells cultured on the COC treated with air plasma (Figure 24B). On the other hand, almost all the cells attached to the untreated COC surface did not survive (Figure 24C).

Different treatment combinations were also tested in order to determine the best surface treatment for bonding purposes. UV treatment showed to be inefficient while plasma allowed strong bonding of COC and PDMS for less exposure times (Table 2). Even though the combination of both techniques has been tried, the results showed weak bonding of COC treated with UV and PDMS treated with air plasma.

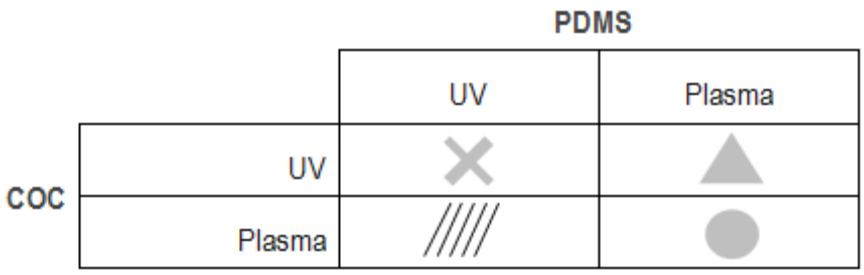

Table 2 - COC and PDMS bonding trials combining different techniques (UV and air plasma) and exposure times: (x) not bonded (for 30 and 60 min of exposure time); (Δ) weakly bonded (for 30 min of UV and 2 min air plasma exposure); (o) bonded (for 2 min of exposure time); (/////) not tested. COC: Cyclic Olefin Copolymer; PDMS: Polymethylsiloxane; UV: Ultraviolet.

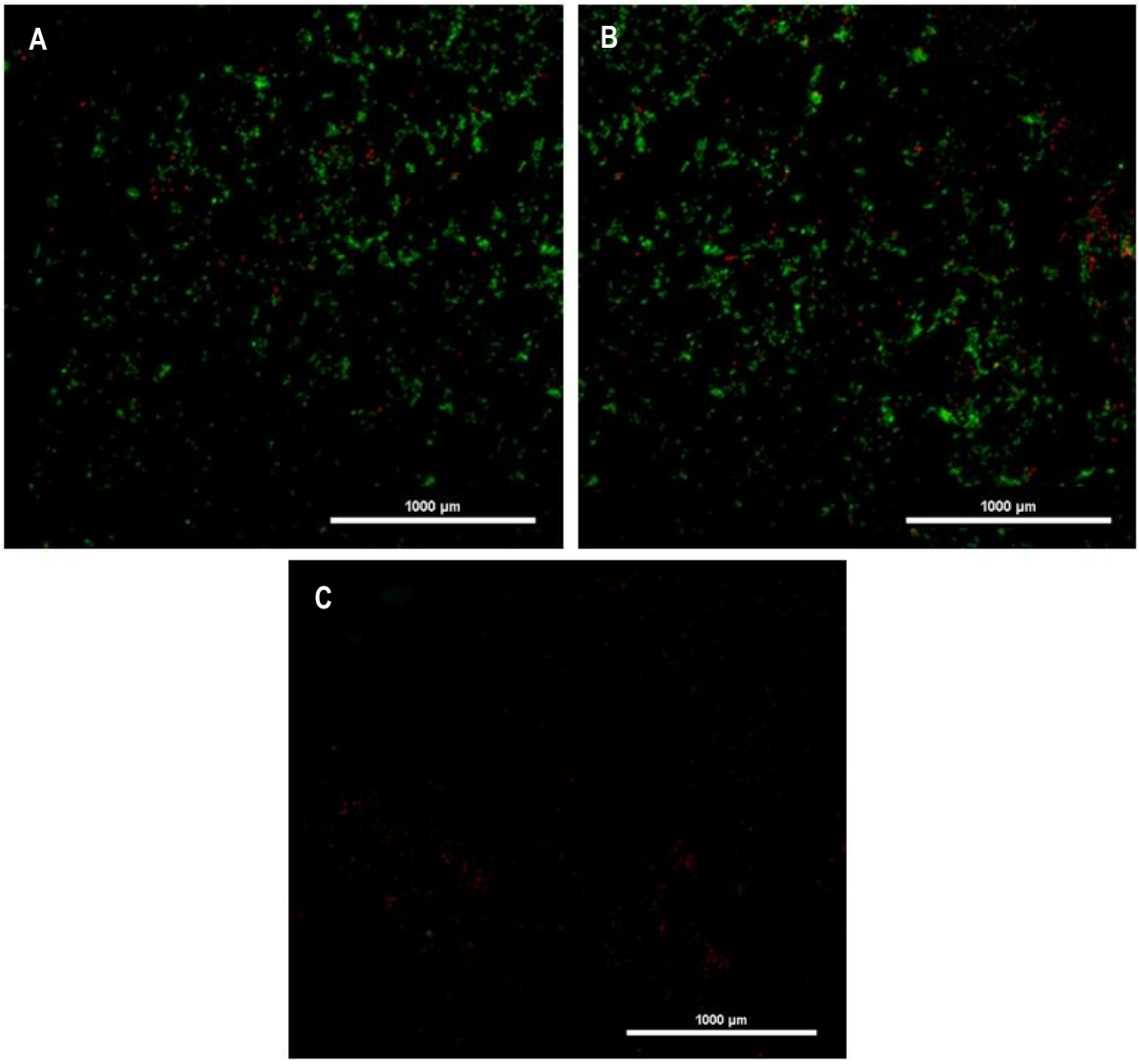

Figure 24 – LIVE/DEAD pictures showing F11 cells cultured on: (A) COC treated with UV; (B) COC treated with air plasma; (C) untreated-COC. Live cells fluoresce green and dead cells fluoresce red. COC: Cyclic Olefin Copolymer.

4.2. Device Optimization

Based on the preliminary results, the air plasma technique was chosen to treat both COC and PDMS surfaces. For that reason, contact angle measurements were performed for different air plasma exposure times in order to obtain the optimal exposure time for culture purposes on COC. The optimal range for cell culture had already been determined (contact angles of 40º-60º) [77], so 6 s was observed to fit this contact angle interval, being the optimal exposure time. Measurements were also performed on PDMS in order to

maximize bonding strength (Figure 25). The exposure values were the same for both surfaces (6 s, 10 s, 15 s, 30 s, 60 s and 120 s). For exposure times above 60 s, there was no significant decrease of contact angles. Thus, PDMS was chosen to be treated with air plasma for 60 s.

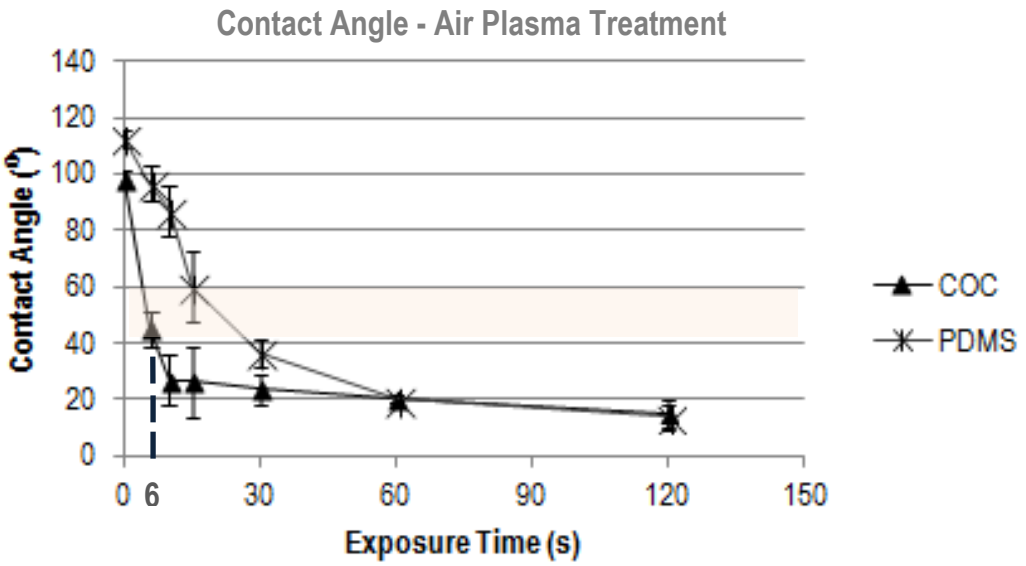

Figure 25 – Contact angle measurements of COC and PDMS for different exposure times of air plasma treatment. Highlighted contact angle interval 40°-60° which was found to be optimal for cell culture. COC: Cyclic Olefin Copolymer; PDMS: Polydimethylsiloxane.

Moreover, NIL parameters were also optimized in order to obtain proper imprinted nanogratings on COC. Pressure was determined by using a calibration curve. First, resistance values were measured for different values of pressure applied on the Flexiforce® sensor (Figure 26). Resistance values were then converted on conductance values in order to obtain a linear equation to calculate the pressure applied on COC sample during NIL process (Figure 27). For that, the conductance value was determined by using the *Flexiforce*® sensor (10.73 µS). From the calibration linear equation (Figure 27), came that the pressure applied on the sensing area (28 mm^2) of the sensor was:

$$10.73 = 5.317x + 0.3708 \leftrightarrow x \cong 1.95\ MPa \qquad (2)$$

Thus, the estimated pressure applied by the papers clips on the COC film (area of 484 mm^2) was determined, considering that pressure is constant per unit of area:

$$P_1 \times A_1 = P_2 \times A_2 \leftrightarrow 1.95 \times 28 = P_2 \times 484 \leftrightarrow P_2 \cong 0.1\,MPa \qquad (3)$$

The pressure applied by the paper clips on the COC film to promote the nanograting imprinting during the NIL process was approximately 0.1 MPa.

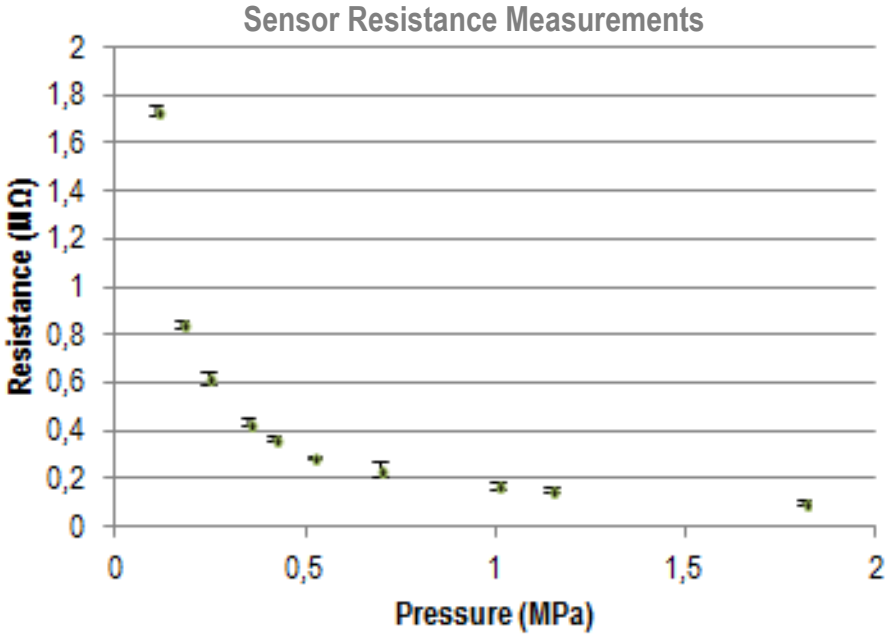

Figure 26 – Resistance values were measured with a multimeter for different values of pressure applied to the sensing area of the *Flexiforce* sensor.

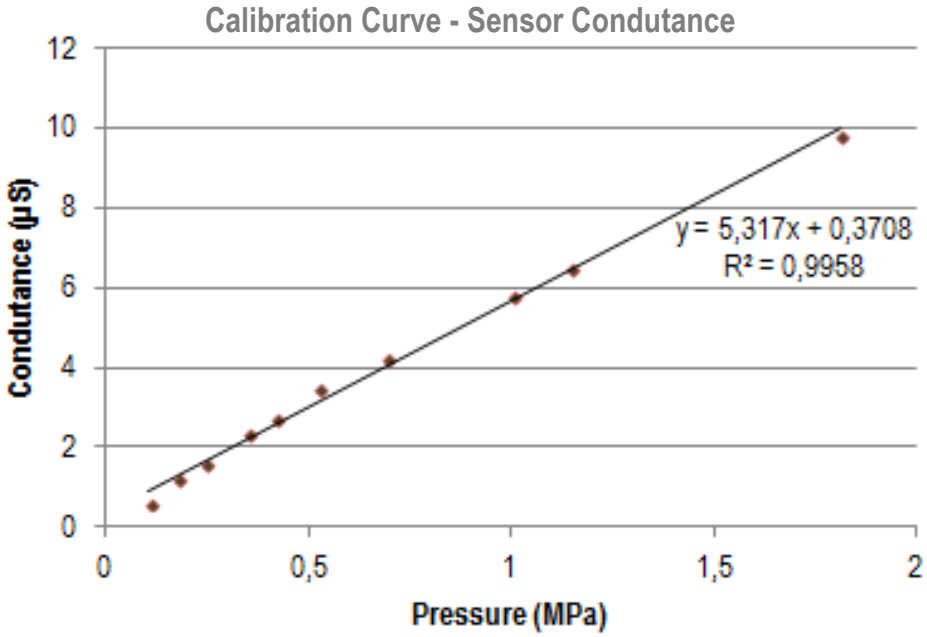

Figure 27 – Calibration curve: Linear regression of conductance was calculated inverting resistance values of Figure 26.

SEM was used to examine if “Y-shaped” nanogratings were correctly imprinted on COC. Based on SEM pictures (Figure 29), optimal conditions for NIL in COC were determined (Temperature 190ºC, pressure 0.1 MPa and time 1h). Cooling step after “hot embossing” procedure revealed to be important for a correct imprinting. Also optimal conditions for PDMS molding were identified by SEM. Pictures showed channels on PDMS baked for 1h at 80ºC temperature (Figure 28). Changes in dimensions of the channels were observed for different baking conditions. The PDMS prepolymer ratio revealed to be essential for peeling the PDMS off from master easily.

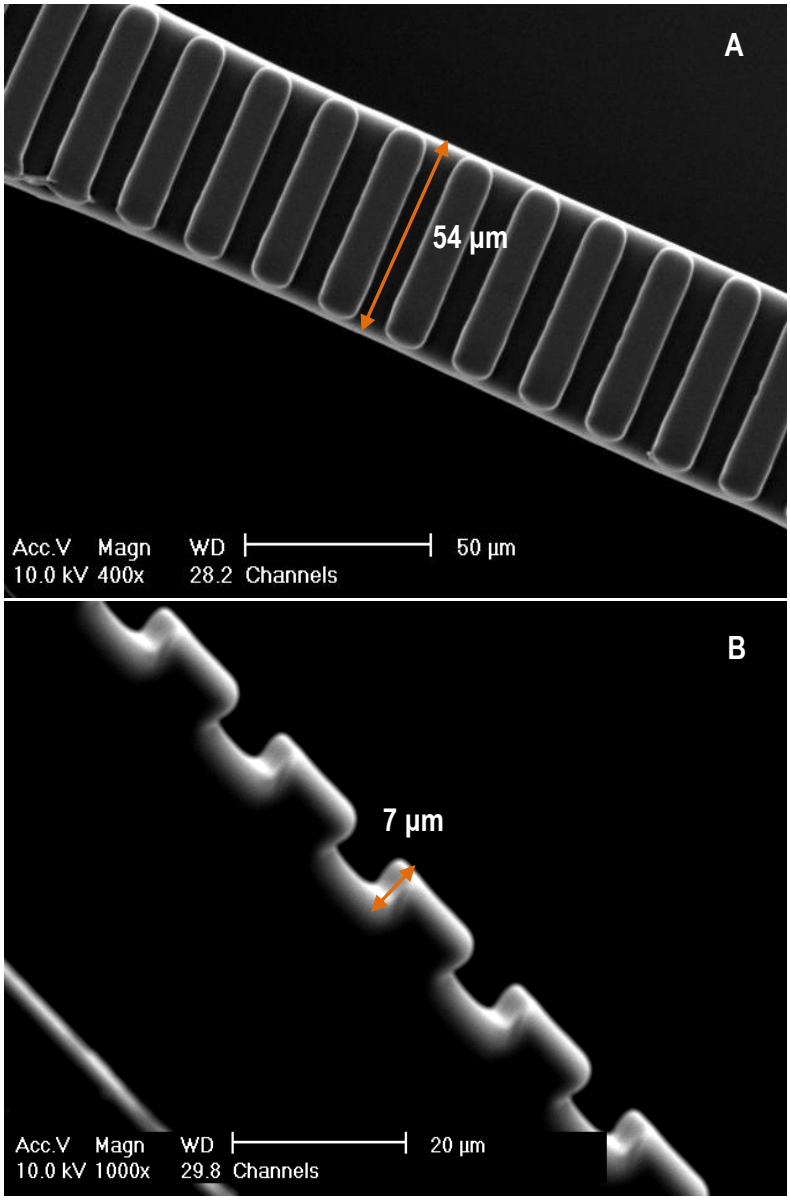

Figure 28 – SEM pictures of channels in PDMS cast: bottom view with lower (A) and higher magnification (B); PDMS baking conditions: 1h, 80ºC. PDMS: Polydimethylsiloxane; SEM: Scanning Emission Microscope. WD: Working Distance.

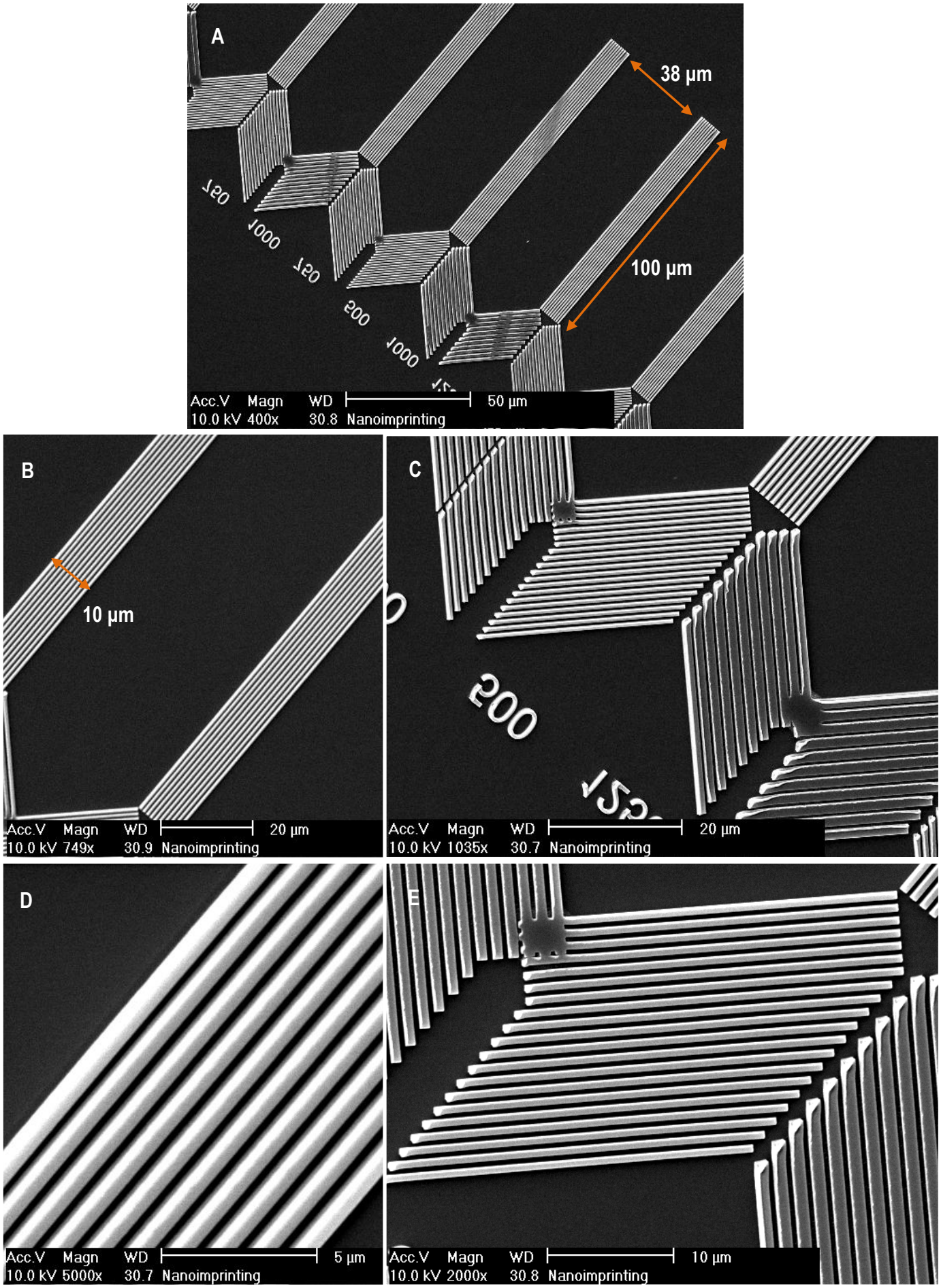

Figure 29 – SEM pictures of imprinted nanopatterns on the surface of the COC: complete "Y"-shape (A); bifurcation part with lower (C) and higher (E) magnification; first part also with lower (B) and higher (D) magnification. COC: Cyclic Olefin Copolymer; SEM: Scanning Emission Microscope; WD: Working Distance.

4.3. Cell Response

Biocompatibility tests were performed to prove that 6 s was effectively the optimal exposure time for F11 culturing purposes. Different surfaces were considered, such as TCT plates, glass coverslips, untreated- and treated-COC films. F11 cells were stained with Phalloidin 488 and DAPI. ATP and DNA assays were also performed.

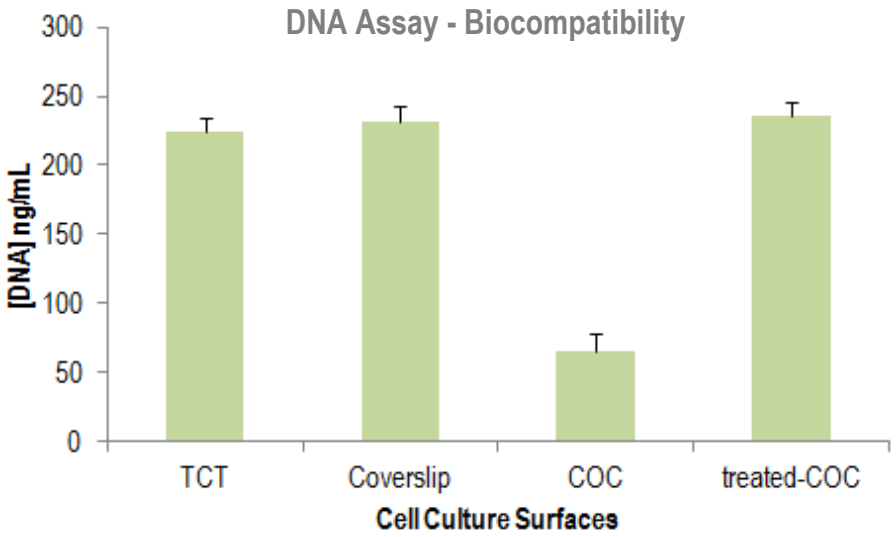

Figure 30 – DNA assay results for one biological experiment. Concentration of DNA detected in each surface for F11 cell culturing (+SD). COC: Cyclic Olefin Copolymer; DNA: Deoxyribonucleic acid; TCT: Tissue Culture Treated; SD: Standard Deviation.

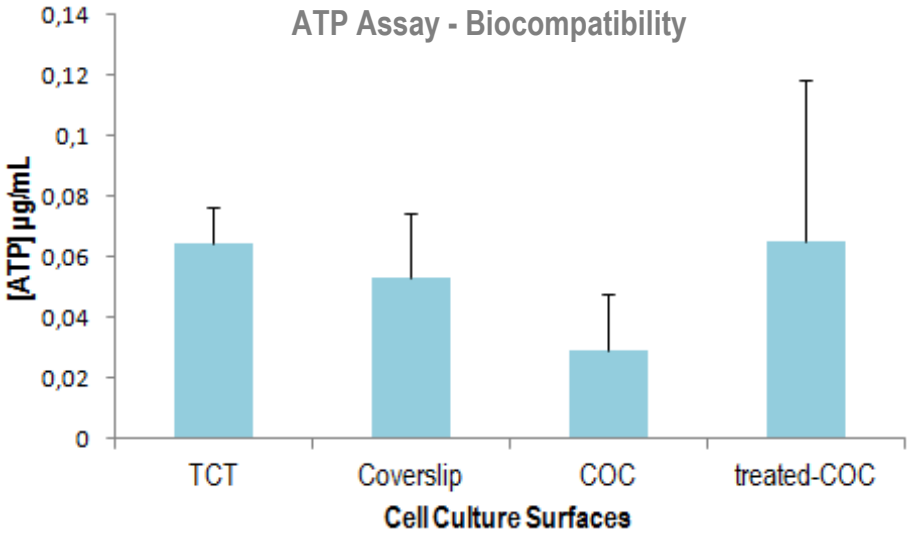

Figure 31 – Concentrations of ATP detected by the Luciferase assay for each cell culture surface (+SD). Samples used were from the same biological experiment performed for DNA assay (Figure 30). ATP: Adenosine Triphosphate; COC: Cyclic Olefin Copolymer; TCT: Tissue Culture Treated; SD: Standard Deviation.

The amounts of DNA and ATP in each cell culture substrate were determined for one biological experiment (Figures 30 and 31). The results were in accordance with the typical range concentrations of DNA and ATP encountered in these kinds of biochemical assays. The detected concentrations of DNA and ATP were higher in COC treated with air plasma as compared to the untreated-COC.

Biological triplicates were performed in order to determine if differences between amounts of DNA in treated- and untreated-COC films were significant (Figure 32). Relative differences between results obtained for studied surfaces were similar to those determined from the first biological experiment. Based on Tukey's statistical test ($\rho<0.05$), the concentration of DNA in treated-COC revealed to be significantly higher as compared to untreated-COC.

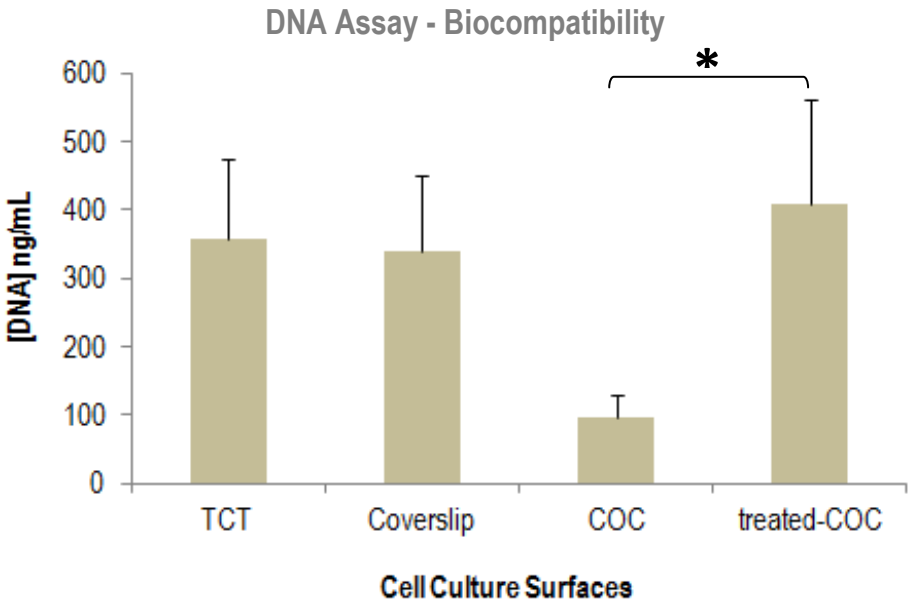

Figure 32 - DNA concentrations measured for different cell culture surfaces. Biological triplicates were performed and averaged (+SD); (*) ANOVA ($\rho<0.05$) and Tukey's test suggests that there is a significant difference between treated-COC as compared with untreated-COC. COC: Cyclic Olefin Copolymer; DNA: Deoxyribonucleic acid; COC: Cyclic Olefin Copolymer; TCT: Tissue Culture Treated; SD: Standard

In addition, F11 cell response to different media conditions was also evaluated. Phalloidin-DAPI staining was performed in order to compare morphological changes between media conditions. ATP and DNA assays were

also made in order to analyse eventual biochemical differences. Also here the results were in accordance with the typical range concentrations of DNA and ATP assays.

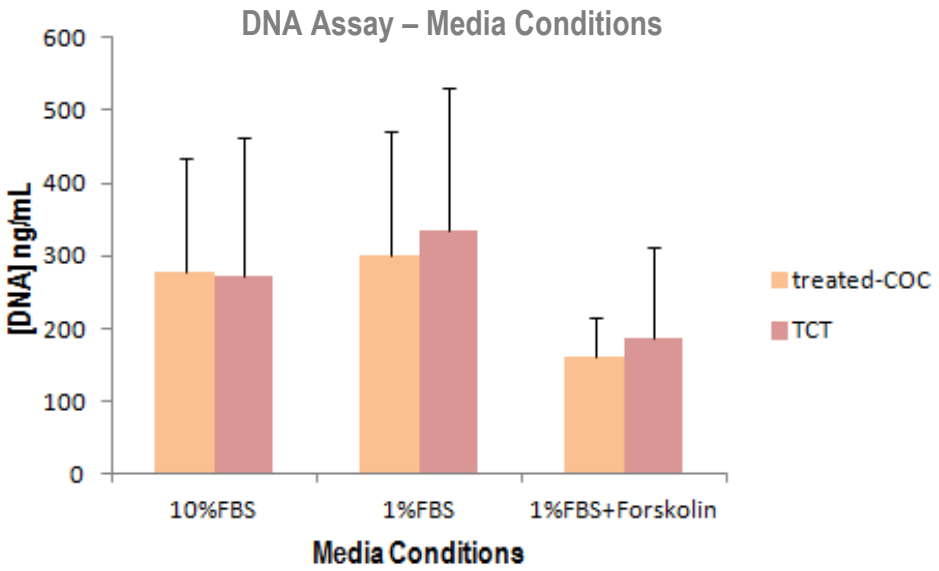

Figure 33 - Amount of DNA measured in each condition of cell culture media (10%FBS, 1%FBS and 1%FBS+FSK), comparing two different cell culture substrates (treated-COC and TCT). Results refer to one biological experiment (+SD). COC: Cyclic Olefin Copolymer; DNA: Deoxyribonucleic acid; FBS: Fetal Bovine Serum; FSK: Forskolin; TCT: Tissue Culture Treated; SD: Standard Deviation.

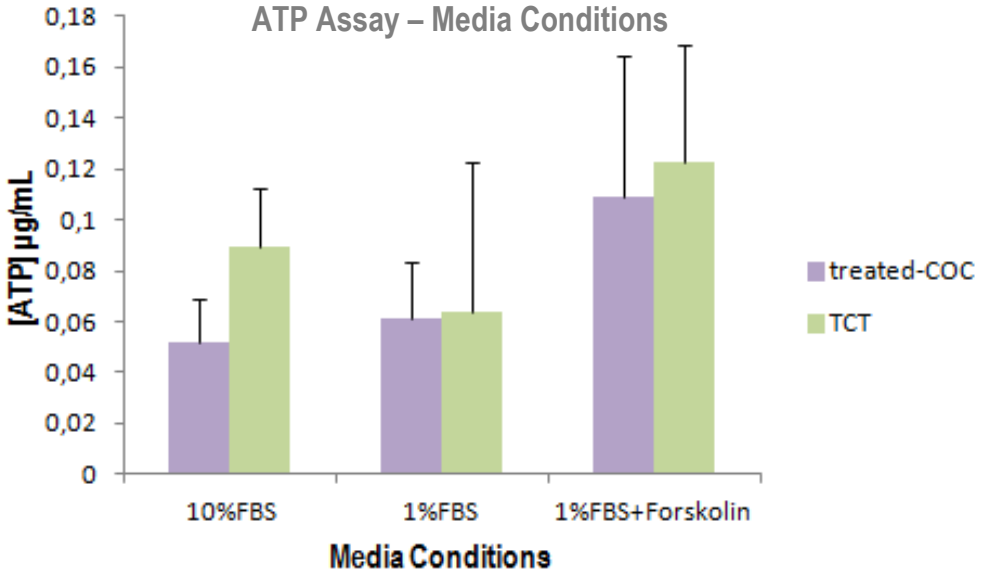

Figure 34 - ATP amounts measured in each condition of cell culture media (10%FBS, 1%FBS and 1%FBS+FSK), comparing treated-COC and TCT. Samples used were from the same biological experiment performed for DNA assay (Figure 33) (+SD). ATP: Adenosine Triphosphate; COC; Cyclic Olefin Copolymer; FBS: Fetal Bovine Serum; FSK: Forskolin. TCT: tissue culture treated. SD: Standard Deviation.

For one biological experiment, the amount of DNA was lower in the 1% FBS + FSK media condition, as compared to the others (Figure 33). On the other hand, the amount of ATP was higher in this media condition when comparing to the remaining ones (Figure 34). The DNA experiment was performed in biological triplicate. Although no significant differences were determined (according to statistical ANOVA analysis), the relative differences between the amounts of DNA in each media condition were in accordance with those detected from the first biological experiment.

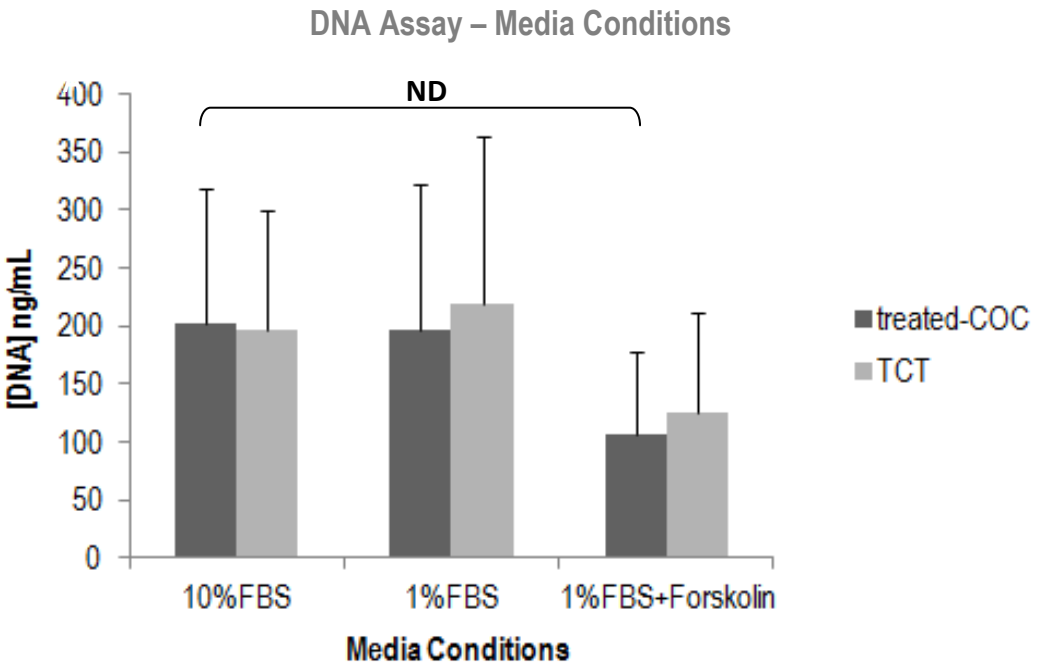

Figure 35 - DNA assay: amount of DNA was measured for each condition of cell culture media (10%FBS, 1%FBS and 1%FBS+FSK), comparing two different cell culture substrates (treated-COC and TCT). Biological triplicates were performed and averaged (+SD). ANOVA statistical analysis shows no significant difference between media conditions ($p<0.05$). COC: Cyclic Olefin Copolymer; DNA: Deoxyribonucleic acid; FBS: Fetal Bovine Serum; FSK: Forskolin; SD: Standard Deviation; ND: Not detected.

Staining pictures revealed different cellular behaviour in different cell culture substrates or media conditions. Cells were widely spread in the treated-COC surface as compared to the multiple cell aggregates formed in the coveslips (Figures 36A and 36C). Few cells attached to the untreated-COC when comparing to the many cells attached to the treated-COC surface (Figures 36A and 36B).

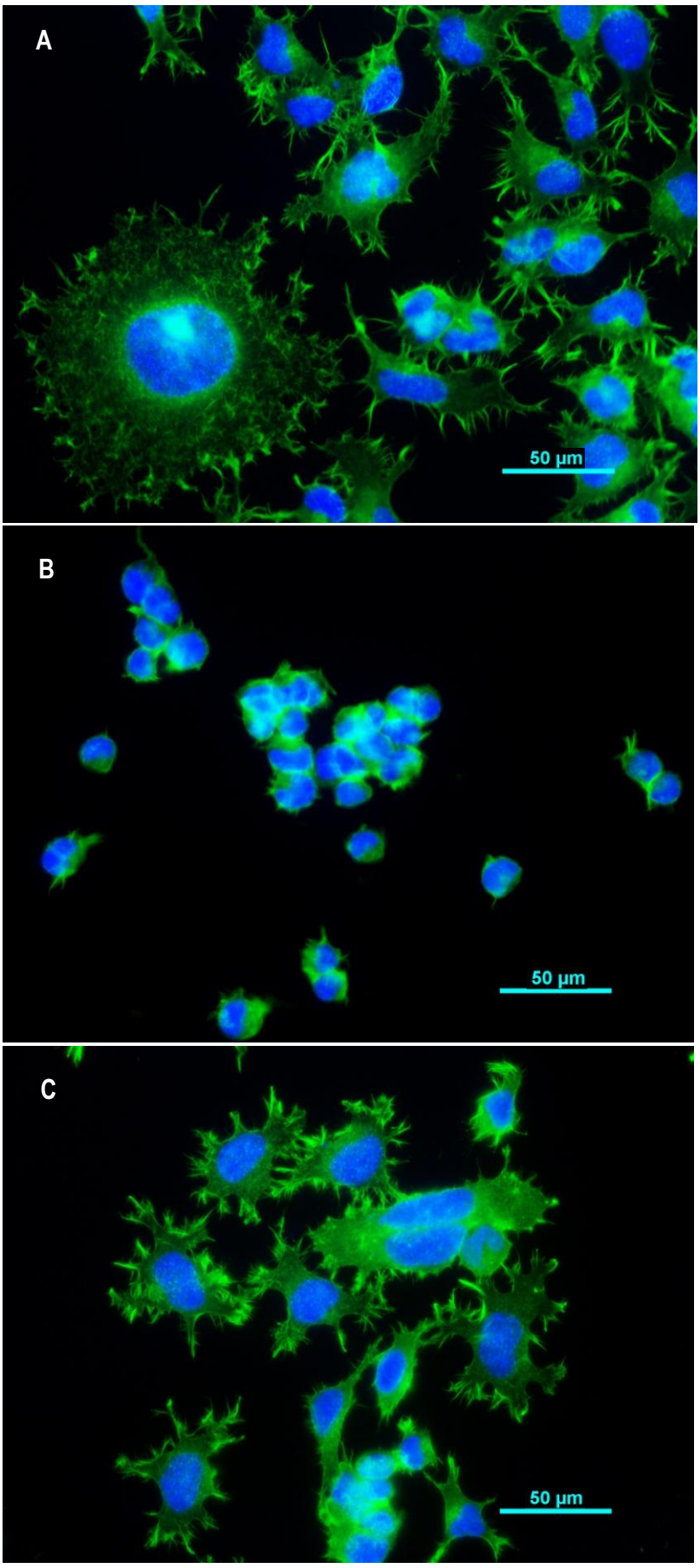

Figure 36 – F11 cells cultured in different substrates: (A) treated-COC, (B) untreated-COC and (C) Coverslip. Actin cytoskeleton staining with Phalloidin 488 (green) and nuclei with DAPI (blue) is shown. COC: Cyclic Olefin Copolymer; DAPI: 4',6-diamidino-2-phenylindole.

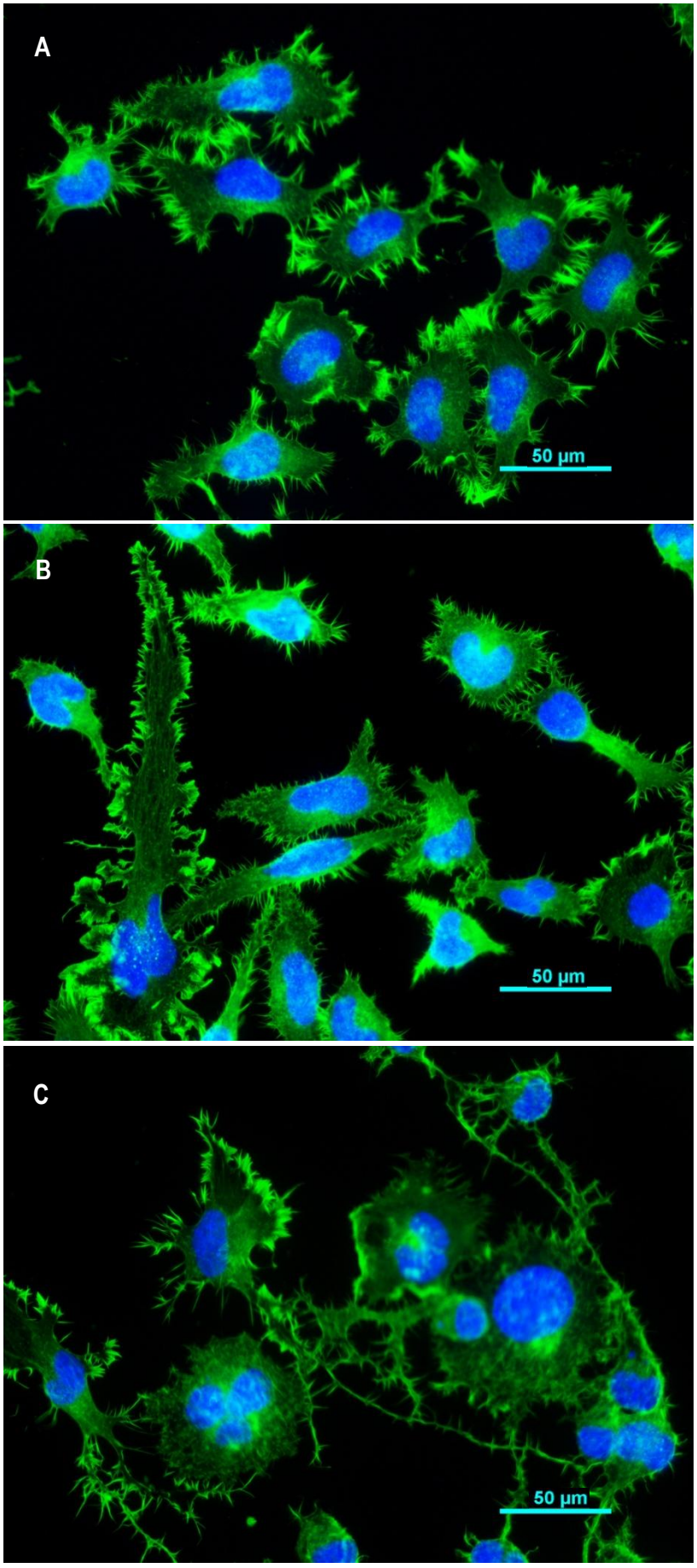

Figure 37 – F11 cells cultured in different media conditions: (A) 10% FBS; (B) 1% FBS; (C) 1% FBS +FSK. Actin cytoskeleton staining with Phalloidin 488 (green) and nuclei with DAPI (blue) is shown. COC: Cyclic Olefin Copolymer; DAPI: 4',6-diamidino-2-phenylindole; FBS: Fetal Bovine Serum; FSK: Forskolin.

Neurites cultured in 1% FBS + FSK media grew longer than those in 10% FBS or 1% FBS media conditions. Moreover, cells cultured in 10% FBS showed more round shape as compared to the others (Figure 37).

4.4. Device Construction Problems

A few problems appeared during the device optimization and construction processes. First, the perfect alignment of “Y-shaped” nanogratings with PDMS channels was not possible. In order to solve this problem, different baking times and temperatures were tested. Channels dimensions revealed to be dependent on the baking conditions. It was observed that different channels and walls widths can be achieved by changing baking conditions. The results demonstrated a complementary behavior between these width values. When the PDMS was baked for 2h at 65ºC, the channels width was 8 µm and the walls width was 11 µm (Figure 38A). On the other hand, the measured widths were respectively 9 µm and 10 µm when the PDMS was baked for 1h at 80ºC (Figure 38B). The channels height was also shown to be dependent on the baking conditions, but in both cases, the device functionality was not compromised.

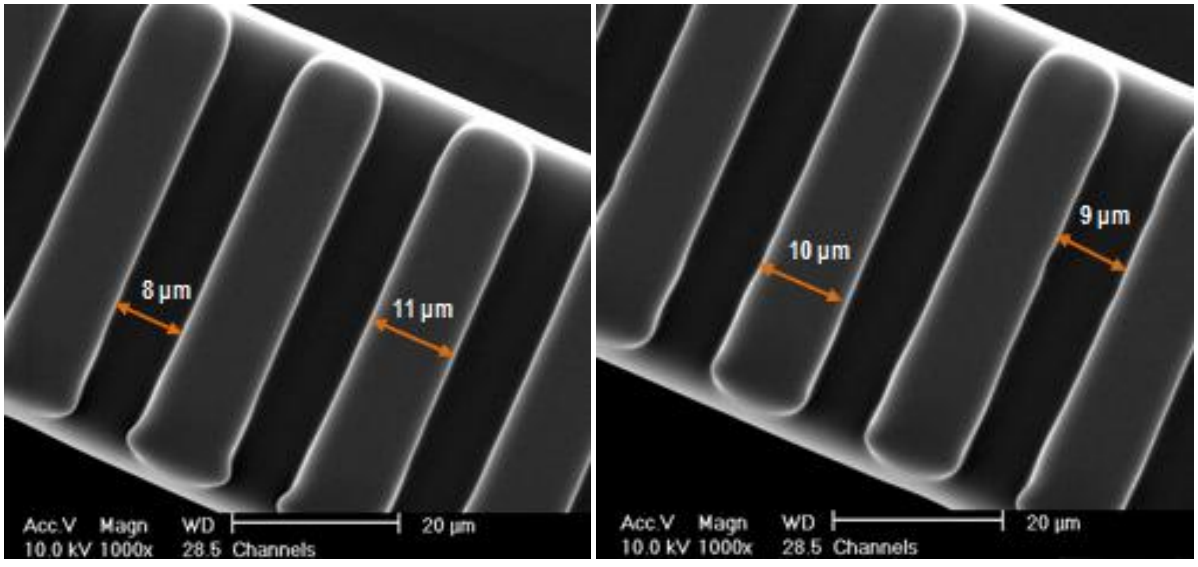

Figure 38 – SEM pictures of PDMS channels: (A) PDMS baked for 2h at 65ºC; (B) PDMS baked for 1h at 80ºC. Channels dimensions are different depending on the baking conditions of the PDMS, such as time and temperature. PDMS: Polymethylsiloxane; SEM: Scanning Emission Microscope; WD: Working Distance.

Second, a leakage problem was observed after device bonding. However, this problem was solved by improving some steps in the bonding protocol. It was observed that treated COC and PDMS surfaces must be dried before bond them together to increase bonding strength and quality. In order to facilitate alignment procedure, a small drop of ETOH was dispensed on the COC surface. As ETOH evaporates before reaction between surfaces, bonding was assured. Thus, the nanotopographic device was properly bonded and constructed in the optimal conditions (Figure 39).

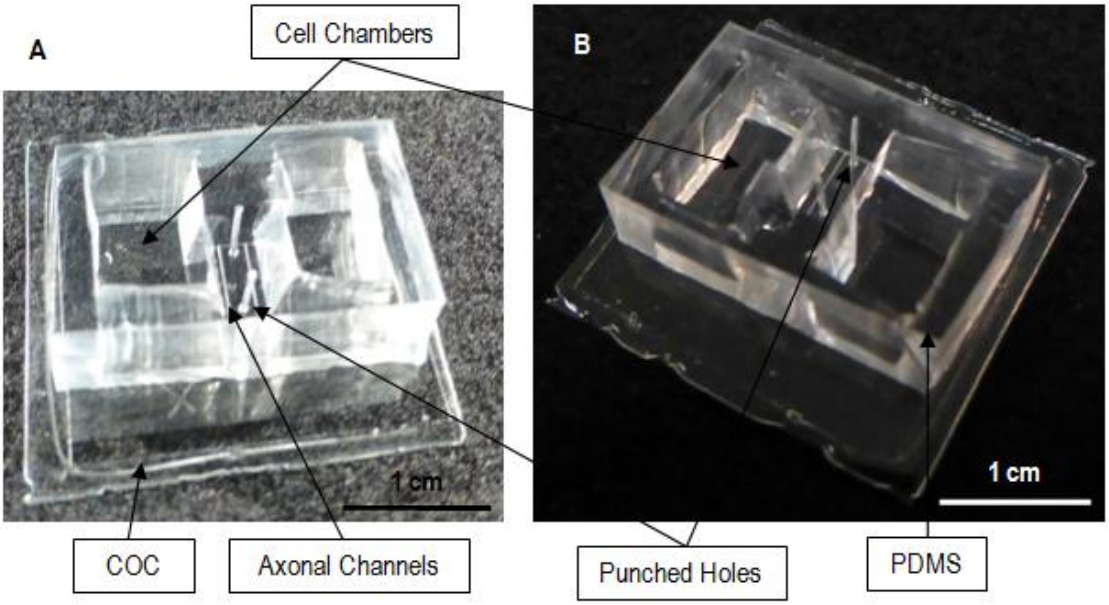

Figure 39 - Nanotopographical device (A-B): bonded device in optimal conditions. COC: Cyclic Olefin Copolymer; PDMS: Polydimethylsiloxane.

Cell seeding density was the third main problem to be solved. Figure 40 showed that the cell seeding density was too high (5000 cells/device) and consequently the neurite outgrowth analysis was impaired by the fact that many neurites were crossing the channels. In addition, some cells completely crossed the channels impairing a proper analysis. Thus, different cell seeding densities and methodologies were tried in order to obtain the optimal F11 seeding conditions in the nanotopographic device. At last, the figure 41 showed that cells were properly seeded by tilting device slightly and the cell seeding density (1000-2000 cells/device) was optimal. Cells were quite close to the channels, but they did not cross them. Staining with phalloidin 488 seemed to be more accurate than those with phalloidin 568.

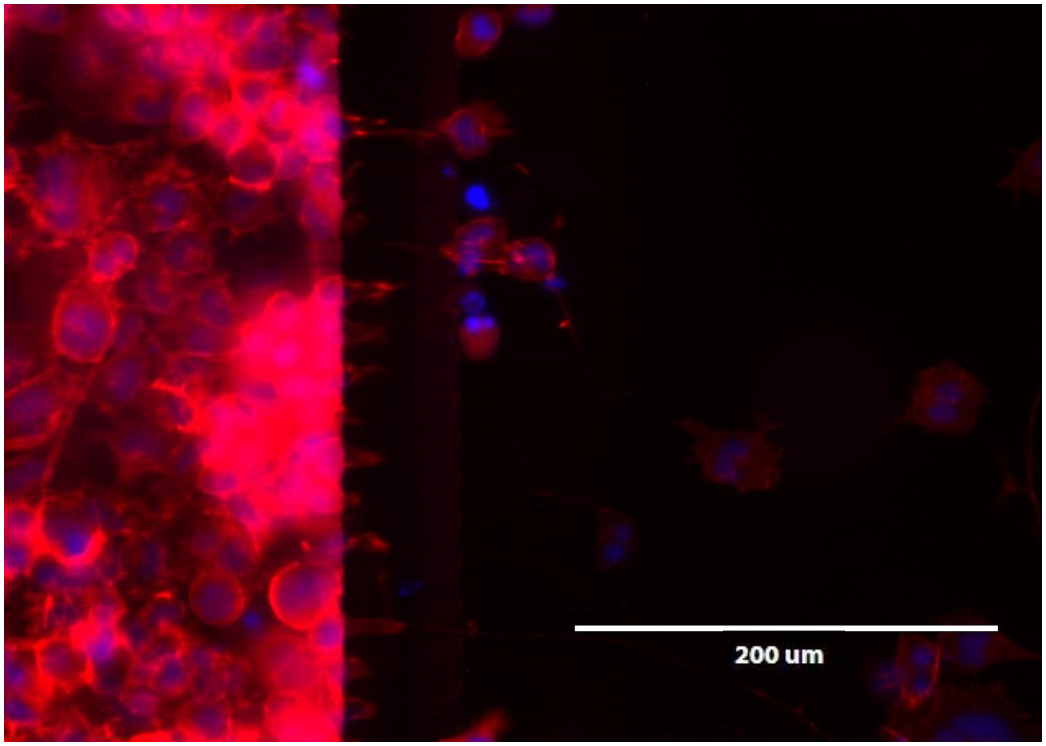

Figure 40 – F11 cells cultured on the nanotopographic device for 2 days. Actin cytoskeleton staining with Phalloidin 568 (red) and nuclei with DAPI (blue) is shown. Although cell seeding density was not optimal and some cells passed through the channels, axons growing across the channels were visible. DAPI: 4',6-diamidino-2-phenylindole.

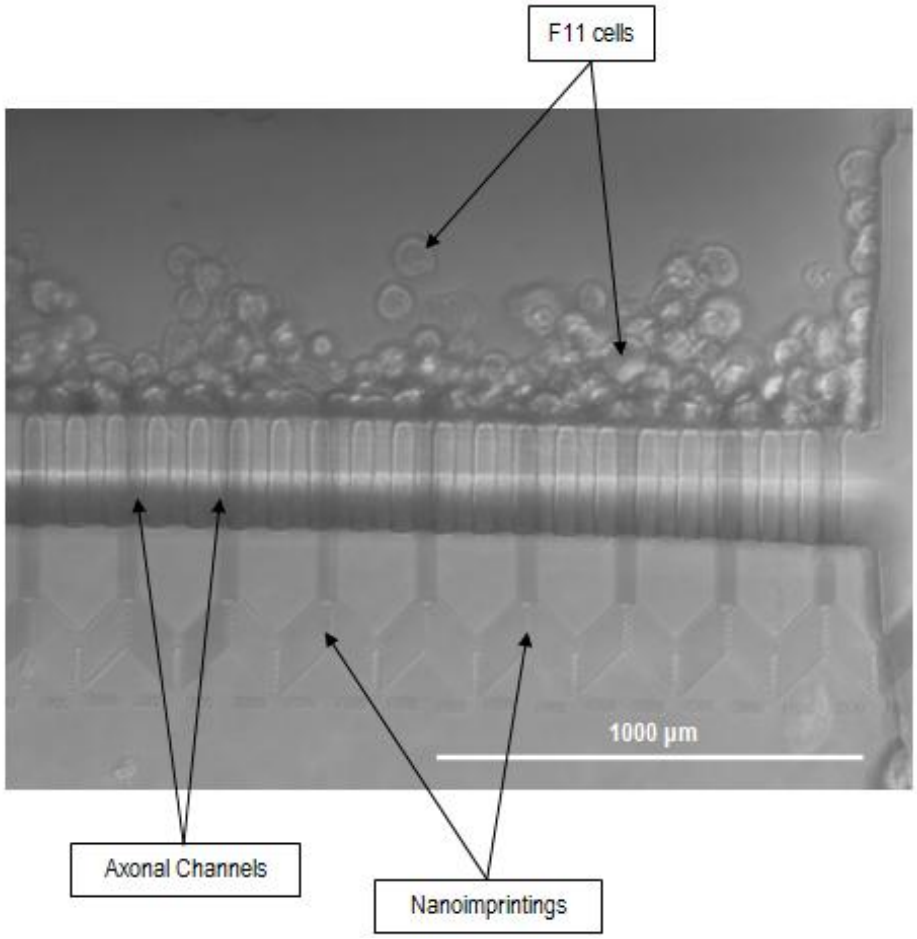

Figure 41 – Bright field picture showing alignment of "Ys" imprinted on COC and PDMS channels, forming axonal channels. After seeding, F11 cells were close to the axonal channels. COC: Cyclic Olefin Copolymer; PDMS: Polydimethylsiloxane.

CHAPTER 5 – *DISCUSSION*

5.1. Device Design Justification

According to literature review, the combination of a nanopatterned substrate for contact guidance with a microfluidic dual-chamber for axonal isolation has not been previously reported. Thus, the nanotopographic device was designed for this purpose.

According to Li et al. [81], to produce high quality microfluidic devices, three main aspects have to be considered: materials and its properties, manufacturing methodologies, and measurements for process control [81]. All these aspects were taken into account during the nanotopographic device construction and optimization.

Materials choice should fit the device performance. Moreover, biocompatible materials must be chosen to do biological experiments. Also the interaction between the materials and tooling or processing methodologies affects device quality and performance [81]. The material cost is another consideration for large-scale, high-volume manufacturing.

PDMS was then chosen for nanotopographic device construction purposes because it is the most used polymer in microfluidic devices for several applications due to advantageous physical and mechanical properties, such as biocompatibility, low cost, optical transparency, ease of fabrication and gas permeability [77] [81]. A PDMS platform was used to create channels for axonal isolation and chambers for cell seeding and culture.

However, PDMS can absorb small hydrophobic molecules or drugs and release oligomers into solution showing disadvantages for some cell studies. Moreover, PDMS is very hydrophobic and shows hydrophobic recovery even after surface treatment [77], requiring more elaborate modification to be used as a suitable culturing substrate. For that reason, thermoplastics are becoming preferable to PDMS for cell culture models in microfluidic [78]. Thermoplastics are polymers that can also be used with the NIL technique to imprint patterns on

the surface, especially because of their stiffness, which is better as compared to PDMS [77]. Thus, thermoplastic materials were considered for the nanogratings layer of the nanotopographic device.

Although thermoplastics are increasingly used for the fabrication of cell culture devices, depending on the application, characterization of the properties of these materials is still needed [77] [94].

Midwoud et al. [77] had already tested PC, PS and COC, and compared them to PDMS in terms of applicability for the fabrication of hydrophilic devices for cell culturing, This comparative study of different thermoplastics revealed that COC is the most suitable for the fabrication of microfluidic cell culture models, especially because this enabled the low-cost production of biocompatible treatable surfaces with low-absorption properties, chemical resistance to organic solvents and gas permeability, beneficial for cell culture. Moreover, COC has the additional advantage of exhibiting a lower autofluorescence, important for optical imaging [94]. For that reason, COC was chosen as F11 culture substrate of the nanotopographic device.

With respect to nanofeature fabrication, EBL was selected as an ideal conventional nanofabrication technique. It has a number of advantages over other lithographic techniques, such as the patterning resolution at nanoscale and the fact that no physical masks are needed, eliminating costs and time delays associated with masks production [8] [35]. Moreover, the products made with EBL can be used as molds for further replications or as final parts.

Also a number of different procedures have been developed for patterning nanoscale structures, such as molding and embossing. For these thermal based techniques, thermal/mechanical/geometry properties should be matched between masters and molds in order to reduce the thermal expansion coefficient and improve replication quality, facilitating peeling off from master and mold. Also bonding quality can be assured by finding the most matched master/mold pair, in terms of stiffness, mechanical stability and adhesive affinity between materials [81].

However, the ability of these thermoplastic materials to produce appropriate surface chemistry for cell attachment (referred to as TCT), their compatibility with standard sterilization methods and their background fluorescence are other important factors on materials selection [78].

Li et al. [81] reviews some properties of materials usually used in microfluidics. COC has proved to be easily demolded from silicon masters and suitable for replication purposes. PDMS casting was also successfully replicated when it is cast on Silicon/SU-8 master [81]. For that reason, an EBL-processed silica master and an SU-8 mold was selected for NIL of COC and PDMS molding, respectively, in order to create the final device.

After a certain manufacturing method is chosen, process quality or quality control has to be conducted to optimize the production parameters, e.g., temperature, pressure, holding time, etc. Defect inspection, critical dimensional measurements, bonding quality characterization and functionality characterization are the main steps for process control [81].

The defects can be in the form of particles, pattern defects, process-induced defects, and many others. Defect inspection aims to find any possible defects in microfluidic devices and/or estimate their distribution or overall sizes.

The common defect inspection technique is the combination of a camera or microscope together with bright filed. SEM is a conventional measurement technique that allows three-dimensional-type topographical views of nanoscale structures [37] and it is usually used to characterize the open features before bonding. The bond should be strong enough to prevent separation, free from air gaps around channels (to prevent fluid leakage), conform to dimensional specifications after deformation, etc. Also here, the camera and microscope are the conventional inspection techniques used to observe the bonding related issues. These techniques are useful to study the interface between materials and cells [37]

Functionality characterization is the last measurement to check the feasibility of the microfluidic devices after the devices are fabricated. It may include examining cellular behavior or if the fluid flows as expected [81].

5.2. Device Optimization

The oxidization of microfluidic devices made of thermoplastics or PDMS to make surfaces more hydrophilic can be achieved using UV-ozone or plasma treatments. Hydrophilicity/hydrophobicity of materials can affect cell attachment by influencing the ability of substratum to absorb protein and/or altering the conformation of the absorbed protein [95]. Welle and Gottwald in 2002 [96] studied the effects of UV-ozone treatment of PS and PC with respect to cell adhesion *in vitro* and it was observed that some products, like peroxides, formed on the surface during or after treatment might be toxic to cells.

However, preliminary experiments were performed in order to conclude which surface oxidization technique was more suitable for F11 culture purposes and for bonding of the COC and PDMS layers. LIVE/DEAD pictures suggested that after both treatments (UV and air plasma), COC became suitable for culture (Figure 24). F11 cells adhered on the treated surfaces and cellular proliferation and viability significantly increased on both cases.

Bonding trials were summarized in table 2. The UV treatment revealed to be inefficient to bond COC and PDMS layers when compared to the air plasma. Even when exposed to 60 min of UV, bonding was not achieved. Moreover, the combination of both techniques was also tried. COC was treated with UV and PDMS was treated with air plasma. Even in this situation, surfaces were not completely bonded. For that reason, air plasma was used to oxidize both COC and PDMS surfaces of the nanotopographic device because stronger bonding was achieved for lower exposure times.

During the air plasma treatment oxygen-containing functional groups are formed on the surface, which results in higher surface free energy and lower hydrophobicity. The surface energy can be assessed by contact angle measurements, indicating the hydrophobicity of the surface [77].

The measured contact angle range of standard TCT PS well plates was 40º-50º, the suggested optimal range for cell culture [77]. Thus, different treatment exposure times were applied to COC and PDMS samples. For this purpose, 6, 10, 15, 30, 60 and 120 seconds were assessed in order to achieve

the optimal range: 6 seconds of air plasma treatment of COC was determined to be the optimal exposure time, resulting in contact angle measurements between 40º and 50º (Figure 25). Moreover, 60 seconds were chosen for PDMS exposure time, because there was no significant decrease of contact angles for exposure times above 60 s. In addition, this value had already been used by others [93] and it also worked for COC and PDMS bonding. Thus, 6 and 60 seconds of air plasma exposure time (for COC and PDMS, respectively) were chosen for device construction purposes as optimal values.

After the choice of the surface treatment for both culture and bonding purposes, the NIL parameters were optimized. Four parameters are involved in the NIL process: molding temperature, molding pressure, holding time and demolding temperature [81].

A calibration curve was used to quantify the molding pressure applied by the paper clips on the COC during imprinting process. Thus, according to the linear equation (Figure 27), a pressure value of 0.1 MPa was estimated for the effective area where the pressure is applied by the paper clips (484 mm^2). As reviewed by Nunes et al. [97], “hot embossing” is generally done using lower pressures. Although the typical value is 0.5 MPa, other pressure values have been tried on different types of materials [97]. Moreover, COC is usually heated at T_g + 50ºC. For that reason, for NIL purposes, COC (T_g = 140ºC) was heated at 190ºC with a constant pressure of 0.1 MPa over a 484 mm^2 square area for 1 hour. COC and master were then disassembled at RT. SEM pictures (Figure 29) showed nanopatterns correctly replicated, proving that NIL conditions were optimized. In addition, the process described here is simpler than NIL existing procedures as well as quick, low cost, and it can be used in regular laboratory settings. Also axonal channels were successfully molded in PDMS (Figure 28), proving that molding conditions were also optimal (PDMS baking: 80ºC, 1 hour).

5.3. Cell Response Analysis

To complete the process of device optimization, the F11 cell response was assessed. The biocompatibility of treated-COC was tested and compared with other surfaces. Phalloidin-DAPI staining, ATP and DNA assays were performed on F11 cells.

DNA assay measures the concentration of DNA (ng/mL) in a sample and can then be used to determine the number of cells in a population that have adhered to a surface as well as to analyze the proliferation rates over different culture substrates. DNA assay results showed that cells highly proliferate on treated-COC surface. Differences were not statistically significant between treated-COC and TCT and glass coverslip (the nominal cell culture substrates, which were chosen as reference), but it was clear that the number of cells attached on the surface was higher on treated-COC, as compared to untreated-COC (Figure 32). The amount of ATP was also measured by performing a luciferase assay for each culture substrate. Although further measurements are required, the results were similar to the DNA assays (Figures 30 and 31). Treated-COC presented more ATP than untreated-COC indicating that F11 cells proliferated more in the treated-COC. However, biological triplicates should be performed in order to analyze eventual significant differences between cell culture substrates in terms of metabolic activity. Thus, the correlation of DNA and ATP experimental data could be also evaluated.

These results were consistent with Phalloidin and DAPI staining pictures: F11 cells were widely spread on treated-COC (Figure 36A) while aggregates of cells were tenderly formed on coverslips (Figure 36C), as compared to treated-COC. Cells did not spread on untreated-COC surfaces and a low number of aggregated cells survived (Figure 36B). Thus, both quantitative and qualitative methods (ATP and DNA assay, and Phalloidin-DAPI staining, respectively) used to cell response assessment indicated that COC treated with air plasma for 6 seconds is biocompatible and constitutes a feasible culture substrate for F11 cells.

The behavior of the F11 cells were also analyzed for different media conditions. According to obtained results, DNA concentration in wells cultured on 10% FBS was close to 1% FBS culture condition, indicating that the number of cells that adhered on the surface and proliferated was similar (Figure 35). It was expectable that cells had proliferated more in the media containing 10% FBS, but these results suggest that maybe cells could be supporting themselves by producing enough growth factors for each others. This maybe happened due to the high amount of seeding density used in these experiments (10000 cells/cm^2). However, the choice of a cell seeding density higher than usual (5000-8000 cells/cm^2) intended to recreate the situation of many cells growing quite close to the channels of the device.

The amount of DNA was lower in the wells cultured on 1% FBS + FSK, indicating that cells proliferated less in these conditions and might have started differentiation instead (Figure 35). This cell behavior was observed in both treated-COC and TCT (control) substrates, establishing that the molecular mechanisms involved on the differentiation of the F11 cells were independent of the chosen substrate. ATP assay results indicated that the ATP amount was higher in the wells cultured on 1% FBS + FSK for both treated-COC and TCT surfaces (Figure 34). These results indicated that although proliferation rates were lower for this media condition (Figure 33), cells were in process of differentiation and ATP was also needed in this case. However, biological triplicates should be performed in order to understand if these differences were significant in terms of metabolic activity.

Actin and nuclear immune staining showed morphological changes, depending on the media culture conditions. Although differences were not so clear, cells cultured on 1% FBS seemed to present a more elongated shape, as compared to cells cultured on 10% FBS conditions (Figure 37A and 37B). Relatively to the 1% FBS + FSK culture conditions, most of the cells presented axonal networks (Figure 37C). For that reason, 1% FBS + FSK were added to DMEM in order to induce F11 cells differentiation inside the device, because axonal outgrowth is essential for the assessment of the axonal nanotopographical preferences. Moreover, FSK has also been used in culturing with the purpose of promoting F11 differentiation [16].

5.4. Device Construction Problems

During the construction of the nanotopographic device, a few problems occurred. Firstly, the alignment of the “Ys” nanoimprintings with channels was not perfectly achieved, due to shrinkage of PDMS after baking. In order to solve this problem, different baking conditions were tried: 65ºC for 2h (usual procedure) and 80ºC for 1h. According to Li et al. [81], at higher curing temperature (85ºC), the shrinkage variation is between 0-1.84%. The SEM pictures showed that when the PDMS is baked at 65ºC for 2 hours, the width of the channels is 8 μm. However, this value increased to 9 μm when baked at 80ºC for 1 hour. On the other hand, the width of the columns that create the channels decreases from 11 μm at 65ºC for 2 hours to 10 μm at 80ºC for 1 hour baking (Figure 38). Despite these slight differences, the alignment was still not perfect. The PDMS was then chosen to be baked at 80ºC for 1 hour in order to reduce the fabrication time of the nanotopographic device. In these conditions, some channels were perfectly aligned, some partially aligned, and others are misaligned (Figure 41). However, as there are several repetitions of nanoimprintings combinatorial series, this problem can be overcome. Moreover, the construction of several devices for the same purpose is another feasible solution.

As Li at al. [81] concluded that no essential shrinkage or distortion was observed when PDMS is cured at room temperature, future trials could also be done in order to improve alignment by changing the baking conditions again. Another solution can also be the fabrication of new silica molds, which patterns dimensions should be created taking into account the predictable shrinkage rates of COC and PDMS. Moraes et al. [98] developed a “sandwich”-based mold fabrication method, which promise to provide an accurate alignment over large areas of multilayered devices. In order to solve the shrinkage problem, this approach could be implemented on the PDMS molding procedure.

Another problem was the fluid leakage in the device. Although the devices seemed to be strongly bonded, leakage of media was observed some hours after cell seeding. In order to solve this problem, some steps of the

bonding protocol were improved. It was observed to be crucial to dry both COC and PDMS surfaces with N_2 flow before the alignment step, most probably because demi-water would take more time to evaporate than the APTES reaction with the OH- groups in the surface. Thus, a layer of water between the surfaces would partially impair the bonding reaction. Then, just to avoid friction between surfaces, a 20 µL drop of ETOH or was used. This small drop would quickly evaporate assuring the correct device bonding and without fluid leakage (Figure 39).

The last main problem was the cell seeding density. First, a low cell seeding density was tested. Approximately 500-1000 cells were seeded in each device. Then, the device was left tilted for 4 hours in order to promote cell attachment close to the channels. However, it was observed that this cell density value was too low and cells died. For that reason, a higher cell seeding density was tried on each device (10000 cells/device), but it was observed that the number of cells was too high and cells also died. Then, 5000 cells were seeded per device. In this situation, cells survived and differentiated quite well inside the device (Figure 40). However, it was observed that some cells passed through the channels during the tilting step. This occurred because, after trypsinization, cells in suspension present round shape and can cross the channels due to media flow between device chambers. On the other hand, when attached to the surface, cells spread and increase their body size. Thus, only axons can pass through the channels.

For that reason, during cell seeding equal drops of media were added in each chamber in order to stop flow between them. Moreover, the tilting time was decreased. The device was gently tilted to promote proximity of cells to the channels and then placed in straight position for 4 hours of cell attachment. After this procedure, media was switched to differentiation media (DMEM + Pen-Strep + 1% FBS + FSK). The optimal number of seeded cells was determined to be 1000-2000 cells/device, because cells were enough close to the channels, without overpopulating them, which facilitates the assessment of the axonal growth through the channels and over the nanogratings (Figure 41).

CHAPTER 6 – *CONCLUSIONS AND FUTURE WORK*

The nanotopographic device shown in this work is the first physically modified microfluic system created with the purpose of single-cell nanotopographical preference analysis. This device incorporates two main aspects: 1) the bifurcation approach with nanogratings of different ridge widths in order to create an axonal selection nanotopographical-based system; 2) the axonal isolation by using channels for neurite outgrowth and guidance. Moreover, the contributions of this work fall into mainly two categories:

1. Device design and fabrication conditions were optimized: advantageous materials and techniques were chosen and the optimal parameters were determined;

2. Cell culture conditions on the device were also determined: seeding density, media conditions and biocompatibility were assessed for F11 cells (feasible *in vitro* cell model).

Although it was observed that F11 axons can grow through axonal channels, more work needs to be done in order to conclude if there is a preferential outgrowth over certain ridge widths. Depending on these results, different combinations of values from the ones tried on this device could also be tested. The production of several devices will be needed to quantify and perform statistical analysis of axonal preference over the nanogratings.

Stroock et al. [99] modelled the flow in a simple geometry, namely, a rectangular channel with a grooved floor (similar situation to those developed in the nanotopographic device). However, much remains to be done in order to quantify more precisely the effects obtainable as well as to explore further the flow for grooves of different dimensions [82] [99].

In spite of that, the nanotopographic device was successfully constructed and can be used as an *in vitro* model to analyze neural cell response to nanotopography. For this purpose, several aspects were taken into account to

choose the most suitable materials and techniques, such as biocompatibility, low-cost, ease of manipulation, and availability in regular laboratory settings.

This device has been designed to evaluate if axons can chose between different nanograting sizes. If cells reveal preferential growth over certain nanotopographical features, scaffolds can be constructed to mimic the natural nanotopography of the cellular microenvironments. Moreover, if different neural cell types have specific growth preferences, selective guidance and physical segregation of axons based on their type and function can be performed. This approach could then be a feasible solution for the selectivity problem in the PNIs, which could improve neuroprostheses performance [100]. For instance, a nanotopographical segregation-based system could be integrated on the PNIs and axons from sensory and motor neurons could be guided towards recording and stimulation specialized-electrodes, respectively.

Furthermore, the nanotopographic device can have many other potential applications. For instance, it can be a significant opportunity to further explore cell-nanotopography interactions, which could lead to refinement and more comprehensive predictive models of these interactions [8, 9] [36, 37].

Optimal nanostructure for a certain cell type is not necessarily optimal for another cell type. For that reason, more systematic approaches are needed to determine the role of nanotopography in conjunction with material characteristics [42]. The nanotopographic device constitutes a feasible systematic approach and can also be easily modified for specific applications.

Although a 2D system like the nanotopographic device does not mimic the *in vivo* 3D cellular microenvironment, 2D models are first required to develop a better fundamental understanding of the interactions between biomaterials and cells [32]. Then, these results can be considered in the optimization *in vitro* of 3D constructs prior to *in vivo* implementation [8] [82] [100]. Moreover, due to limitations in the nanofabrication of uniform features in 3D, most applications are based on 2D surfaces. Application of 2D structures to 3D biomaterials and the fabrication of novel 3D structures remain challenges for the future [8] [100].

Although the synergistic or competitive effect between chemistry, topography and mechanical properties of surfaces has to be understood, nanoscale surface topographies may present new ways to modulate cell function, compared to chemical treatments which are non-specific [30] [32].

More attention should also be paid to the research of “contact guidance” *in vivo* in the future [33], because recent studies have demonstrated that the cells cultured on flat surfaces behave differently from those in native tissues [42]. In addition, clinical evidences suggest that nanotopographies incorporated into scaffolds does not merely improve regeneration, but are in fact essential for meaningful restoration of peripheral nerve function [101].

As neurons are highly sensitive to the surrounding environment, the use of biocompatible materials improves culture reliability and *in vivo* implantation [45] [70]. Moreover, it would also be interesting to analyse how the cells of the immune system interact with nanotopographies [8]. Thus, signal transmission between tissue-prosthesis interface could also be improved, by developing structured nanoscale topographies able to suppress the immune response, and SCs proliferation, for instance [40].

Thompson et al. [102] demonstrated that axonal guidance was determined by both the topography of the SC monolayer and molecules expressed on the SC surface. Thus, the second chamber of the device can be used to culture SCs and analyse contact guidance of F11 cells in the presence of the SCs. This new coculture device could then be useful to further elucidate the contributions of these guidance cues to axonal guidance and to investigate other SC-neuronal interactions [103].

Micro- and nanotechnologies and microfluidics clearly have great potential in NTE and it will be extremely useful in this field, but the definitive proof of this assumption in the specific context of the approach described in this thesis is still lacking [70]. However, the nanotopographic device has the potential to be important in the development of this new field of neurofluidics.

REFERENCES

1. *O&P Trends & Statistics* 2008; Retrieved, November 2013, from http://www.opcareers.org/assets/pdf/OP_Trends_and_Statistics.pdf].
2. Farina, D., Jensen, W., Akay, M., ed. *Introduction to Neural Engineering for Motor Rehabilitation*. Series in Biomedical Engineering, ed. I. Press 2013, Wiley, New Jersey.
3. Esquenazi, A., *Amputation rehabilitation and prosthetic restoration. From surgery to community reintegration.* Disability and Rehabilitation, 2004. **26**: p. 831-836.
4. Marks, L.J. and J.W. Michael, *Artificial limbs.* BMJ, 2001. **323**(7315): p. 732-735.
5. Lai, J.C., et al., *Prosthetic devices: challenges and implications of robotic implants and biological interfaces.* Proc Inst Mech Eng H, 2007. **221**(2): p. 173-83.
6. San Jose, C. *Global Orthopedic Prosthetics Market to Reach US$19.4 Billion by 2015, according to a New Report by Global Industry Analysts, Inc.* 2011; Retrieved, November 2013, from http://www.prweb.com/pdfdownload/8072141.pdf].
7. Kumar, S., *Microfluidic Devices in Nanotechnology: Applications*2010: Wiley.
8. Popat, K., ed. *Nanotechnology in Tissue Engineering and Regenerative Medicine*. 1st ed. 2011, CRC Press. 302.
9. Leach, J.B., A.K. Achyuta, and S.K. Murthy, *Bridging the Divide between Neuroprosthetic Design, Tissue Engineering and Neurobiology.* Front Neuroeng, 2010. **2**: p. 18.
10. Khademhosseini, A., et al., *Microscale technologies for tissue engineering and biology.* Proc Natl Acad Sci U S A, 2006. **103**(8): p. 2480-7.
11. Norman, J.J. and T.A. Desai, *Methods for fabrication of nanoscale topography for tissue engineering scaffolds.* Ann Biomed Eng, 2006. **34**(1): p. 89-101.

12. Roco, M., *The long view of nanotechnology development: the National Nanotechnology Initiative at 10 years.* J Nanopart Res, 2011. **13**: p. 427-455.
13. Silva, G.A., *What impact will nanotechnology have on neurology?* Nat Clin Pract Neurol, 2007. **3**(4): p. 180-1.
14. Kelleher, C.M. and J.P. Vacanti, *Engineering extracellular matrix through nanotechnology.* J R Soc Interface, 2010. **7 Suppl 6**: p. S717-29.
15. Brunello, C.A., et al., *Microtechnologies to fuel neurobiological research with nanometer precision.* J Nanobiotechnology, 2013. **11**: p. 11.
16. Wieringa, P., et al., *Nanotopography induced contact guidance of the F11 cell line during neuronal differentiation: a neuronal model cell line for tissue scaffold development.* Nanotechnology, 2012. **23**(27): p. 275102.
17. Rod R. Seeley, T.D.S., Philip Tate, ed. *Anatomy and Physiology*. 6th ed. 2003, McGraw Hill Education, Idaho. p. 1105.
18. Schmidt, C.E. and J.B. Leach, *Neural tissue engineering: strategies for repair and regeneration.* Annu Rev Biomed Eng, 2003. **5**: p. 293-347.
19. Clemens van Blitterswijk, P.T., Jeffrey Hubbell, Ranieri Cancedda, Joost de Bruijn, Anders Lindahl, Jerome Sohier, David F. Williams, ed. *Tissue Engineering*. 1st ed. Academic Press Series in Biomedical Engineering 2008, Elsevier, Amsterdam. p. 740.
20. Navarro, X., et al., *A critical review of interfaces with the peripheral nervous system for the control of neuroprostheses and hybrid bionic systems.* J Peripher Nerv Syst, 2005. **10**(3): p. 229-58.
21. Salihu. *Three types of neurons*. Studyblue 2014; Retrieved, December 2013, from http://www.studyblue.com/notes/note/n/final-exam-review/deck/4847677].
22. Koaboi. *The Central Nervous System (CNS)*. 2009; Retrieved, December 2013, from http://koaboi.wordpress.com/].
23. Ulrich Meyer, J.H., Hans Peter Wiesmann, Thomas Meyer, ed. *Fundamentals of Tissue Engineering and Regenerative Medicine*. 1st ed. 2009, Springer, New York. p. 1054
24. Huebner, E.A. and S.M. Strittmatter, *Axon regeneration in the peripheral and central nervous systems.* Results Probl Cell Differ, 2009. **48**: p. 339-51.

25. Allodi, I., E. Udina, and X. Navarro, *Specificity of peripheral nerve regeneration: interactions at the axon level.* Prog Neurobiol, 2012. **98**(1): p. 16-37.
26. Roytta, M. and V. Salonen, *Long-term endoneurial changes after nerve transection.* Acta Neuropathol, 1988. **76**(1): p. 35-45.
27. Torigoe, K., et al., *Basic behavior of migratory Schwann cells in peripheral nerve regeneration.* Exp Neurol, 1996. **137**(2): p. 301-8.
28. Bellamkonda, R.V., *Peripheral nerve regeneration: an opinion on channels, scaffolds and anisotropy.* Biomaterials, 2006. **27**(19): p. 3515-8.
29. Chang, W.C., M. Kliot, and D.W. Sretavan, *Microtechnology and nanotechnology in nerve repair.* Neurol Res, 2008. **30**(10): p. 1053-62.
30. Li, G.N. and D. Hoffman-Kim, *Tissue-engineered platforms of axon guidance.* Tissue Eng Part B Rev, 2008. **14**(1): p. 33-51.
31. Silva, G.A., *Introduction to nanotechnology and its applications to medicine.* Surg Neurol, 2004. **61**(3): p. 216-20.
32. Lord, M.S., M. Foss, and F. Besenbacher, *Influence of nanoscale surface topography on protein adsorption and cellular response.* Nano Today, 2010. **5**(1): p. 66-78.
33. Zhou, F., et al., *Phenomenon of "contact guidance" on the surface with nano-micro-groove-like pattern and cell physiological effects.* Chinese Science Bulletin, 2009. **54**(18): p. 3200-3205.
34. Silva, G.A., *Neuroscience nanotechnology: progress, opportunities and challenges.* Nat Rev Neurosci, 2006. **7**(1): p. 65-74.
35. Gates, B.D., et al., *New approaches to nanofabrication: molding, printing, and other techniques.* Chem Rev, 2005. **105**(4): p. 1171-96.
36. Bettinger, C.J., R. Langer, and J.T. Borenstein, *Engineering substrate topography at the micro- and nanoscale to control cell function.* Angew Chem Int Ed Engl, 2009. **48**(30): p. 5406-15.
37. Silva, G.A., *Introduction to nanotechnology and its applications to medicine.* Surgical Neurology, 2004. **61**(3): p. 216-220.
38. Xie, J., et al., *Neurite Outgrowth on Nanofiber Scaffolds with Different Orders, Structures, and Surface Properties.* ACS Nano, 2009. **3**(5): p. 1151-1159.

39. Lim, J.Y. and H.J. Donahue, *Cell sensing and response to micro- and nanostructured surfaces produced by chemical and topographic patterning.* Tissue Eng, 2007. **13**(8): p. 1879-91.
40. Jung, D.R., et al., *Topographical and physicochemical modification of material surface to enable patterning of living cells.* Crit Rev Biotechnol, 2001. **21**(2): p. 111-54.
41. Tay, C.Y., et al., *Micro-/nano-engineered cellular responses for soft tissue engineering and biomedical applications.* Small, 2011. **7**(10): p. 1361-78.
42. Kim, H.N., et al., *Nanotopography-guided tissue engineering and regenerative medicine.* Adv Drug Deliv Rev, 2013. **65**(4): p. 536-58.
43. Dent, E.W., S.L. Gupton, and F.B. Gertler, *The growth cone cytoskeleton in axon outgrowth and guidance.* Cold Spring Harb Perspect Biol, 2011. **3**(3).
44. Ferrari, A., et al., *The effect of alternative neuronal differentiation pathways on PC12 cell adhesion and neurite alignment to nanogratings.* Biomaterials, 2010. **31**(9): p. 2565-73.
45. Millet, L.J. and M.U. Gillette, *Over a century of neuron culture: from the hanging drop to microfluidic devices.* Yale J Biol Med, 2012. **85**(4): p. 501-21.
46. Millet, L.J. and M.U. Gillette, *New perspectives on neuronal development via microfluidic environments.* Trends Neurosci, 2012. **35**(12): p. 752-61.
47. Dalby, M.J., D. Pasqui, and S. Affrossman, *Cell response to nano-islands produced by polymer demixing: a brief review.* IEE Proc Nanobiotechnol, 2004. **151**(2): p. 53-61.
48. Martinez, E., et al., *Effects of artificial micro- and nano-structured surfaces on cell behaviour.* Ann Anat, 2009. **191**(1): p. 126-35.
49. Moxon, K.A., et al., *Bioactive properties of nanostructured porous silicon for enhancing electrode to neuron interfaces.* J Biomater Sci Polym Ed, 2007. **18**(10): p. 1263-81.
50. Ferrari, A., et al., *Nanotopographic control of neuronal polarity.* Nano letters, 2011. **11**(2): p. 505-511.
51. Cecchini, M., et al., *PC12 differentiation on biopolymer nanostructures.* Nanotechnology, 2007. **18**(50): p. 505103.

52. Koh, H.S., et al., *Enhancement of neurite outgrowth using nano-structured scaffolds coupled with laminin.* Biomaterials, 2008. **29**(26): p. 3574-82.
53. Naka, Y., et al., *Neurite outgrowths of neurons on patterned self-assembled monolayers.* J Biosci Bioeng, 2002. **94**(5): p. 434-9.
54. Kim, Y.T., et al., *The role of aligned polymer fiber-based constructs in the bridging of long peripheral nerve gaps.* Biomaterials, 2008. **29**(21): p. 3117-27.
55. Corey, J.M., et al., *Aligned electrospun nanofibers specify the direction of dorsal root ganglia neurite growth.* J Biomed Mater Res A, 2007. **83**(3): p. 636-45.
56. Kofron, C.M., V.J. Fong, and D. Hoffman-Kim, *Neurite outgrowth at the interface of 2D and 3D growth environments.* J Neural Eng, 2009. **6**(1): p. 016002.
57. Long, Y., et al., *Formation of Highly Aligned Grooves on Inner Surface of Semipermeable Hollow Fiber Membrane for Directional Axonal Outgrowth.* Journal of Manufacturing Science and Engineering, 2008. **130**(2): p. 021011-021011.
58. Miller, C., S. Jeftinija, and S. Mallapragada, *Synergistic effects of physical and chemical guidance cues on neurite alignment and outgrowth on biodegradable polymer substrates.* Tissue Eng, 2002. **8**(3): p. 367-78.
59. Goldner, J.S., et al., *Neurite bridging across micropatterned grooves.* Biomaterials, 2006. **27**(3): p. 460-72.
60. Wang, H.B., et al., *Creation of highly aligned electrospun poly-L-lactic acid fibers for nerve regeneration applications.* J Neural Eng, 2009. **6**(1): p. 016001.
61. Dubey, N., P.C. Letourneau, and R.T. Tranquillo, *Guided neurite elongation and schwann cell invasion into magnetically aligned collagen in simulated peripheral nerve regeneration.* Exp Neurol, 1999. **158**(2): p. 338-50.
62. Krsko, P., et al., *Length-scale mediated adhesion and directed growth of neural cells by surface-patterned poly(ethylene glycol) hydrogels.* Biomaterials, 2009. **30**(5): p. 721-9.

63. Gupta, D., et al., *Aligned and random nanofibrous substrate for the in vitro culture of Schwann cells for neural tissue engineering.* Acta Biomater, 2009. **5**(7): p. 2560-9.
64. Kulangara, K. and K.W. Leong, *Substrate topography shapes cell function.* Soft Matter, 2009. **5**(21): p. 4072-4076.
65. Yim, E.K. and K.W. Leong, *Significance of synthetic nanostructures in dictating cellular response.* Nanomedicine, 2005. **1**(1): p. 10-21.
66. Johansson, F., et al., *Axonal outgrowth on nano-imprinted patterns.* Biomaterials, 2006. **27**(8): p. 1251-8.
67. Fozdar, D.Y., et al., *Selective axonal growth of embryonic hippocampal neurons according to topographic features of various sizes and shapes.* Int J Nanomedicine, 2011. **6**: p. 45-57.
68. Curley, J.L. and M.J. Moore, *Facile micropatterning of dual hydrogel systems for 3D models of neurite outgrowth.* J Biomed Mater Res A, 2011. **99**(4): p. 532-43.
69. Wieringa, P.A., et al., *Bifurcating microchannels as a scaffold to induce separation of regenerating neurites.* J Neural Eng, 2010. **7**(1): p. 16001.
70. Andersson, H. and A. van den Berg, *Microfabrication and microfluidics for tissue engineering: state of the art and future opportunities.* Lab Chip, 2004. **4**(2): p. 98-103.
71. Durand, D.M., *What is Neural Engineering?* JOURNAL OF NEURAL ENGINEERING, 2007. p. 4.
72. Thomas D. Coates Jr., P.D., ed. *Neural Interfacing: Forging the Human-Machine Connection*. 1st ed. Synthesis Lectures on Biomedical Engineering, ed. U.o.C. John D. Enderle 2008, California. p. 112.
73. Luca Rossini, D.I., Leopold Summerer, ed. *Brain machine interfaces for space applications: enhancing astronaut capabilities*. 1st ed. International Review of Neurobiology. Vol. 86. 2009, Academic Press, Amsterdam. p. 268.
74. Pancrazio, J.J., *Neural interfaces at the nanoscale.* Nanomedicine (Lond), 2008. **3**(6): p. 823-30.
75. Grill, W.M., S.E. Norman, and R.V. Bellamkonda, *Implanted neural interfaces: biochallenges and engineered solutions.* Annu Rev Biomed Eng, 2009. **11**: p. 1-24.

76. Taylor, A.M., et al., *Microfluidic Multicompartment Device for Neuroscience Research.* Langmuir, 2003. **19**(5): p. 1551-1556.
77. van Midwoud, P.M., et al., *Comparison of biocompatibility and adsorption properties of different plastics for advanced microfluidic cell and tissue culture models.* Anal Chem, 2012. **84**(9): p. 3938-44.
78. Meyvantsson, I. and D.J. Beebe, *Cell culture models in microfluidic systems.* Annu Rev Anal Chem (Palo Alto Calif), 2008. **1**: p. 423-49.
79. Nelson, C.M. and J. Tien, *Microstructured extracellular matrices in tissue engineering and development.* Curr Opin Biotechnol, 2006. **17**(5): p. 518-23.
80. Kim, S.M., S.H. Lee, and K.Y. Suh, *Cell research with physically modified microfluidic channels: a review.* Lab Chip, 2008. **8**(7): p. 1015-23.
81. Li, S., et al. *Review of production of microfluidic devices: material, manufacturing and metrology*. Proc. SPIE, France, 2008. p. 6993.
82. Gross, P.G., et al., *Applications of microfluidics for neuronal studies.* J Neurol Sci, 2007. **252**(2): p. 135-43.
83. Tsao, C.-W. and D. DeVoe, *Bonding of thermoplastic polymer microfluidics.* Microfluidics and Nanofluidics, 2009. **6**(1): p. 1-16.
84. Campenot, R.B., *Local control of neurite development by nerve growth factor.* Proceedings of the National Academy of Sciences, 1977. **74**(10): p. 4516-4519.
85. Tharin, S., et al., *A microfluidic device to investigate axon targeting by limited numbers of purified cortical projection neuron subtypes.* Integr Biol (Camb), 2012. **4**(11): p. 1398-405.
86. Majumdar, D., et al., *Co-culture of neurons and glia in a novel microfluidic platform.* J Neurosci Methods, 2011. **196**(1): p. 38-44.
87. Dinh, N.D., et al., *Microfluidic construction of minimalistic neuronal co-cultures.* Lab Chip, 2013. **13**(7): p. 1402-12.
88. Park, J.W., et al., *Microfluidic culture platform for neuroscience research.* Nat Protoc, 2006. **1**(4): p. 2128-36.
89. Li, L., et al., *Spatiotemporally controlled and multifactor involved assay of neuronal compartment regeneration after chemical injury in an integrated microfluidics.* Anal Chem, 2012. **84**(15): p. 6444-53.

90. Taylor, A.M., et al., *A microfluidic culture platform for CNS axonal injury, regeneration and transport.* Nat Methods, 2005. **2**(8): p. 599-605.
91. Goral, V.N., et al., *Hot embossing of plastic microfluidic devices using poly(dimethylsiloxane) molds.* Journal of Micromechanics and Microengineering, 2011. **21**(1): p. 017002.
92. Tekscan, I. *FlexiForce® Sensors: standard flexiforce sensors for force measurement*. 2013; Retrieved, February 2014, from http://www.tekscan.com/flexible-force-sensors].
93. Sunkara, V., et al., *Simple room temperature bonding of thermoplastics and poly(dimethylsiloxane).* Lab Chip, 2011. **11**(5): p. 962-5.
94. Sollier, E., et al., *Rapid prototyping polymers for microfluidic devices and high pressure injections.* Lab on a Chip, 2011. **11**(22): p. 3752-3765.
95. Khan, S. and G. Newaz, *A comprehensive review of surface modification for neural cell adhesion and patterning.* J Biomed Mater Res A, 2010. **93**(3): p. 1209-24.
96. Welle, A. and E. Gottwald, *UV-Based Patterning of Polymeric Substrates for Cell Culture Applications.* Biomedical Microdevices, 2002. **4**(1): p. 33-41.
97. Nunes, P., et al., *Cyclic olefin polymers: emerging materials for lab-on-a-chip applications.* Microfluidics and Nanofluidics, 2010. **9**(2-3): p. 145-161.
98. Moraes, C., Y. Sun, and C.A. Simmons, *Solving the shrinkage-induced PDMS alignment registration issue in multilayer soft lithography.* Journal of Micromechanics and Microengineering, 2009. **19**(6): p. 065015.
99. Stroock, A.D., et al., *Patterning flows using grooved surfaces.* Anal Chem, 2002. **74**(20): p. 5306-12.
100. Cullen, D.K., et al., *Neural tissue engineering and biohybridized microsystems for neurobiological investigation in vitro (Part 1).* Crit Rev Biomed Eng, 2011. **39**(3): p. 201-40.
101. Spivey, E.C., et al., *The fundamental role of subcellular topography in peripheral nerve repair therapies.* Biomaterials, 2012. **33**(17): p. 4264-76.
102. Thompson, D.M. and H.M. Buettner, *Neurite outgrowth is directed by schwann cell alignment in the absence of other guidance cues.* Ann Biomed Eng, 2006. **34**(1): p. 161-8.

103. Goubko, C.A. and X. Cao, *Patterning multiple cell types in co-cultures: A review.* Materials Science and Engineering: C, 2009. **29**(6): p. 1855-1868.